Stability and Bifurcations of Modes of Current Transfer to Cathodes of DC Gas Discharges

TESE DE DOUTORAMENTO

Maria José Gomes Faria

DOUTORAMENTO EM FÍSICA

UNIVERSIDADE da MADEIRA

A Nossa Universidade

www.uma.pt

Maio | 2011

Acknowledgments

To my supervisor, Professor Mikhail Benilov, who has always accompanied and motivated me throughout this work.

To Dr. Mário Cunha, for providing numerical solutions describing different modes of current transfer to cathodes of high-pressure arc discharges and for discussions that enriched my vision.

To Pedro Almeida, for providing numerical solutions describing different modes of current transfer of glow discharges and for helpful discussions.

To Dr. Nelson Almeida, for his support with LaTeX.

Preface

This dissertation was performed within activities of the following projects:

- Fellowship SFRH/BD/35883/2007 from FCT.
- Fellowship from Secretaria Regional da Educação e Cultura da RAM in the academic year 2008/09.
- Project POCTI/FIS/32411/2000 *Theory and modelling of plasma-cathode interaction in high-pressure arc discharges* of the program POCTI of FCT and FEDER.
- Project POCI/FIS/60526/2004 *Modes of current transfer to cathodes of high-pressure arc discharges and their stability* of FCT, POCI 2010 and FEDER.
- Project PTDC/FIS/68609/2006 *Cathode spots in high-pressure DC gas discharges: self-organization phenomena* of FCT and FEDER.
- Project *Centro de Ciências Matemáticas* of FCT, POCTI-219 and FEDER.

Results presented in this thesis are published in the following articles:

- M. S. Benilov and M. J. Faria, *Stability of direct current transfer to thermionic cathodes: II. Numerical simulation* (2007) J. Phys. D: Appl. Phys. **40** 5083–5097.
- M. S. Benilov, M.D. Cunha, and M. J. Faria, *Effect of protrusions on cathodic-arc-attachment mode in high-pressure arc discharges* (2008) IEEE Trans. Plasma Sci. **36**, No. 4, pp. 1034-1035.
- M. S. Benilov, M. D. Cunha and M. J. Faria, *Simulating different modes of current transfer to thermionic cathodes in a wide range of conditions* (2009) J. Phys. D: Appl. Phys. **42** 145205 (17pp).
- P. G. C. Almeida, M. S. Benilov, M.D. Cunha and M. J. Faria, *Analysing bifurcations encountered in numerical modelling of current transfer to cathodes of DC glow and arc discharges* (2009) J. Phys. D: Appl. Phys. **42** 194010 (21pp).

Results presented in this thesis were reported at a number of conferences:

- M. S. Benilov and M. J. Faria, *Numerical investigation of stability of current transfer to thermionic cathodes*, Proceedings of the 59th Gaseous Electronics Conference (October 10-13, 2006, Columbus, Ohio).

- M. S. Benilov and M. J. Faria, *Stability of current transfer to cathodes of HID lamps*, Cost Strategic Workshop on Lighting – Light Sources and Light Systems – Technology for the Future (December 1-3, 2006, Heraklion Crete, Greece).

- M. S. Benilov and M. J. Faria, *Numerical investigation of stability of steady-state current transfer to thermionic cathodes*, Proceedings of the 28th International Conference on Phenomena in Ionized Gases (July 15-20, 2007, Prague, Czech Republic).

- M. S. Benilov, M. D. Cunha and M. J. Faria, *Effect of cathode geometry on modes of current transfer to cathodes of high-pressure arc discharges*, Proceedings of the 35th IEEE International Conference on Plasma Science (July 15-19, 2008, Granada, Spain).

- M. S. Benilov and M. J. Faria, *Investigation of stability of current transfer to thermionic cathodes*, Proceedings of the European COMSOL Conference (November 4-6, 2008, Hannover, Germany).

- M. S. Benilov, M.D. Cunha and M. J. Faria, *Patterns of current transfer to thermionic cathodes in a wide range of conditions*, Proceedings of the 29th International Conference on Phenomena in Ionized Gases (July 12-19, 2009, Cancún, México).

- P. G. C. Almeida, M. S. Benilov, M.D. Cunha and M. J. Faria, *Understanding bifurcations encountered in numerical modelling of current transfer to cathodes of DC glow and arc discharges*, Proceedings of the 29th International Conference on Phenomena in Ionized Gases (July 12-19, 2009, Cancún, México) - **invited talk** delivered by M. J. Faria.

- M. S. Benilov, M.D. Cunha and M. J. Faria, *Modelling current transfer to thermionic cathodes in a wide range of conditions*, Proceedings of the 19th International Symposium on Plasma Chemistry (July 26-31, 2009, Bochum, Germany).

- P. G. C. Almeida, M. S. Benilov and M. J. Faria, *Axially symmetric modes of current transfer to cathodes of DC glow discharges and their stability*, Proceedings of the 20th European Conference on the Atomic and Molecular Physics of Ionized Gases (July 13-17, 2010, Novi Sad, Sérvia).

- P. G. C. Almeida, M. S. Benilov, M. J. Faria and V. V. Mikhailenko, *Stability of current transfer to cathodes of DC glow discharges*, Proceedings of the 63rd Annual Gaseous Electronics Conference and 7th International Conference on Reactive Plasmas (October 4-8, 2010, Paris, France).

Resumo

A estabilidade de diferentes modos estacionários de transferência de corrente para cátodos de arco a alta pressão e de diferentes modos estacionários axialmente simétricos de transferência de corrente em descargas luminescentes em relação a pequenas perturbações é investigada no âmbito da teoria da estabilidade linear. O problema de valores próprios para as perturbações é resolvido através do software COMSOL Multiphysics. Na descarga de arco, verificou-se que apenas o modo difuso e o primeiro modo mancha 3D podem ser estáveis. A transição entre os dois modos é não-estacionária e acompanhada por histerese. Na descarga luminescente, as variações dos incrementos das perturbações com a corrente são investigadas para o caso 1D e para diferentes modos axialmente simétricos. Incrementos reais e complexos foram detectados, o que significa que as perturbações podem variar com o tempo tanto monotonicamente como com oscilações. Em geral, os resultados fornecidos pela teoria da estabilidade linear confirmam os conceitos intuitivos desenvolvidos na literatura e estão em conformidade com as experiências. A teoria também fornece sugestões para trabalhos teóricos e experimentais. As bifurcações encontradas durante a modulação numérica da transferência de corrente para os cátodos de arco a alta pressão e em descargas luminescentes são analisadas. Todos os tipos básicos de bifurcações estacionárias foram identificados e analisados. A análise fornece explicações para muitos dos resultados obtidos na modulação numérica. Em particular, é mostrado que mudanças dramáticas dos padrões de transferência de corrente para ambos os cátodos das descargas luminescente e de arco ocorrem por meio de perturbações de bifurcações transcríticas de contato de primeira e segunda ordem. No caso da descarga de arco, o efeito da geometria do cátodo e da temperatura de arrefecimento sobre a estabilidade foi estudado. Verificou-se que as mudanças dos padrões dos modos estacionários ocorrem devido a uma interação entre auto-organização e fatores geométricos.

Palavras-chave: descarga de arco a alta pressão, descarga luminescente, manchas catódicas, auto-organização, estabilidade, bifurcações.

Abstract

Stability of different steady-state modes of current transfer to cathodes of DC high-pressure arcs and of different axially symmetric modes of current transfer of DC glow discharges against small perturbations is investigated in the framework of the linear stability theory. The eigenvalue problem for perturbations is solved with the use of software COMSOL Multiphysics. For the arc discharge, it was found that only the diffuse mode and the first 3D spot mode can be stable. The transition between the two modes is non-stationary and accompanied by hysteresis. For the glow discharge, variations of the increments of perturbations with discharge current are investigated for the 1D glow discharge and different modes of axially symmetric glow discharge. Both real and complex increments have been detected, meaning that perturbations can vary with time both monotonically and with oscillations. In general, results given by the linear stability theory confirm intuitive concepts developed in the literature and conform to the experiment. On the other hand, the theory provides suggestions for further experimental and theoretical work. Bifurcations encountered in numerical modelling of current transfer to cathodes of DC high-pressure arcs and of DC glow discharges are analyzed. All basic types of steady-state bifurcations (fold, transcritical, pitchfork) have been identified and analyzed. The analysis provides explanations to many results obtained in numerical modelling. In particular, it is shown that dramatic changes of patterns of current transfer to cathodes of both glow and arc discharges, described by numerical modelling, occur through perturbed transcritical bifurcations of first and second order contact. For the case of the arc discharge, effect over stability of cathode geometry and temperature of cooling was studied. It was found that changes of patterns of the steady-state modes occur due to interplay of self-organization and geometric factors.

Keywords: high-pressure arc discharge, glow discharge, cathode spots, self-organization, stability, bifurcations.

Contents

List of Figures

List of Tables

Chapter 1

Introduction

1.1 Concept of self-organization in complex dissipative systems

Spontaneous formation of well organized structures in complex systems (systems involving a large number of interactions between its various subunits) is a fascinating phenomenon. These structures are found in a wide spectrum of disciplines ranging from mathematics to physics to computer science to sociology. As examples of these phenomena one can mention the formation of stars, the evolution of species to more complex levels, the evolution of financial markets and the emergence of new words.

According to Haken [1], a system is self-organized if it acquired a spatial, temporal or functional structure without specific correlation to the environment, i.e., if the structure is not imposed from outside. In order to explain the meaning of the last words, let us turn to an example from gas discharge physics which is relevant to this work: cathodes of high-pressure arc discharges can operate in the diffuse mode, where the current is more or less uniformly distributed over the front surface of the cathode, and in the spot mode, where the most of the current is collected by a small area (cathode spot). Cathode spots can be provoked by non-uniformities of geometrical and/or physical properties of the current-collecting surface, such as the presence of protrusions or areas with a reduced work function. However, they can occur also on uniform cathodes, and such cases should be treated as self-organization.

Let us consider, following Nicolis and Prigogine [2], an example of a pan with liquid being heated from below. While the temperature gradient remains low, the heat spreads through the liquid by conduction. As the temperature of the bottom of the pan increases, convection cells arise spontaneously at a certain value of the temperature gradient. One could say that the mode without convection is unstable and the system jumped to another mode. Note that the mode without convection includes the state where the pan is cold, i.e., the equilibrium state which occurs when the system (the pan) is isolated. In [2], this mode is called the thermodynamic branch. The mode with convection cells results from a self-organization of the system as a response to a change in its environment; a self-organized mode, or a mode with dissipative structures.

Let us analyze the previous example from another perspective. One can think that there are always small convection currents (fluctuations or spontaneous perturbations) in the system considered. Below a certain value of the temperature gradient, these fluctuations are damped and disappear. On the contrary, above the critical value of the temperature gradient the fluctuations are amplified and give rise to macroscopic currents, i.e., the system self-organizes itself.

Nicolis and Prigogine [2] generalize this example as follows. Let us suppose that an external force takes a system away from the equilibrium state. Two situations can occur: the thermodynamic branch may either persist or, if appropriate feedback conditions appear, become unstable. In the latter case, the system evolves to a new structure radically different from the structure of the thermodynamic branch: a self-organized mode.

Note, however, that self-organization can occur when the external force is low enough, instead of high enough. In the above-mentioned example of cathodes of high-pressure arc discharges the diffuse mode occurs at high values of the discharge current and the spot mode occurs at low values. It is natural to consider the spot mode as self-organized, however one would not term the diffuse mode the thermodynamic branch since it does not include the zero-current state, which represents the equilibrium state of an isolated discharge system. In fact, the term "thermodynamic branch", introduced by Nicolis and Prigogine, seems not to have gained wide recognition. In this work, the terms "diffuse mode" or "fundamental mode" are used.

Self-organization in complex systems can be studied by means of different tools. A natural approach to solving the problem of the appearance of self-organization is to invoke the bifurcation theory. This theory studies the appearance of new solutions of differential equations when control parameters (parameters on which the system depends) vary. Points where new solutions arise are called bifurcation points or critical points. The bifurcation theory usually gives qualitative information on behavior of emerging solutions in the vicinity of the bifurcation points. In some cases, the asymptotic behavior may be found analytically. Concepts of bifurcation theory are extensively used in this dissertation. Since this theory is not a tool of everyday use in the gas discharge physics, a brief summary of relevant information from this theory for convenience is given in appendix B.

Stability theory is another common tool for investigation of self-organization in complex systems. The formalism of stability theory is well-known and may be briefly described as follows. Consider a set of differential equations describing temporal evolution of a system. Assume that $u(t)$ is a solution of this system of equations, where t is time, and that it is uniquely determined by values at the initial instant. What happens to the trajectory $u(t)$ if the initial conditions are not exactly the same as considered? Intuitively we can say that the trajectory $u(t)$ is stable if trajectories that are close to $u(t)$ at the initial moment will remain close to it at all subsequent moments. Otherwise, $u(t)$ is unstable.

There are two different approaches in the stability theory: stability can be studied using the local criterion (linear stability analysis) or the global criterion. In the first approach, the study is done considering a new solution which represents the sum of the solution under investigation and of a small perturbation dependent on time, which describes an external perturbation or an internal fluctuation. This new solution is substituted into the system of equations and initial and/or boundary conditions and the problem is linearized with respect to the perturbation. After the (linear) problem for perturbations has been solved, the evolution of perturbations with time is analyzed. Thus, times of relaxation or development of perturbations are obtained. In the second approach, stability is analyzed based on Lyapunov function.

The catastrophe theory is based on calculation of potential functions associated with forces acting in the system under consideration. An analysis of the points where the first derivative of the potential function is zero is made. Depending on the sign of the second derivative, these points can be stable (minimum of the potential function), unstable (maximum) or neutrally stable (inflection point). If (some of) the parameters of the potential function change, it may happen that the number of minima changes. If this change occurs, it is said that there was a catastrophic change, i.e., a bifurcation occurs.

Both the stability theory based on the global criterion and the catastrophe theory only provide qualitative information. The linear stability theory is extensively used in this work.

There are cases where the above-described deterministic methods are not adequate. This means that even if the initial condition (starting point) is known, there are many possibilities for where the system can evolve. Nevertheless, some of these possibilities are more probable than others. In such situations, the evolution of the system must be analyzed in probabilistic terms, by means of stochastic methods.

Another concept important for this dissertation is the coexistence of phases, i.e., simultaneous occurrence of different modes in different domains inside the system. (Inevitably, coexistence of phases is found in systems that are in phase transition.) It is necessary that some control parameters take specific values for a coexistence of phases be possible. A typical example is found in the coexistence of a liquid and its vapor: for a given temperature, coexistence is possible only for one pressure value (value of the saturated vapor for the temperature being considered). A condition that defines values of the control parameter for which coexistence is possible (in this example, the pressure value) is referred to as Maxwell construction; e.g., [2, 3]. A classic example of this construction is the pressure-volume diagram of a van der Waals gas, where the pressure at which the coexistence occurs is chosen from a geometric rule of equal area, which follows from the second law of thermodynamics.

1.2 Self-organization near electrodes of gas discharges

Self-organized patterns in gas discharges are well-known and represent an important particular case of self-organization phenomena; see, e.g., the recent review [4] and references therein. Of interest for this work is self-organization occurring in the vicinity of electrodes. This section is devoted to a review of relevant experimental and theoretical results. Note that self-organization phenomena occurring in the discharge column, which are unrelated to electrodes, are left beyond the scope of this work and are not reviewed here; this includes such classic examples as striations and filaments appearing under certain conditions in the column of a glow discharge (e.g., [5, 6]) and a recent example of plasma bullets [7–14], which, according to the experiments [15], also are likely to represent self-organized patterns.

1.2.1 Experiment

The occurrence of self-organization in near-electrode regions of gas discharges is a very frequent phenomenon. Being of considerable scientific interest by itself, the understanding of this phenomenon is of vital importance for the design of a number of technical devices.

It has been known for many decades that the steady-state current transfer to cathodes of glow discharges can occur in the so-called abnormal mode, where most of the discharge cross section near the cathode is bright, or in a mode called normal, in which only part of the cross section near the cathode is bright (e.g., books [5, 6, 16]). Modes with more than one spot have been observed on cathodes of non-self sustained DC glow discharges [17–19] and of DC glow microdischarges [20–24]. One should note that usually the bright areas in the discharge volume are called "filaments" in works related to the glow discharge, and this term is used also in [20–23]. However, lateral photographs [19, 22] show that the maximum brightness is observed in the near-cathode region (i.e., in a region between the cathode and the positive column). For this reason, the term "spots" will be used in this dissertation to designate the bright areas.

Patterns with several spots were also observed on anodes of DC glow discharge; e.g. [25–29].

Alternating periodic-chaotic sequences were observed in [30] on a DC glow discharge.

Observations of different modes of current transfer from high-pressure arc plasmas to thermionic cathodes were reported many years ago for arcs with both low currents [31] and with currents of several hundred amperes [32]. These observations were also reported in more recent works, e.g., [33–38]. In these works, a variety of modes is observed, being often called diffuse and spot (or constricted) modes.

Patterns with several spots were observed in cathodes of vacuum arcs; e.g., [39–41].

Diffuse, constricted and multiple spots modes may occur on anodes of high-pressure arc discharges [42, 43].

A variety of different patterns was observed in DC planar discharges in which an electrode is made of a semiconductor material (e.g., [4, 44–47]) and in dielectric barrier discharges (DBD's) (e.g., [48–60]).

Structures were also observed on cathodes of a glow discharge generated by pulses [61].

Single and multiple spots in a DC planar glow discharge were observed in [62]. The authors [63] brought to attention the fact that parameter pd, where p is the gas pressure and d is the distance between the electrodes, takes values that correspond to the left-hand side (lhs) of the Paschen curve under conditions of experiments [62]; the so-called obstructed discharge. This is of considerable interest for the following reason. It is general understanding that instabilities occur and self-organization arises in nonlinear bi-stable dissipative systems. In particular, in the case of gas discharges it is believed that instabilities occur and self-organization arises in discharges with an N-shaped current density-voltage characteristic (CDVC). (The latter means that the CDVC, $U(j)$, consists of two rising sections, which are supposedly stable, separated by a decreasing section, which is supposedly unstable.) The CDVC of a DC glow discharge is monotonically increasing if the pd takes values that correspond to the lhs of the Paschen curve and is N-shaped if pd takes values that corresponding to the right-hand side (rhs) of the Paschen curve; e.g., [6]. (Note that the derivation [6] has been put in question in [64], but these doubts were subsequently clarified [65].) Self-organization observed in [62] in an obstructed planar glow discharge seems to contradict the above-described understanding.

Experiments [63] confirmed the patterns detected in [62], when observed on the same time scale. However, the patterns show a more complex intrinsic dynamics when observed on a shorter time scale: the appearance of spots is accompanied by peaks of currents. Each cycle includes a phase of rapid change with duration of approximately 1 μs and a phase of slower variation with duration of tens of microseconds. There is no more than one spot burning at any given moment. A conclusion was drawn that the mechanism of self-organization in this case has to do with gas heating, not only with the electronic avalanche mechanism described by the Paschen curve. Then, the results [62] are not in contradiction with the above understanding, but are rather beyond its scope.

It is interesting to note that spot patterns have been observed on the rising section of the current-voltage characteristic (CVC), $U(I)$, of non-self sustained DC glow discharges [19].

It has been known for many years that spots can occur on electrodes of corona discharge [66]. In [67], macroscopic structures of other types were observed on corona cathodes of a spiral shape in an electrostatic precipitator: a part of the cathode was dark with light spots, the other part was bright with dark longitudinal stripes.

1.2.2 Theory

Modelling of different modes

Many authors have tried to explain the existence of different modes of current transfer as a manifestation of different physical mechanisms. For example, the authors of [20, 22, 23] believe that the basic mechanisms of glow discharge are insufficient to describe the modes with multiple spots and that additional mechanisms are needed, such an increasing dependence of the coefficient of secondary emission on the reduced electric field or the heating of the gas. An alternative point of view is that multiple modes of current transfer to the electrodes of gas discharges do not necessarily involve different physical mechanisms but rather represent a self-organization phenomenon. Therefore, an adequate theoretical description of multiple modes is a mathematical problem of finding non-unique solutions: an appropriate theoretical model that describes current transfer to electrodes of gas discharges in some cases must allow the existence of different solutions for the same conditions, with different solutions describing different modes of current transfer. It should be noted that according to this point of view, different modes can involve, or not, different physical mechanisms, but mechanisms that characterize each mode arise as a result of the treatment performed and not by an *a priori* imposition.

Authors who adopt this latter point of view use two approaches to theoretical description of the different modes. One approach, which can be called phenomenological, is based on similarities between patterns observed on electrodes of gas discharge and patterns that appear in nonlinear dissipative systems in other fields such as biology, chemistry, and optics. In the framework of this approach, it is assumed that the distribution of parameters along the electrode surface is governed by a reaction-diffusion equation (a model equation that describes variation of the concentration of a substance distributed in space under the effect of two processes: chemical reactions in which the substance is produced and/or consumed, and propagation of the substance over the space available) or by a system of two or three coupled reaction-diffusion equations, e.g., [28, 68–70]. In some special cases, equations of reaction-diffusion type can be derived by means of application of asymptotic techniques to basic equations that govern the discharge under study, such as the conservation equations of ions and electrons and the Poisson equation; [71–73]. In most cases, however, reaction-diffusion equations for the distribution of parameters along the surface of the electrode are just postulated on the basis of the similarities mentioned above.

The other approach used for theoretical description of multiple modes of current transfer to electrodes of gas discharges is based on a direct numerical solution of the basic equations describing a particular discharge. There are works concerned with a two-dimensional numerical simulation of the normal mode on glow cathodes (e.g., [74, 75]) and of the simplest axially symmetrical patterns (a single spot, a central spot surrounded by a ring spot) on glow anodes (e.g., [76]). The transition from a Townsend discharge to a normal glow

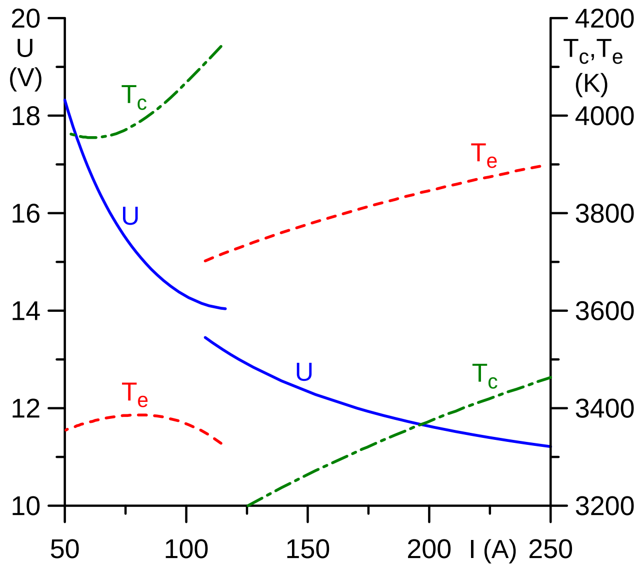

Figure 1.1: CVC of the near-cathode region of the arc discharge and temperatures at the center and the edge of the front surface of the cathode. Simulation by means of the Internet tool [90] with the use of the built-in initial approximation. Ar plasma, $p = 1$ bar, W cathode of 2 mm radius and 10 mm height.

discharge was investigated numerically in [74, 77, 78]. Temporal and spatiotemporal patterns in a thin glow-discharge layer sandwiched with a semiconductor layer between planar electrodes were studied in [79, 80] by non-stationary one- and two-dimensional numerical simulations, respectively. Self-organized patterns in DBD's were calculated by means of a direct two- and three-dimensional numerical simulation of the discharge; [59, 60, 81] and [51], respectively. Stationary modes with different patterns of spots on cathodes of high-pressure arc discharges were described by solving the numerical equation of heat conduction in the cathode [82–89].

The pattern of stationary modes of current transfer to high-pressure arc cathodes is rather complex: a large number of modes with different patterns of spots may exist for the same discharge current [89]. At present, this pattern is in general well understood. However, there are important aspects that remain unclear. One of these aspects is as follows. Figure 1.1 shows the CVC of the near-cathode region and temperatures T_c and T_e at the center and, respectively, edge of the front surface of a cylindrical arc cathode, calculated by means of the free Internet tool for modelling axially symmetric modes of current transfer to cathodes of high-pressure arc discharges [90]. The code starts from a 1D initial approximation, describing the diffuse mode on a cathode with an insulated lateral surface, and then gradually eliminates the insulation until a solution for a fully active lateral surface has been found. Under the conditions considered, this approach works nicely at the near-cathode voltages U below approximately 13.46 V. The obtained CVC is falling and $T_c < T_e$; typical features of the diffuse mode of operation of an arc cathode. There is no convergence at U between 13.46 V and 14.04 V. The convergence re-appears at $U \gtrsim 14.04$ V.

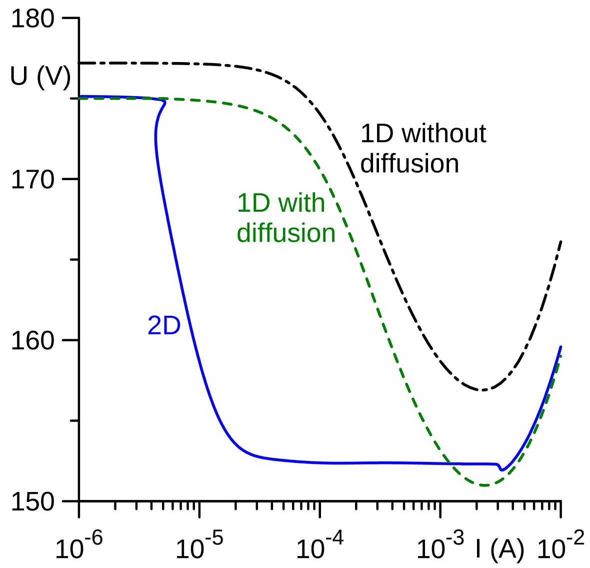

Figure 1.2: CVC's of the glow discharge. Xe plasma, $p = 30\,\mathrm{Torr}$, the discharge radius 1.5 mm and height 0.5 mm.

The CVC remains falling, however $T_c > T_e$: it looks like a mode with a spot at the center of the front surface of the cathode. Questions arise why simulations which start from the diffuse mode on a cathode with the insulating lateral surface are unable to arrive at the diffuse mode on a cathode with the active lateral surface and what significance has the value $U = 13.46\,\mathrm{V}$ at which the troubles start.

There is an important aspect which remains unclear also in results of numerical simulation of the normal mode on glow cathodes. Figure 1.2 shows CVC's of a DC glow discharge calculated in the framework of a simple drift-diffusion model under different approximations: in one dimension (1D) without account of diffusion of the ions and the electrons; in 1D with account of (axial) diffusion; in two dimensions (2D) under the approximation of axial symmetry with account of diffusion both in the axial direction and to the (absorbing) wall.

The 1D solutions with and without diffusion are rather close to each other and represent in essence the classic solution of von Engel and Steenbeck (e.g., [6]). The physical meaning of this solution is well known: it describes the Townsend discharge at very low currents, the abnormal discharge at relatively high currents, and a mode associated with the falling section of the CVC at intermediate currents, which is unstable and is not realized. The 2D solution is close to the 1D solution with account of diffusion at low and high currents, however at intermediate currents it describes the subnormal and normal modes rather than the mode associated with the falling section of the CVC. Note that the ratio of the electron current to the wall of the discharge tube to the discharge current, evaluated with the use of the 2D solution, is of the order of 10^{-3} or lower at all discharge currents. In other words, diffusion of the charged particles to the wall is a weak effect and a question arises why this weak effect originates such a large difference.

Normal modes as coexistence of phases

From the point of view of the theory of self-organization, the normal glow discharge is an example of phase coexistence: a region that collects electric current (hot phase) coexists with a region where almost no electric current flows (cold phase). From this point of view, the fact that the CVC of the normal discharge is more or less horizontal, represents an analog of the pressure-volume diagram during phase transitions. A necessary condition for the appearance of phase coexistence on electrodes of gas discharges is that the cross section of the electrode be large enough to accommodate more than one phase. That is, the width of the electrodes should be much bigger than the characteristic length scale in the normal direction. The latter scale is represented by the thickness of the layer near the cathode in the case of the glow discharge and by the height of the cathode in the case of the plasma-cathode interaction in the arc discharge.

A basis of the mathematical theory of the normal regime of a glow discharge was developed in [71]. However, the particular form of the Maxwell construction for glow discharges has not been deduced. In [91], the particular form of the Maxwell construction was deduced for cathodes of arc discharges and the normal voltage was determined.

The treatment [91] represents an interesting example where an accurate Maxwell construction can be explicitly derived for a multidimensional problem. On the other hand, the normal regime would occur on arc cathodes provided the spot radius were much larger than the height of the cathode. In reality, however, the spot radius is usually smaller than the height of the cathode, meaning that spots on arc cathodes are not normal in reality. In vacuum arcs, the spot radius is typically much smaller than the radius of the cathode and the spots can be considered as isolated. In this case one can again speak of phase coexistence, with the difference that these phases are not 1D. In [92], the particular form of the Maxwell construction for these spots was derived and the radius of the spot determined.

Self-organization vs. imposed non-uniformities

As discussed in section 1.1, not all structures observed on electrodes of gas discharges originate in self-organization. As another example, one can indicate the work [93] where an attempt was made to explain in terms of self-organization the appearance of bright and dark stripes on the cathodes of a corona discharge that was observed in [67]. It was found that there are no bifurcation points on the 1D stationary solution in the theory of a negative corona. The conclusion was that the appearance of a pattern in this case is due to geometry of the discharge. This example clearly shows that the appearance of patterns on the surface of electrodes may be due, in addition to self-organization, to the specific geometry of the discharge or, eventually, to variation of physical properties of the surface that collects electric current.

The interplay of self-organization and non-uniformities of geometrical or physical properties of the electrodes has not been studied. For example, three modes of current transfer were observed in experiment [36]: the diffuse mode, the spot mode, and a new mode called by the authors the super spot mode. The cathodes were manufactured as rods with a flat tip. After operation in the spot mode, the edge of the front surface became rounded due to local melting. After some hours of operation in the spot mode, structures of the dimension of about $20 - 200\,\mu$m appeared, which were interpreted as attachment locations for the super spot mode. An important question is to what extent is this spot a result of self-organization or of geometric effects. This question remains unanswered.

Steady-state modes and their stability

This work is concerned with the case where all existing modes of current transfer to the electrodes are stationary, non-DC discharges and DC discharges with non-stationary patterns being set aside. In this case, a theory must have the capability of predicting all the modes that are possible under the particular conditions of the discharge and indicating which of these modes are stable. In mathematical terms, the task is to find multiple stationary solutions of a strongly nonlinear multidimensional boundary-value problem that describes a particular discharge, and to investigate stability of each of these solutions.

Obviously, this task cannot be solved without advanced numerical modelling. (It should be noted that in order to find all the solutions allowed by the system, one should not use the method of relaxation in time, in which stationary solutions are found as a result of evolution of the system with time and which is widely used in gas discharge modelling. The reason is that this approach only allows calculation of stationary solutions which are stable with the particular external circuit.) On the other hand, this task can hardly be solved by means of numerical modelling alone: qualitative information about characteristics and range of existence of each of the solutions is needed in order to ensure the convergence of iterations to a desired solution. (In particular, one should know in advance whether the desired solution does exist under specific discharge conditions, a question that is difficult to answer purely through numerical simulation. In fact, if iterations diverge or converge to another solution, one can hardly know whether this is a numerical problem or whether the solution sought simply does not exist under the specified conditions.) This information was obtained using the ideas and methods of the theory of self-organization in nonlinear dissipative systems described in section 1.1. The bifurcation theory was used in [84, 91] and [94, 95] in order to locate points of junction of the one-dimensional mode with multidimensional steady-state modes of current transfer to arc and glow cathodes, respectively. In [96], bifurcation points were found where 3D steady-state modes of current transfer to arc cathodes join the axially symmetric modes.

Investigation of stability of stationary states is very common in many areas of physics.

However, studies on stability of gas discharges in low-temperature plasma physics are not common and usually refer to the volume of the discharge (e.g., the books [6, 97]; one can mention [73, 98–101] as further examples). The study of stability is particularly important in cases where several stationary modes are possible for the same conditions, since it will determine which of the modes will be realized.

This is the case, in particular, of current transfer from high-pressure arc plasmas to thermionic cathodes, where a "zoo" of different steady-state modes was found [89]. However, this information is insufficient: one needs to know which of these modes are stable and under what conditions. Results of investigation of stability of the diffuse mode on a cathode of a cylindrical shape with an isolated lateral surface were given without derivation in [84]. Stability of other modes was hypothesized in [84] on the basis of general trends of self-organization in nonlinear dissipative systems. The authors [88] used arguments based on Steenbeck's principle of minimum voltage for discharges with fixed current in order to find out stability of different branches of the spot mode. However, it was shown [89] that general trends of self-organization in nonlinear dissipative systems predict stability of different branches of the spot mode contrary to Steenbeck's principle. On the other hand, experimental information is insufficient to judge which branch of the spot mode occurs in the experiment. In addition, it has been shown [102–104] that there are serious problems with Steenbeck's principle in gas discharges and that this principle should not be used. Therefore, a consistent theory of stability of different modes of current transfer of high-pressure arc plasma to thermionic cathodes is necessary.

Equally unexplored is stability of stationary modes of current transfer in glow discharges. In part, this is explained by the fact that most researchers working in the field compute steady-state solutions by means of simulating temporal evolution of the discharge with the use of a non-stationary code: one could think that temporal evolution cannot lead to an unstable steady state and therefore all stationary solutions obtained by means of a non-stationary code are stable. However, the latter is only true with respect to perturbations having the same symmetry to which the code is adjusted. For example, an axially symmetric (2D) steady-state solution calculated by means of a non-stationary 2D code is stable against 2D perturbations but is not necessarily stable against 3D perturbations, which are frequently the most dangerous ones.

1.3 This dissertation: objectives, the method, organization

One of the aims of this dissertation is to numerically investigate stability of different modes of steady-state current transfer to cathodes of high-pressure DC arc and glow discharges in the framework of the linear stability theory. In particular, main features of stability of DC arc and glow discharges will be found and compared with intuitive concepts developed in the literature and with the experiment.

Another aim is to analyze bifurcations of steady-state modes encountered in numerical modelling of current transfer to cathodes of high-pressure DC arc and glow discharges. This study helps to understand results on stability, provides guidelines for numerical calculation of different steady-state modes, and explains dramatic changes of patterns of steady-state modes encountered in the numerical modelling which remained obscure (see figures 1.1 and 1.2 and their discussion in section 1.2.2).

A third objective is to investigate the interplay of self-organization and effects of non-uniformities of geometrical or physical properties of the electrodes, considering as an example changes of pattern of steady-state modes of current transfer to thermionic cathodes induced by variations of control parameters. The treatment will heavily rely on results of the previous task, since changes of patterns occur through bifurcations.

This work is focused on treating different steady-state modes of current transfer to cathodes of DC arc and glow discharges as self-organization phenomena. Self-organization in very different systems is governed by the same rules. One should expect therefore that patterns of different modes on cathodes of DC arc and glow discharges follow the same trends, although the physical mechanisms involved in each type of discharge are different. One of the objectives of this work is to identify similarities and differences between the two patterns and explain them.

This work represents a part of a larger project on investigation of multiple modes of steady-state current transfer to cathodes of DC arc and glow discharges and their stability ongoing at Universidade da Madeira. In the framework of this project, calculations of multiple modes of steady-state current transfer to cathodes of high-pressure arc discharges have been performed by Dr. Mário Cunha, calculations of multiple modes of steady-state current transfer to cathodes of glow discharges have been performed by Pedro Almeida, and investigation of stability and analysis of bifurcations in both cases have been performed by the author of this thesis. Obviously, results on stability and bifurcations cannot be presented without connection to the steady-state modes to which these results refer. Therefore relevant information on these modes has to be included in this thesis, however we stress once again that what is studied are not the steady-state modes as such but rather their stability and bifurcations.

The numerical investigation of stability of steady-state current transfer in this work is performed with the use of commercial finite element software COMSOL Multiphysics both in the case of arc and glow cathodes. This software includes, in addition to powerful steady-state solvers, also an eigenvalue solver, which makes it fit for the task. Note that its application is not straightforward, however the difficulties can be overcome in a number of ways, which are described in detail.

The main body of the thesis consist of four chapters. Chapter 2 is dedicated to study of stability of different modes of steady-state current transfer to cathodes of high-pressure arc discharges. The eigenvalue problem describing stability is formulated. Two approaches to its numerical solution by means of software COMSOL Multiphysics are discussed. Calculation results are compared with trends observed in the experiment. Related to this chapter is appendix A, where an analytical study of stability of a model problem is given. Material of this chapter is published in [105].

Stability of different modes of steady-state current transfer in glow discharges is studied in chapter 3. The eigenvalue problem for the perturbations is formulated and an efficient approach to its numerical solution by means of COMSOL Multiphysics devised. Calculation results for conditions of microdischarges in xenon are given. Results confirm intuitive concepts developed in the literature, conform to the experiment, and provide suggestions for further experimental and theoretical work. Material of this chapter has been submitted for publication.

Chapter 4 is dedicated to identification and analysis of bifurcations encountered in numerical modelling of steady-state current transfer to cathodes of DC glow and arc discharges. All basic types of steady-state bifurcations (fold, transcritical, pitchfork) have been identified and analyzed. Explanations to many results obtained in numerical modelling are given. Related to this chapter is appendix B, where a brief summary is given of relevant information from the bifurcation theory. Material of this chapter is published in [106].

Changes of patterns of steady-state modes of current transfer to cathodes of arc discharge of complex shapes are studied in chapter 5. Variations of the pattern of current transfer for different geometries and different temperatures of the cathode base are described and analyzed. It is shown that these changes occur through perturbed transcritical bifurcations. A comparison with experimental data is given. Material of this chapter is published in [107, 108].

Conclusions of the work are summarized and considerations on future research given in chapter 6.

Chapter 2

Stability of current transfer to cathodes of arc discharges

Spectra of perturbations of steady-state current transfer to cathodes of high-pressure argon arcs are computed in the framework of the model of nonlinear surface heating. The following pattern of stability has been established for a current-controlled arc on a cylindrical cathode on the basis of the numerical results: the diffuse (fundamental) mode is stable beyond the first bifurcation point and unstable at lower currents; steady-state modes with more than one spot are unstable; the axially symmetric mode with a spot at the center of the front surface of the cathode is unstable; the 3D steady-state mode with a spot at the edge is unstable between the bifurcation point and the turning point and stable beyond the turning point; the transition between the latter mode and the fundamental mode is non-stationary and accompanied by hysteresis. Theoretical results are in agreement with trends observed in the experiment.

2.1 Introduction

Interaction of high-pressure arc plasmas with thermionic cathodes is a challenging issue of high scientific interest and technological importance. In spite of many decades of research, a self-consistent theory and modelling methods have started to emerge only recently; see [96, 109–117] and also references cited in section 1.2.2. Still, some important questions are far from being answered. Stability of different modes of steady-state current transfer from high-pressure arc plasmas to thermionic cathodes is one of such questions.

In addition to being highly important for science and applications of arc discharges, understanding of trends of stability of DC current transfer to high-pressure arc cathodes is also of a more general interest due to its contribution to understanding stability of different modes under other conditions of interest for gas discharge physics as already discussed in section 1.3.

An analytical theory of stability of steady-state current transfer from high-pressure arc plasmas to thermionic cathodes has been developed in [118]. A number of results of general character have been obtained and a pattern of stability has been established of the diffuse mode and of three-dimensional, or 3D, spot modes that branch off from the diffuse mode on axially symmetric cathodes. (In the case of a cylindrical cathode, these are modes with spots at the edge of the front surface of the cathode.) The present work is concerned with a numerical investigation of stability, with the aim to supplement qualitative results [118] with quantitative data and to investigate important questions outside the scope of the treatment [118], in particular: stability of the axially symmetric mode with a spot at the center of the front surface of a cylindrical cathode; stability of 3D modes with spots both at the center and at the edge; bifurcations of other kinds than those treated in [118] and their effect on stability. Besides, the present treatment does not rely on the specific assumption on transfer functions made in [118]. One can hope that a combination of such numerical results with the analytical results will elucidate a complete pattern of stability of all steady-state modes.

Another goal of the present dissertation is to obtain quantitative data on spectrum of perturbations under conditions of experimental interest. Apart from being of interest by itself, such data will allow one to independently verify conclusions drawn for these conditions in [118]. Note that the necessity of such verification stems from a contradiction between the conclusions [118] and the pattern of stability of the diffuse and first spot modes that has been proposed in the preceding work [88] and is seemingly supported by the experiment.

The outline of the chapter is as follows. A mathematical model is introduced in section 2.2. Relevant aspects of numerical solution of the eigenvalue problem for perturbations with the use of software COMSOL Multiphysics are discussed in section 2.3. Numerical data on spectra of perturbations of various steady-state modes on a cylindrical cathode are given and analyzed in section 2.4. Results of the chapter are summarized and compared with trends observed in the experiment in section 2.5. In appendix A, an exact analytical solution is given of the problem of stability of the diffuse mode on a cylindrical cathode with an insulating lateral surface, which provides data for validation of the numerical code and reference points for analysis of numerical results.

2.2 Model

2.2.1 Physical basis of the model of nonlinear surface heating

Processes governing current transfer from high-pressure arc plasmas to thermionic cathodes are many and of different nature and occur on strongly different time scales; e.g., review [119] and references therein. Processes governing distributions of the ions, electrons, and the electric field in the near-cathode plasma are the fastest. The relevant time scale is represented by the time of motion of the ions across the near-cathode layer where the energy flux to the cathode is generated. (This layer includes the space-charge sheath and the ionization layer; [119] and references therein.) This time is comparable to the ionization time and, if estimated with the use of characteristic parameters of near-cathode region of the atmospheric-pressure argon arc taken from [120], is of the order of $1\,\mu$s or lower.

Formation of diffuse and spot modes of current transfer, as well as switching between the modes, is governed by the process of conduction of heat in the body of the cathode. Since the temperature distribution inside the cathode is characterized by a variety of length scales, this process comprises several phases characterized by different time scales. The smallest and, respectively, biggest time scales are represented by the times of diffusion of heat over distances of the order of the radius of the cathode spot and, respectively, of the order of the cathode height. Taking $10^{-5}\,\mathrm{m}^2/\,\mathrm{s}$ as a typical value of thermal diffusivity of electrode materials and assuming $50\,\mu$m as a lower estimate of the radius of the cathode spot and 10 mm as a characteristic height of the cathode, one finds that the time scales of heat conduction in the cathode body are comprised between 0.25 ms and 10 s.

It happens frequently that cathodes of high-pressure arc discharges change their shape due to melting and/or evaporation of the cathode material with subsequent return of a part of the evaporated metal to the cathode in the form of either neutral atoms (condensation of the vapor) or ions (the so-called recycling). These changes usually take from several minutes to several hours (e.g., sections 3.2 and 3.4 of [36] and section 2 of [37]).

Thus, heat propagates in the cathode body much slower than processes in the near-cathode plasma occur, but much faster than the cathode changes its shape. It follows that, while treating the formation of diffuse and spot modes of current transfer and switching between the modes, one may assume that variations of distributions of the ions, electrons, and the electric field in the near-cathode plasma, caused by variations of the potential and the distribution of temperature of the cathode surface, occur instantaneously, while variations of the cathode shape are frozen. A theoretical approach to description of diffuse and spot modes on thermionic cathodes which is developed along these lines and makes use of the thinness of a near-cathode plasma layer where the energy flux to the cathode surface is generated is frequently termed the model of nonlinear surface heating.

The model of nonlinear surface heating does not account for the effect of convective motion of the gas over the plasma-cathode interaction, on the grounds that the normal component of the gas velocity can hardly be sufficiently high in the above-mentioned very thin near-cathode plasma layer where the energy flux to the cathode surface is generated. It is difficult to estimate the effect of convective motion of the gas theoretically, since the distribution of the gas velocity in the immediate vicinity of the cathode surface is unknown. The experiment seems to indicate that a convective motion of the gas is necessary for the formation of the so-called blue-core mode [121], which can occur on cathodes of low-current free-burning arcs, especially on those made of thoriated tungsten. However, there are no indications that a convective motion plays a role in the formation of the diffuse or spot modes. (It is interesting to note that the situation is different as far as modes of anode attachment are concerned: it is believed [122] that in the diffuse mode the power is supplied to the anode by a plasma flow from the bulk.) Therefore, the model of nonlinear surface heating represents an adequate tool for investigation of the diffuse and spot modes.

The model of nonlinear surface heating was proposed long ago [123], however its power has been universally appreciated only during the last decade; see review [119]. By now, this model has been widely recognized as an adequate tool of simulation of interaction of high-pressure arc plasmas with thermionic cathodes [85–89, 91, 96, 109, 110, 112–115], including under non-steady state conditions [112, 113, 115]. The most important feature of this model is the existence, under the same conditions, of multiple solutions describing the diffuse mode of current transfer and different spot modes. This feature has made a self-consistent modelling of the diffuse and spot modes on cathodes of a given shape a matter of routine. One can mention, as an example, a free Internet tool [90] for simulation of diffuse and axially symmetric spot modes on cylindrical cathodes in a wide range of arc currents, plasma compositions, and cathode materials and dimensions, which serves also as a tutorial on finding multiple solutions describing diffuse and spot modes.

In this work, the model of nonlinear surface heating is used for investigation of stability of current transfer to cathodes of high-pressure arc discharges, similarly to how it was done in [118]. In the framework of this model, the (in)stability of steady-state modes of current transfer to thermionic cathodes of high-pressure arc discharges originates in a competition of a positive feedback which is present on the growing section of the dependence of the density of energy flux from the plasma on the local temperature of the cathode surface, and of thermal conduction, which represents a stabilizing mechanism.

2.2.2 System of equations and boundary conditions

The model of nonlinear surface heating is mathematically formulated as follows. Let us consider a cathode (see figure 2.1) that is made of a substance of thermal conductivity κ, density ρ and specific heat c_p which are known function of the temperature T: $\kappa = \kappa(T)$, $\rho = \rho(T)$, $c_p = c_p(T)$. Joule heat production inside the cathode is neglected; see e.g., estimates in [119]. The temperature distribution inside the cathode is governed by the non-stationary equation of heat conduction:

$$\rho(T)\, c_p(T)\, \frac{\partial T}{\partial t} = \nabla \cdot [\kappa(T)\, \nabla T], \tag{2.1}$$

where t is time.

The base of the cathode, Γ_c, is maintained at a fixed temperature T_c by external cooling. The rest of the cathode surface, Γ_h, is in contact with the plasma or the cold gas and

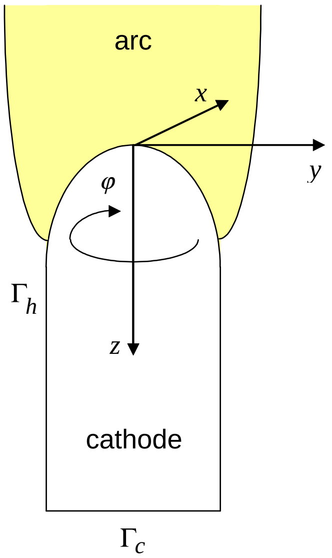

Figure 2.1: Geometry of the problem.

exchanges energy with it. The corresponding boundary conditions read

$$\Gamma_c: \quad T = T_c, \qquad \Gamma_h: \quad \kappa \frac{\partial T}{\partial n} = q\,(T, U)\,. \tag{2.2}$$

Here n is the direction locally orthogonal to the cathode surface and oriented outward, $q = q\,(T, U)$ is the density of the energy flux to the cathode surface from the arc plasma or the cold gas, and U is the voltage drop across the near-cathode layer (which is constant along the current-collecting surface).

The total electric current I to the cathode surface (the arc current) may be evaluated in terms of a distribution of the cathode surface temperature and of the value of U by means of the formula

$$I = \int_{\Gamma_h} j\,(T, U)\; dS, \tag{2.3}$$

where $j = j\,(T, U)$ is the density of electric current to the current-collecting part of the cathode surface. A relation between U and I is given by an equation modelling the external circuit

$$U + I\Omega = \varepsilon, \tag{2.4}$$

where Ω represents the external resistance (ballast) and the resistance of the arc column, and ε is the electromotive force.

Densities of the energy flux and of the electric current to the cathode surface, q and j, are governed by equations describing the near-cathode layer in a high-pressure plasma that are summarized in [124] and in the present analysis are treated as known functions of the local surface temperature and of the voltage drop across the near-cathode layer: $q = q\,(T, U)$ and $j = j(T, U)$. (A module realizing calculation of these functions is written in Fortran and the produced data are transferred to COMSOL Multiphysics in the form of tables.) It should be stressed that what is specified is not a distribution of q and j over the cathode surface, but rather a dependence of q and j on the local surface temperature and voltage drop across the near-cathode layer, being this temperature and voltage unknown *a priori*. After the problem (2.1)-(2.4) has been solved, one will have complete information on a temperature distribution in the cathode and also on a distribution of the energy flux and electric current over the cathode surface. It should be emphasized that functions q and j depend on time only through T and U. This approach is justified by the fact that processes in the near-cathode plasma layer are much faster than propagation of temperature perturbations in the cathode body as discussed in the latter section.

As far as steady-state solutions are concerned, there is in principle no need to introduce the equation of external circuit (2.4): a natural control parameter is the voltage drop in the near-cathode plasma layer U. However, this parameter is clearly inappropriate in the vicinity of extreme points of the CVC of the mode being computed. Another possible control parameter is the discharge current I. (It should be stressed that stationary solvers of COMSOL Multiphysics allow specifying I as a control parameter without invoking equation of external circuit.) However it is inappropriate in the vicinity of turning points. On the other hand, one can calculate all steady-state modes by switch between U and I.

The situation turns different as far as bifurcations and stability are concerned: for example, an extreme point of the CVC of a given mode, while being a regular point if the control parameter is I, becomes a turning point if the control parameter is U; conditions of stability of current- and voltage-controlled DC gas discharges are not the same as will be shown below. Therefore, equation (2.4) with Ω and ε considered as fixed parameters must be used in investigation of stability.

2.2.3 Eigenvalue problem for perturbations

To investigate stability of a steady state, a solution to the problem (2.1)-(2.4) is sought as sum of a steady-state solution and a small perturbation with the exponential time dependence

$$T(\mathbf{r},t) = T_0(\mathbf{r}) + e^{\lambda t} T_1(\mathbf{r}) + \dots, \tag{2.5}$$

$$U(t) = U_0 + e^{\lambda t} U_1 + \dots, \tag{2.6}$$

$$I(t) = I_0 + e^{\lambda t} I_1 + \dots. \tag{2.7}$$

Here $\mathbf{r}$ is the space vector, index 0 is attributed to the steady-state solution, index 1 is attributed to the amplitude (time-independent factor) of perturbations, and λ is the growth increment of the perturbations. Substituting these expansions into equations (2.1)-

(2.4), linearizing and equating linear terms, one obtains

$$\rho(T_0)\, c_p\,(T_0)\ \lambda T_1 = \nabla \cdot \left[\frac{d\kappa}{dT}\,(T_0)\ T_1 \nabla T_0 + \kappa\,(T_0)\ \nabla T_1 \right], \tag{2.8}$$

$$\Gamma_c: \quad T_1 = 0, \qquad \Gamma_h: \quad T_1 \frac{d\kappa}{dT}(T_0)\frac{\partial T_0}{\partial n} + \kappa \frac{\partial T_1}{\partial n} = \frac{\partial q}{\partial T}\,(T_0, U_0)\ T_1 + \frac{\partial q}{\partial U}\,(T_0, U_0)\ U_1, \tag{2.9}$$

$$I_1 = \int_{\Gamma_h} \frac{\partial j}{\partial T}\,(T_0, U_0)\ T_1\, dS + U_1 \int_{\Gamma_h} \frac{\partial j}{\partial U}\,(T_0, U_0)\ dS, \tag{2.10}$$

$$U_1 + I_1 \Omega = 0. \tag{2.11}$$

Here $\rho\,(T_0)$, $\frac{\partial q}{\partial T}\,(T_0, U_0)$ *etc* are evaluated in terms of the temperature distribution of the steady state, T_0, and of the near-cathode voltage drop U_0 corresponding to the steady state.

Equation (2.8) with the boundary conditions (2.9), and equations (2.10) and (2.11) represent a closed linear eigenvalue problem for the function T_1 and the eigenvalue λ. By means of solving this problem, one will determine a set of eigenvalues λ (spectrum) for every stationary state of interest. If real parts of all eigenvalues of a state are non-positive, this state is stable; if at least one eigenvalue has a positive real part, the state is unstable.

Gas discharges are operated usually with a high external resistance. In this case equation (2.11) is reduced to $I_1 = 0$; a current-controlled arc. The most of analysis of this work has been performed for this case. In order to gain physical insight, some spectra in this chapter have been calculated for the case where the external resistance is absent and equation (2.11) is reduced to $U_1 = 0$; a near-cathode region with a fixed voltage.

High-pressure arc cathodes in most cases possess axial symmetry; in particular, modeling results presented in this chapter refer to cathodes in the form of a right circular cylinder. It is convenient at this point to discuss some properties of the eigenvalue problem (2.8)-(2.11) originating in this symmetry. Steady-state temperature distributions on axially symmetric cathodes may be axially symmetric or 3D. Axially symmetric distributions correspond to the diffuse mode and to modes with axially symmetric spot systems, 3D distributions correspond to modes with 3D spot systems. Let us restrict the consideration to steady-state temperature distributions that are either axially symmetric or 3D with planar symmetry. Let us introduce Cartesian coordinates (x, y, z) with the origin at the center of the front surface of the cathode and the z-axis directed along the axis inside the cathode, in such a way that the steady-state temperature distribution be even with respect to y.

Every 3D perturbation of an even steady-state distribution may be treated without losing generality as either even or odd. Indeed, let us consider an eigenfunction $T_1\,(x, y, z)$ associated with an eigenvalue λ. The eigenvalue problem (2.8)-(2.11) is invariant with respect to the symmetry $(x, y, z) \to (x, -y, z)$, therefore $T_1\,(x, -y, z)$ also is an eigenfunction associated with the same λ. The functions $T_1^{(1)} = T_1\,(x, y, z) + T_1\,(x, -y, z)$ and

$T_1^{(2)} = T_1(x,y,z) - T_1(x,-y,z)$ also represent eigenfunctions associated with the same λ. If this eigenvalue λ is non-degenerate, then the functions $T_1^{(1)}$ and $T_1^{(2)}$ must be linearly dependent. If both these functions were non-zero, then $T_1^{(1)}$ would be even with respect to y while $T_1^{(2)}$ would be odd, therefore these functions would be linearly independent. Hence, $T_1^{(1)}$ or $T_1^{(2)}$ must be zero, which means that $T_1(x,y,z)$ must be either odd or, respectively, even with respect to y. Thus, eigenfunctions associated with non-degenerate eigenvalues are necessarily even or odd. Eigenfunctions associated with degenerate eigenvalues are not necessarily even or odd, however each of them can be chosen as even or odd.

The 3D eigenvalue problem (2.8)-(2.11) for an axially symmetric steady-state temperature distribution, if written in cylindrical coordinates (r,ϕ,z), allows separation of variables and admits solutions of the form

$$T_1(r,\phi,z) = w_m(r,z)\left\{\begin{array}{c}\cos m\phi \\ \sin m\phi\end{array}\right\}. \tag{2.12}$$

Here $m = 0,1,2,\ldots$. If $m = 0$, the perturbation being considered is axially symmetric. If $m = 1,2,\ldots$, the perturbation is 3D with period in ϕ equal to $2\pi/m$. Function $w_m = w_m(r,z)$ satisfies the axially symmetric problem

$$\rho(T_0)c_p(T_0)\lambda w_m = \nabla\cdot\left[\frac{d\kappa}{dT}(T_0)w_m\nabla T_0 + \kappa(T_0)\nabla w_m\right] - \left(\frac{m}{r}\right)^2\kappa(T_0)w_m \tag{2.13}$$

$$\gamma_c: \quad w_m = 0, \qquad \gamma_h: \quad w_m\frac{d\kappa}{dT}(T_0)\frac{\partial T_0}{\partial n_1} + \kappa\frac{\partial w_m}{\partial n_1} = \frac{\partial q}{\partial T}(T_0,U_0)\,w_m + \frac{\partial q}{\partial U}(T_0,U_0)\,U_1, \tag{2.14}$$

$$I_1 = 2\pi\delta_{m0}\int_{\gamma_h}\frac{\partial j}{\partial T}(T_0,U_0)\,w_m r\,dl + 2\pi U_1\int_{\gamma_h}\frac{\partial j}{\partial U}(T_0,U_0)r\,dl \tag{2.15}$$

and, additionally, equation (2.11). Here γ_h and γ_c are generatrices of the revolution surfaces Γ_h and Γ_c, respectively [lines in the plane (r,z) which produce, on being rotated around the z-axis, surfaces Γ_h and Γ_c]; n_1 is a direction in the plane (r,z) locally orthogonal to γ_h and directed outside the cathode. It should be stressed that although equation (2.13) is written in terms of ∇, there are no azimuthal derivatives in this equation since T_0 and w_m are functions only of r and z. Kronecker delta δ_{m0} on the rhs of the first term of equation (2.15) originates in integration over ϕ.

In the case $m \neq 0$, the first term on the rhs of equation (2.15) vanishes and one gets from this equation and equation (2.11): $I_1 = 0$ and $U_1 = 0$. This means that perturbations which are harmonic in ϕ are not affected by the external resistance. In this case, second term in the rhs on the second boundary condition of equation (2.14) vanishes, too.

The linear homogeneous problem (2.13)-(2.15) and equation (2.11) represent a linear eigenvalue problem, λ being the eigenvalue. By means of solving this problem for a given

m, one will determine a set of eigenvalues λ (spectrum) associated with this m. By means of repeating this procedure for each m and joining the obtained spectra, one will find the whole spectrum of the stationary state being treated.

2.3 Numerical solution of the eigenvalue problem with COMSOL Multiphysics

Commercial software COMSOL Multiphysics provides, in addition to stationary and non-stationary solvers, also a powerful eigenvalue solver, which may be used for investigation of stability of stationary solutions. However, its application is not straightforward, as is seen from the following.

A straightforward approach is to introduce the non-stationary problem of section 2.2.2 in the 3D geometry in the heat transfer application mode (or in the PDE mode) and then invoke for each value of the discharge current first the stationary solver, thus finding a solution describing the steady state being considered, and then the eigenvalue solver, thus finding spectrum of perturbations of this steady state. The weak point of this approach originates in the fact that COMSOL Multiphysics does not allow imposing different boundary conditions on a steady-state solution and on its perturbations. This difficulty may be explained as follows.

While numerically calculating a steady-state 3D distribution on an axially symmetric cathode, one must impose an additional condition in order to specify azimuthal position of the 3D spot system, and thus to ensure convergence of iterations. (In mathematical terms: each 3D steady-state solution on an axially symmetric cathode represents an element of a continuous set of 3D solutions that are identical to the accuracy of a rotation about the cathode axis; hence, one must impose an additional condition in order to single out one solution from this set, otherwise the problem will be ill-stated and iterations will not converge.) The simplest and most natural way to do so is the one used in [88, 89, 113, 115], which consists in restricting the calculation domain to half of the cathode, $y \geq 0$, and imposing the symmetry condition at the plane $y = 0$: $\partial T_0/\partial y = 0$. Of course, this approach allows one not only to fix the azimuthal position of a 3D spot system but also to save RAM and CPU time.

There is in principle no problem in restricting the calculation domain to half of the cathode also while stability of steady-state solutions is investigated. However, the use of heat transfer application (or PDE) mode of COMSOL Multiphysics with the stationary and eigenvalue solvers implies that the symmetry boundary condition is imposed also on perturbations: $\partial T_1/\partial y = 0$ at $y = 0$. In other words, the straightforward application of COMSOL Multiphysics allows one to study stability against axially symmetric perturbations and 3D perturbations that are even with respect to y, but not against 3D perturbations that are odd with respect to y. This does not pose a problem while stability of axially symmetric steady states is investigated: 3D even and odd perturbations of an axially symmetric steady state are identical to the accuracy of a rotation and are therefore associated with the same eigenvalue (which is, consequently, doubly degenerated), hence an account of 3D odd perturbations will not change conclusions on stability. The situation is different as far as stability of 3D steady states is concerned: odd and even perturbations of 3D steady states are essentially different and are therefore associated with different eigenvalues, and eigenvalues associated with odd perturbations cannot be computed.

Hence, while conclusions on instability of 3D steady states, reached with the use of COMSOL Multiphysics, can be accepted without reservations, conclusions on stability of 3D steady states should be dealt with caution: a part of the spectrum that is associated with odd eigenfunctions remains unknown, and if that part includes an eigenvalue with a positive real part, then the steady state in question is unstable rather than stable.

Another approach to investigation of stability by means of COMSOL Multiphysics consists in introducing the steady-state problem and the eigenvalue problem for perturbations separately. Of course, this approach requires more effort, because it involves a manual derivation and introduction of the perturbation problem instead of letting COMSOL to generate it. However, this approach allows one to overcome the above difficulty and a modelling of a complete spectrum became possible. The procedure is as follows. First, the steady-state problem is solved through the heat transfer application mode (or the PDE mode) and function T_0 and quantities U_0, and I_0 determined. After this, the eigenvalue problem (2.8)-(2.11) for perturbations is solved by means of the (added) PDE mode with the boundary condition $\partial T_1/\partial y = 0$ at the plane $y = 0$ for even perturbations and $T_1 = 0$ at the plane $y = 0$ for odd perturbations. Of course, the spectrum of even perturbations can be calculated also by solving the system of equations (2.1)-(2.4) through the heat transfer application mode using the stationary and eigenvalue solvers.

One of advantages of this approach is the possibility of treating cases where the stationary state and its perturbations possess different symmetries. Another advantage appears in cases where the steady state is axially symmetric: it is natural to formulate the perturbation problem in the form (2.13)-(2.15), (2.11) and solve both the stationary and eigenvalue problems in the 2D geometry. In addition to a dramatic reduction in RAM and CPU time, this results in the elimination of difficulties originating in an extreme sensitivity of results of 3D stability calculations with respect to details of the steady state in the vicinity of the axis of symmetry.

The first above-described approach was used in work [105]. The problem that this approach does not allow one to find a part of the spectrum of perturbations of 3D stationary states associated with odd eigenfunctions was realized and got round by means of qualitative considerations based on the analytical theory [118]. The second above-described approach was employed and the whole of the spectrum was computed in [125].

Results reported in this section have been obtained with the use of versions 3.3 and 3.4 of COMSOL Multiphysics.

2.4 Spectra of different modes of steady-state current transfer

Before proceeding to particular results on stability, it is worth to stress the following. For a given steady state, the COMSOL Multiphysics software allows one to compute all the eigenvalues λ in the whole complex plane. In all the simulations performed for the arc cathodes, all the spectra turned out to be real, i.e., included only real values of λ. This result confirms a conclusion on the growth increment being real drawn in [118] on the basis of an approximate analytical treatment and conforms to the well-known experimental fact that transitions between the diffuse and spots modes are monotonic, i.e., occur without oscillations of the surface temperature and luminosity.

Numerical calculations reported in this work have been performed for a tungsten cathode and an argon plasma. Data on thermal conductivity and heat capacity of tungsten have been taken from [126] and [127], respectively. The density of tungsten equals $19250\,\mathrm{kg\,m^{-3}}$ and the value of $4.55\,\mathrm{eV}$ was assumed for the work function of tungsten. Note that data used for ρ and c_p affect values of the increment of perturbations, but they do not affect the sign of the increment and, therefore, conclusions on stability. The cooling temperature T_c was set equal to $293\,\mathrm{K}$.

Results given in this section refer to a cathode in the form of a right cylinder as shown in figure 2.2. The cathode radius R is assumed equal to $2\,\mathrm{mm}$ and the cathode height h to $10\,\mathrm{mm}$; a kind of standard geometry convenient for illustrative purposes. The plasma pressure is set equal to 1 bar. Note that not all results obtained for such geometry are quantitatively correct. For example, the first 3D spot mode branches off from the diffuse mode (see the next section) at relatively high currents where the temperature of the front surface of the cathode is above the melting point of tungsten, while melting is disregarded in the present model. However, the mere fact that 3D spot modes do branch off from the diffuse mode is critical for understanding stability. Therefore, the above geometry is more suitable for demonstration of general trends than slimmer cathodes typical for HID lamps, for which branching occurs at very low currents and very high voltages and cannot be conveniently represented on graphs.

2.4.1 Modes of steady-state current transfer

CVC's of different steady-state modes of current transfer under the specified conditions are shown in figure 2.3 that has been taken from the work [89]. Note that main features of this pattern have been established theoretically [91] with the use of ideas from the theory

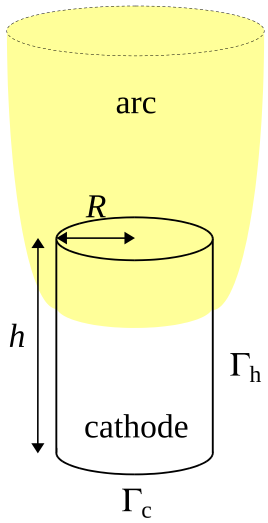

Figure 2.2: Schematic of a cylindrical cathode.

of self-organization in nonlinear dissipative systems. In order to prevent a frequently occurring doubt, it is helpful to stress that modern solvers for steady-state partial differential equations, like those implemented in the software COMSOL Multiphysics employed in [89], allow one to find stationary solutions regardless of their stability in time. Therefore, the mere fact that a steady-state solution has been computed does not mean that this solution is necessarily stable in time, and indeed most of the solutions plotted in the figure 2.3 will be shown to be unstable.

The open circles in the figure 2.3 and the following represent points of minimum of CVC's of axially symmetric modes, namely, of the diffuse mode and of the first axially symmetric spot mode. The corresponding values of the arc current will be designated $I_0 = I_{\min}$. The full circles in the figure 2.3 represent bifurcation points, i.e., points at which a 3D spot mode becomes exactly identical with an axially symmetric mode. The number ν characterizing each bifurcation point represents the number of spots at the edge of the front surface of the cathode in the 3D mode that branches off at this point. In the following, value of the arc current corresponding to a bifurcation point with a given ν will be designated I_ν. Note that the same designation is used for bifurcation points positioned on different axially symmetric modes; for example, $I_2 = 276\,\mathrm{A}$ for the diffuse mode and $I_2 = 106\,\mathrm{A}$ for the first axially symmetric spot mode.

A detailed information on different steady-state modes of current transfer represented in figure 2.3 can be found elsewhere [89]; here we note only the following. The first axially symmetric spot mode corresponds to steady states with a spot at the center of the front surface of the cathode. The 3D spot modes branching off from the diffuse mode at the bifurcation point with numbers $\nu = 1, 2, 3, 4$ correspond to steady states with one, two, three or, respectively four spots at the edge. The 3D spot mode branching off from the first axially symmetric spot mode at the bifurcation point with $\nu = 2$ corresponds to steady

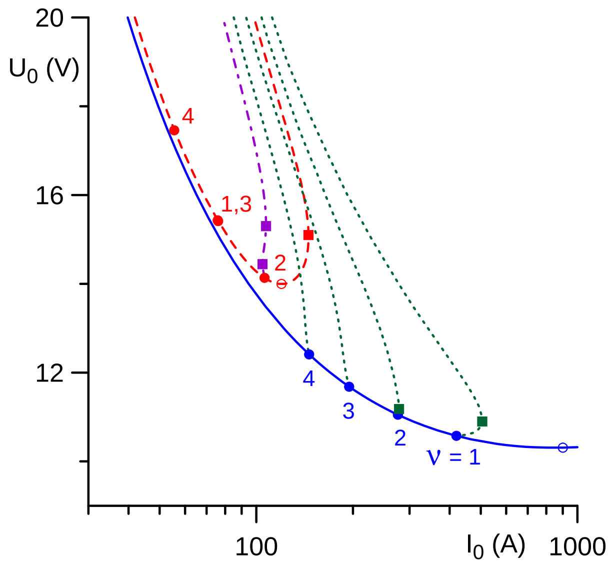

Figure 2.3: CVC's of different modes of steady-state current transfer. $R = 2\,\mathrm{mm}$, $h = 10\,\mathrm{mm}$. Solid line: diffuse (fundamental) mode. Dashed line: first axially symmetric spot mode. Dotted lines: 3D spot modes branching off from the diffuse mode. Dash-and-dotted line: 3D spot mode branching off from the first axially symmetric spot mode.

states with a spot at the center and two spots at the edge.

The first axially symmetric steady-state spot mode has two branches, a low-voltage branch and a high-voltage branch, separated by a turning point.

The 3D steady-state mode with a spot at the edge of the front surface of the cathode bifurcates from the diffuse mode into the range of higher currents, $I_0 > I_1$, then turns back and moves into the direction of lower currents. The 3D steady-state mode with two spots at the edge behaves in a similar way, although this behavior is less pronounced and is hardly visible on the graph. The 3D steady-state mode with a spot at the center and two spots at the edge bifurcates from the first axially symmetric spot mode into the range of lower currents, $I_0 < I_2$, then it turns back and starts moving into the direction of higher currents, then it turns back once again and moves into the direction of lower currents.

The above-described turning points are represented in the figure 2.3 by squares.

The above discussion is based on the (usual) concepts of diffuse and spot modes. However, a question arises: if multiple regimes have been found in a certain current range, are there any reasons to associate one (or several) of them with diffuse mode(s) and others with spot modes? This question was addressed in previous works [87, 112]. The following simple definition was proposed in [87]: a mode which exists in a wide current range, including high currents, is a diffuse mode; modes which cease to exist as current grows are spot modes. However, this definition is not quite adequate for the purposes of this work. First, it is not general enough, which is seen from the following example: in the case of glow discharge in a cylindrical tube with an absorbing wall, the mode which exists in a wide current range, including high currents, is the one shown by the solid line in figure

1.2, however this mode includes a section with a normal current spot. Second, in the case of bifurcating modes this definition may be ambiguous; for example, in the case shown in figure 2.3 the term “mode which exists in a wide current range, including high currents” may, strictly speaking, refer not only to the mode represented by the solid line, but also to a “composed” mode represented by the solid line at high currents down to the bifurcation point marked with $\nu = 1$ and by the dotted line which starts at this point.

A definition used in this work is as follows: the mode of the highest symmetry admitted by the discharge which exists at all discharge currents is termed “fundamental mode”, and the other modes are termed non-fundamental, or spot, modes. We stress once again that the fundamental mode looks diffuse in some situations but is clearly non-diffuse in others. In other words, the concept of fundamental mode does not coincide with the concept of diffuse mode, but rather represents the only meaningful generalization of the latter concept.

The importance of the concept of fundamental mode stems from the fact that this is the only mode that exists at currents high and (in the case of glow discharge) low enough. Since a steady-state discharge at these currents is observed in the experiment, it must operate in the fundamental mode, which, therefore, should be stable. With decrease or increase of current the fundamental mode may turn, or not, unstable and give way to other (non-fundamental) modes.

2.4.2 Spectrum of the fundamental (diffuse) mode on a cathode with an insulating lateral surface

If a cathode has the form of a right cylinder with a thermally and electrically insulating lateral surface, the second boundary conditions in equations (2.2), (2.9), and (2.14) are valid only at the front surface of the cathode. At the lateral surface, the boundary conditions are $\partial T_0/\partial n = \partial T_1/\partial n = 0$ and the contribution of the lateral surface to the integrals (2.3), (2.10), and (2.15), governing discharge current, is discarded. The steady-state solution describing the fundamental mode is one-dimensional (1D): $T_0 = T_0\,(z)$. If, additionally, thermal diffusivity of the cathode material, $\chi = \kappa/\rho c_p$, is constant, then the eigenvalue problem describing stability of the fundamental mode admits an analytic solution; see appendix A. Results of numerical calculations for this particular case are given and compared with the analytical results in the present section, with the aim of validating the code and providing reference points for analysis of subsequent numerical results.

Results given in this section have been calculated for the (constant) thermal conductivity equal to $100\,\mathrm{W\,m^{-1}\,K^{-1}}$ and the specific heat equal to $200\,\mathrm{J\,kg^{-1}\,K^{-1}}$; these values may be assumed as characteristic for tungsten in the range of temperatures between 1000 K and 3000 K. The pattern of CVC's of different steady-state modes of current transfer to the cathode under these conditions will be discussed in some detail below (see figure 4.2); for now, it is sufficient to say that it is similar to the one shown in figure 2.3, except that the

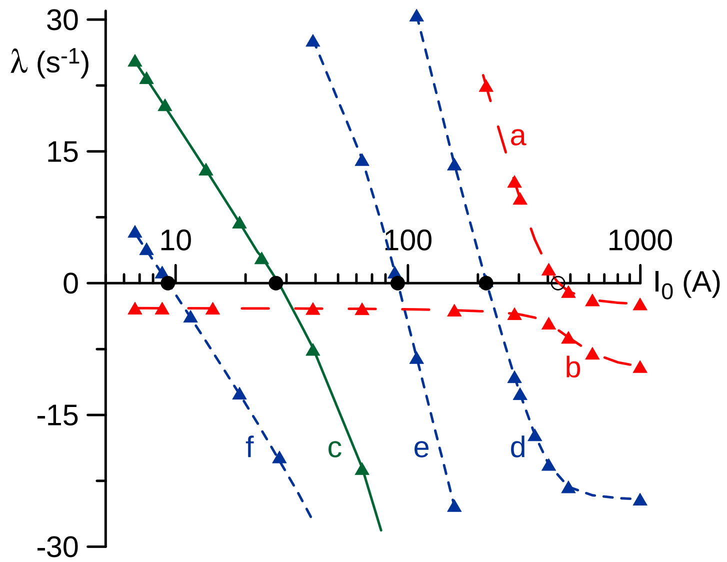

Figure 2.4: Increments of different modes of perturbations of the fundamental mode on a cathode with an insulating lateral surface. $R = 2\,\mathrm{mm}$, $h = 10\,\mathrm{mm}$, near-cathode region with a fixed voltage. Lines: analytical spectra. Triangles: numerical spectra. a, b: first and second modes of 1D perturbations. c: first mode of axially symmetric perturbations. d, e, f: first, second and third modes of 3D perturbations.

first axially symmetric spot mode on the cathode with an insulating lateral surface joins the fundamental mode [87, 91].

Figure 2.4 shows the analytical and numerical spectra of several perturbation modes for the case of a near-cathode region with a fixed voltage, $U_1 = 0$. (As usual in the linear stability theory, a value of the increment λ of each perturbation mode may be interpreted as an inverse time of development of the instability against perturbations of this mode, if $\lambda > 0$, or an inverse time of decay of perturbations of this mode, if $\lambda < 0$.) Modes chosen for representation in this figure and in similar figures below are those with the biggest values of the increment. Full circles in this and similar figures designate values of the arc current corresponding to the bifurcation points. Bifurcation points positioned on the fundamental mode are ordered: $\cdots < I_3 < I_2 < I_1 < I_{\min}$, so the right-most full circle represents I_1, the next one represents I_2 *etc.* The analytical data represented by the lines have been obtained by means of equations (A.7) and (A.20) of appendix A in accord to table A.1 of appendix A. The numerically calculated distributions of perturbations of these modes are shown in figure 2.5 for the state with $U_0 = 12\,\mathrm{V}$ on the falling section of the CVC.

One can see from figure 2.4 that the numerical data on increments of perturbations coincide with the analytical results. The numerical data on distributions of perturbations, such as those shown in figure 2.5, conform to the analytical formulas (A.8), (A.21) and (A.22) of appendix A. This agreement attests to accurate operation of the code.

All modes of perturbations have negative increments on the rising section of the CVC of the fundamental mode, i.e., in the current range $I_0 > I_{\min}$. Hence, this section is stable.

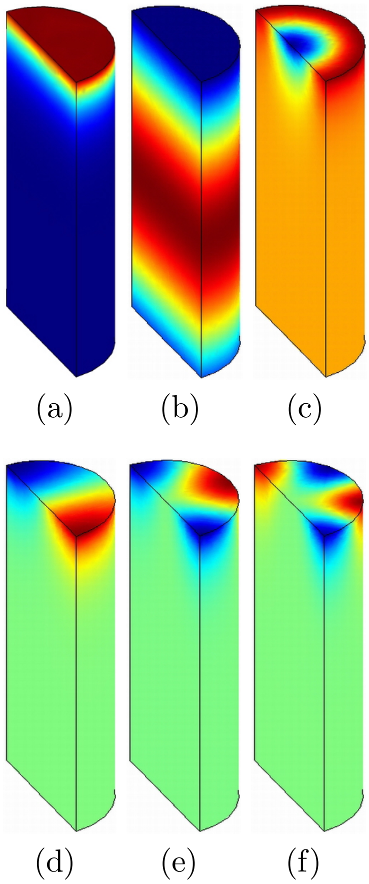

Figure 2.5: Different modes of perturbations of the state with $U_0 = 12\,\mathrm{V}$ on the falling section of the CVC of the fundamental mode. $R = 2\,\mathrm{mm}$, $h = 10\,\mathrm{mm}$, cathode with an insulating lateral surface, near-cathode region with a fixed voltage. (a), (b): first and second modes of 1D perturbations. (c): first mode of axially symmetric perturbations. (d), (e), (f): first, second and third modes of 3D perturbations.

This conclusion is consistent with the fact that there is no positive feedback on this section: the rising section of the CVC of the fundamental mode on a cathode with an insulating lateral surface is associated with a falling dependence $q(T, U)$ on T [91].

On the falling section of the CVC, i.e., in the range $I_0 < I_{\min}$, there is a mode of 1D perturbations with a positive increment. The increment of this mode is depicted by the line a in figure 2.4 and the distribution of temperature perturbations associated with this mode is shown in figure 2.5a. Taking into account an analytical solution for the spectrum given in the appendix A (see table A.1), this mode can be termed the first 1D mode. The second 1D mode (line b in figure 2.4 and figure 2.5b) and all the higher 1D modes (which are not shown on the graph) are decaying at all currents.

At $I_0 < I_1$, another mode of perturbations becomes growing. The increment of this mode is depicted by the line d in figure 2.4 and the distribution of temperature perturbations associated with this mode is shown in figure 2.5d. The perturbations of this mode are 3D and their dependence on the azimuthal angle ϕ is described by the factor $\cos\phi$; the first 3D mode.

The perturbation mode that becomes growing next, at $I_0 < I_2$ (line e in figure 2.4 and figure 2.5e), is proportional to $\cos 2\phi$; the second 3D mode. The next perturbation mode to become growing, at $I_0 < I_3$, is the first axially symmetric mode; line c in figure 2.4 and figure 2.5c. The next perturbation mode to become growing, at $I_0 < I_4$, is the third 3D mode; line f in figure 2.4 and figure 2.5f, *etc.*

Thus, states belonging to the growing section, $I_0 > I_{\min}$, of the CVC of a voltage-controlled fundamental mode on a cathode with an insulating lateral surface are stable. States belonging to the falling section of the CVC, $I_0 < I_{\min}$, are unstable against 1D perturbations. With decreasing current, one more perturbation mode, 3D or axially symmetric one, turns growing at each bifurcation point.

The above results refer to a near-cathode region with a fixed voltage, $\Omega = 0$. The analytical solution given in the appendix A as well as the numerical modelling show that axially symmetric and 3D perturbations in this case are not affected by external resistance. 1D perturbations are affected by external resistance; in particular, if the arc is powered by a current source, i.e., if Ω is large enough, then the first 1D perturbation mode becomes decaying at all currents while all the higher 1D modes remain decaying at all currents. Thus, the current-controlled fundamental mode on a cathode with an insulating lateral surface is stable in the current range $I_0 > I_1$, i.e., on the growing section of the CVC and on a segment of the falling section beyond the first bifurcation point, and turns unstable at $I_0 < I_1$.

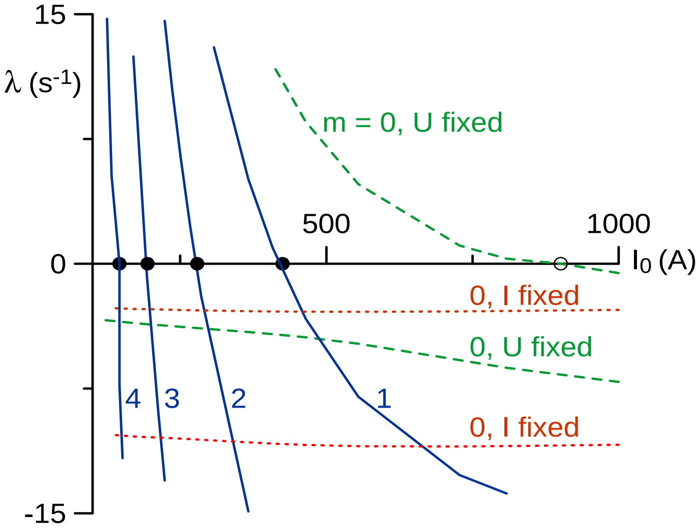

Figure 2.6: Increments of different modes of perturbations of the fundamental mode. $R = 2\,\mathrm{mm}$, $h = 10\,\mathrm{mm}$. Solid: 3D perturbations with $m = 1, 2, 3, 4$. Dashed: axially symmetric perturbations, near-cathode region with a fixed voltage. Dotted: axially symmetric perturbations, current-controlled arc.

2.4.3 Spectrum of the fundamental mode on a cathode with an active lateral surface

Modelling results presented in this and the following sections have been calculated numerically for a cathode with an active lateral surface with account of variability of κ and c_p.

Since steady-state temperature distributions associated with the fundamental mode are axially symmetric, perturbations of the fundamental mode are harmonic in ϕ, i.e., proportional to $\cos m\phi$, $m = 0, 1, 2, \ldots$. Therefore, one can associate each perturbation mode with the corresponding value of m. Perturbations with $m = 0$ are axially symmetric, those with $m \geq 1$ are 3D.

Increments of several modes of perturbations of the fundamental mode are shown in figure 2.6. Numbers on curves indicate values of m. For the case of a near-cathode region with a fixed voltage, there is a mode of axially symmetric perturbations that turns growing at $I_0 < I_{\min}$. The other mode of axially symmetric perturbations that is shown on the graph for U fixed remains decaying at all currents, as well as all the other axially symmetric perturbation modes which are not shown. At $I_0 < I_1$, a mode of 3D perturbations with $m = 1$ turns growing. Modes of 3D perturbations with $m = 2, 3, 4$ become growing at, respectively, $I_0 < I_2$, $I_0 < I_3$, $I_0 < I_4$.

Distributions of perturbations of these modes are shown in figure 2.7. The distributions of the 3D perturbations modes with $m = 1, 2, 3$, shown in figures 2.7c-2.7e, are qualitatively similar to corresponding perturbations calculated for a cathode with an insulating lateral

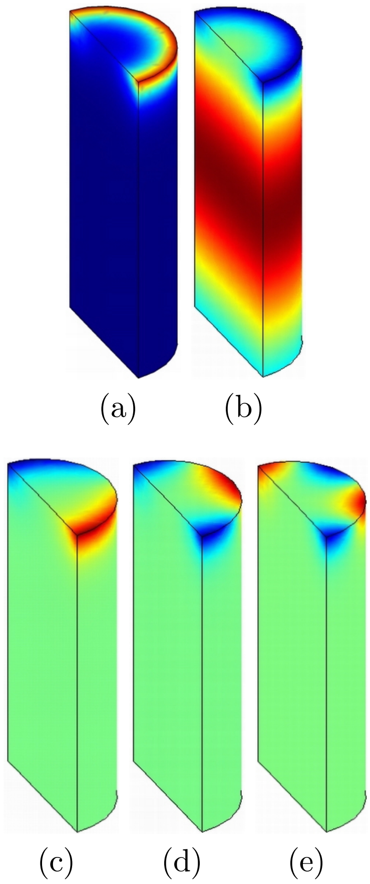

Figure 2.7: Different modes of perturbations of the state with $U_0 = 12\,\mathrm{V}$ on the falling section of the CVC of the fundamental mode. $R = 2\,\mathrm{mm}$, $h = 10\,\mathrm{mm}$. (a), (b): axially symmetric perturbations, near-cathode region with a fixed voltage. (c), (d), (e): 3D perturbations with $m = 1, 2, 3$, respectively.

surface and shown in figures 2.5d-2.5f. The axially symmetric perturbation mode with the biggest increment shown in figure 2.7a is analogous to the first 1D mode on a cathode with an insulating lateral surface shown in figure 2.5a. (Note that the non-uniformity of perturbations on the front surface of the cathode, seen in figure 2.7a and absent from figure 2.5a, is a consequence of the non-uniformity of the steady-state distribution of the temperature of the front surface in the fundamental mode on a cathode with an active lateral surface.) Similarly, the axially symmetric perturbation mode with the second biggest increment shown in figure 2.7b is analogous to the second 1D mode on a cathode with an insulating lateral surface shown in figure 2.5b.

The above results refer to a near-cathode region with a fixed voltage. 3D perturbations are not affected by external resistance, similarly to what happens on a cathode with an insulating lateral surface. On the other hand, axially symmetric perturbations are affected by external resistance, on the contrary to what happens on a cathode with an insulating lateral surface. One can say that both in the case of a cathode with an insulating lateral surface and in the case of a cathode with an active lateral surface, the presence of external resistance affects perturbations with the same symmetry that the steady-state temperature distribution.

Calculations showed that all axially symmetric perturbations of a current-controlled fundamental mode are decaying at all currents; see dotted lines in figure 2.6.

The above results show that patterns of stability of the fundamental mode on a cathode with an active lateral surface and on a cathode with an insulating lateral surface are similar, except that the steady-state solution describing the fundamental mode on a cathode with an active lateral surface is axially symmetric rather than 1D, so 1D perturbations do not exist. The above results conform to conclusions on stability of the fundamental mode reached by means of an analytical treatment [118].

2.4.4 Spectrum of the first axially symmetric spot (non-fundamental) mode

Modelling results presented in this section refer to a current-controlled arc. Note that 3D perturbations of axially symmetric spot modes are not affected by external resistance, similarly to 3D perturbations of the fundamental mode. In all the cases studied in this and the following sections, the finite element mesh was locally refined in the vicinity of each spot in order to obtain a good accuracy.

Perturbations of axially symmetric steady-state spot modes are harmonic in ϕ and may be characterized by the corresponding value of m, similarly to perturbations of the fundamental mode. Increments of several modes of perturbations of the first axially symmetric steady-state spot mode are shown in figure 2.8. Here and in the following figures, squares represent values of arc current corresponding to turning points of the steady-state mode being under stability investigation. The solid and dashed lines in figure 2.8 represent values of the increments on high- and, respectively, low-voltage branches of the first axially symmetric steady-state spot mode.

There is a mode of axially symmetric perturbations, $m = 0$, that is growing on the low-voltage branch of the first axially symmetric steady-state spot mode. On passing through the turning point, switching between growing and decaying occurs and this mode is decaying on the high-voltage branch. The other modes of axially symmetric perturbations (one of these modes is shown on the graph) are decaying in the whole range of existence of the steady-state mode in question. The steady-state mode in question is neutrally stable against four modes of 3D perturbations (see figure 2.8) with $m = 1, 2, 3, 4$ at the corresponding bifurcation point $I_0 = I_m$. These modes of perturbations are growing on the low-voltage branch at lower currents, $I_0 < I_m$, and are decaying on the low-voltage branch at higher currents and on the high-voltage branch. (I_ν in the present section designates the value of arc current corresponding to the bifurcation point with a given ν positioned on the first

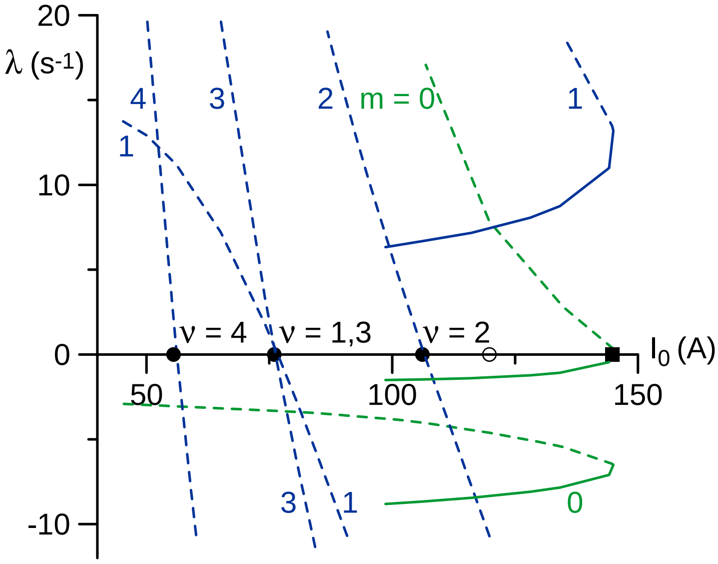

Figure 2.8: Increments of different modes of perturbations of the first axially symmetric spot mode. $R = 2\,\text{mm}$, $h = 10\,\text{mm}$, current-controlled arc.

axially symmetric spot mode; note that $\cdots < I_4 < I_3 = I_1 < I_2 < I_{\min}$.) The other mode of 3D perturbations with $m = 1$ shown on figure 2.8 is growing in the whole range of existence of the steady-state mode in question.

The change of stability against axially symmetric perturbations occurring at the turning point is similar to the change of stability of a voltage-controlled fundamental mode against perturbations of the same symmetry that occurs at the point of minimum of the CVC of the fundamental mode, as discussed in the two preceding sections. [As long as a near-cathode region with a fixed voltage is concerned, every extremum of the CVC $U_0\,(I_0)$ represents a limit of the range of existence of a solution, i.e., a turning point.] Modes of 3D perturbations that switches between growing and decaying do so at the corresponding bifurcation points: a ν-th mode is growing at $I_0 < I_\nu$ and decaying at $I_0 > I_\nu$. Again, this is similar to what happens in the case of the fundamental mode.

As far as changes of stability are concerned, the above results conform to conclusions of the analytical treatment [118]. On the other hand, there is a mode of 3D perturbations with $m = 1$ that is always growing, and this result is outside the scope of [118]. Because of this mode, the first axially symmetric steady-state spot mode is unstable in the whole range of its existence.

2.4.5 Spectra of 3D spot modes

All perturbations of 3D steady-state spot modes are 3D and their azimuthal dependence is not harmonic, therefore the classification of perturbations in terms of m employed in the preceding two sections is not applicable. However, one can extend this classification using the fact that the "initial" state of each 3D steady-state spot mode, $I_0 = I_\nu$, being a bifurcation point, is axially symmetric, hence perturbations of this state are harmonic. In the following, a mode of perturbations of a 3D steady-state spot mode that is proportional to $\cos m\phi$ at $I_0 = I_\nu$ will be associated with this value of m. Note that a perturbation mode with a given m, while having the azimuthal period of $2\pi/m$ at the initial state, does not necessarily have the same period outside the initial state. In fact, in all the cases treated in this chapter periods of different even and odd perturbation modes of different 3D steady-state spot modes coincided with those given in table 1 of [118].

Increments of several modes of even perturbations of various 3D steady-state spot modes are shown in figures 2.9 and 2.10. Figures 2.9a to 2.9d refer to the 3D steady-state modes with, respectively, one to four spots at the edge of the front surface of the cathode. These modes are represented by the dotted lines in figure 2.3 and branch off from the fundamental mode at the bifurcation points with $\nu = 1, 2, 3, 4$, respectively. Figure 2.10 refers to the 3D steady-state mode with two spots at the edge of the front surface of the cathode and a spot at the center of the front surface, which is shown in figure 2.3 by the dash-and-dotted line. In figure 2.10, circles representing the initial state of the mode in question have been added to each line.

Steady-state temperature distributions $T_0\,(x, y, z)$ associated with two spots at the edge, or four spots at the edge, or two spots at the edge and one spot at the center are even with respect to x. According to what has been said in section 2.2.3, every perturbation of any of these steady states may be treated without losing generality as either even or odd with respect to x. (Note that every perturbation of all these states found numerically indeed turned out to be even or odd with respect to x, which is not surprising since all spectra found in these calculations were non-degenerate.) For odd perturbations, the first term on the rhs of equation (2.10) vanishes and equation (2.11) is reduced to $U_1 = 0$. Hence, odd perturbations are not affected by external resistance, but even perturbations in a general case are. Modelling results presented in this section refer to a current-controlled arc.

The 3D steady-state mode with one spot at the edge, to which data plotted in figure 2.9a refer, possesses a turning point. The dashed lines in figure 2.9a represent values of increments on that section of the steady-state spot mode that is comprised between the initial state and the turning point, solid lines represent values of increments on the section beyond the turning point. One can see that the steady-state mode in question is neutrally stable against one mode of even perturbations with $m = 1$ at the initial state and at the turning point, unstable between the initial state and the turning point, and stable beyond the turning point. Calculations of spectrum for odd perturbations (which are skipped for brevity) showed that the steady-state mode in question is neutrally stable against one mode of odd perturbations with $m = 1$. Perturbations of all the other modes are decaying in the whole range of existence of the steady-state spot mode in question.

The 3D steady-state mode with two spots at the edge, to which data plotted in figure 2.9b refer, possesses one turning point as well, so the dashed and solid lines in figure 2.9b

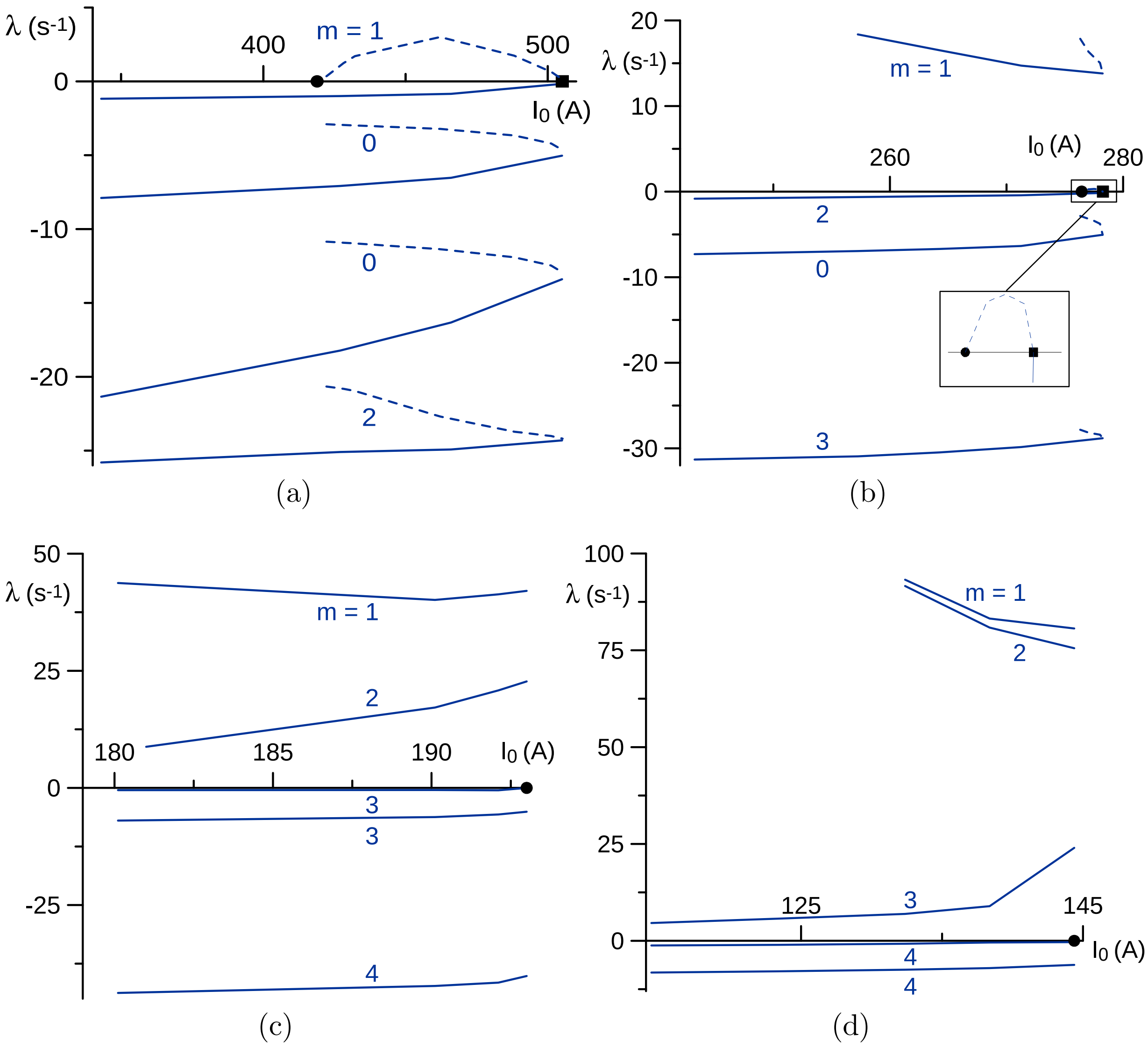

Figure 2.9: Increments of different modes of even perturbations of the steady-state modes with one, two, three, and four spots at the edge of the front surface of the cathode. $R = 2\,\mathrm{mm}$, $h = 10\,\mathrm{mm}$, current-controlled arc. (a), (b), (c), (d): steady-state modes with, respectively, one, two, three, and four spots.

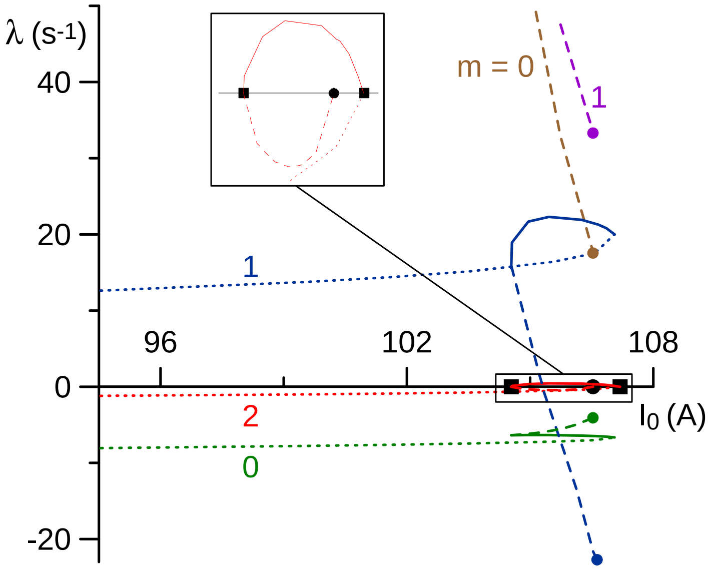

Figure 2.10: Increments of different modes of even perturbations of the steady-state mode with two spots at the edge of the front surface of the cathode and a spot at the center. $R = 2\,\mathrm{mm}$, $h = 10\,\mathrm{mm}$, current-controlled arc.

has the same meaning as on figure 2.9a. This steady-state mode is neutrally stable against one mode of even perturbations with $m = 2$ at the initial state and at the turning point; unstable between the initial state and the turning point; stable beyond the turning point. There is a mode of even perturbations with $m = 1$ that is growing in the whole range of existence of the steady-state spot mode in question. Calculations of spectrum of odd perturbations showed that the steady-state mode in question is neutrally stable against one mode of odd perturbations with $m = 2$ and unstable against one mode of odd perturbations with period $m = 1$. Perturbations of all the other modes are decaying in the whole range of existence.

The 3D steady-state modes with three or four spots at the edge possess no turning points. Under conditions of figure 2.9c (or, respectively, of figure 2.9d), the steady-state mode is neutrally stable against a mode of even perturbations with $m = 3$ (or, respectively, with $m = 4$) at the initial state and stable outside this state. Absolute values of the increments of these modes are very small, so the corresponding lines are barely distinguishable from the axis of abscissas. There are two (or, respectively, three) modes of even perturbations, one of these modes with $m = 1$ and the other one with $m = 2$ (or, respectively, with $m = 1$, $m = 2$, and $m = 3$), that are growing in the whole range of existence of the steady-state spot mode in question. The steady-state mode is neutrally stable against one mode of odd perturbations with $m = 3$ ($m = 4$) and is unstable against two modes of odd perturbations with $m = 1$ (two modes of odd perturbations with $m = 1$ and one mode of odd perturbations with $m = 2$). Perturbations of all the other modes are decaying in the whole range of existence.

In all the cases above-described, odd perturbations do not change sign of their increment along 3D steady-state spot modes and do not add new windows of instability compared to even perturbations. This result is in accordance with theory [118]. Therefore, spectra of odd perturbations will not be computed in the following.

The mode with two spots at the edge of the front surface of the cathode and a spot at the center, to which data plotted in figure 2.10 refer, possesses two turning points, at arc currents $I_0 = 104.5\,\mathrm{A}$ and $I_0 = 107.2\,\mathrm{A}$. (Let us indicate, for completeness, the value of arc current corresponding to the initial state: $I_2 = 106.5\,\mathrm{A}$.) The dashed, solid and dotted lines in figure 2.10 represent values of increments on the section of the steady-state spot mode that is, respectively, comprised between the initial state and the first turning point; between the first and second turning points; beyond the second turning point. There is a mode of even perturbations with $m = 2$ that is decaying between the initial state and the first turning point; growing between the first and second turning points; decaying beyond the second turning point. There is a mode of even perturbations with $m = 1$ that is decaying at the initial state and in its vicinity and then turns growing. Switching between decay and growth occurs at $I_0 = 105.3\,\mathrm{A}$, i.e., outside the turning points. There are a perturbation mode with $m = 0$ and a mode of even perturbations with $m = 1$ that are growing in the whole range of existence of the steady-state spot mode in question. Perturbations of all the other modes of perturbations are decaying in the whole range of existence.

Since points of neutral stability against perturbations of any kind represent points of bifurcation of steady-state solutions, one should conclude that another 3D steady-state mode branches off from the mode with two spots at the edge of the front surface of the cathode and a spot at the center at $I_0 = 105.3\,\mathrm{A}$. While the steady-state temperature distribution corresponding to the mode with two spots at the edge and a spot at the center is symmetric with respect to the plane $x = 0$, the perturbation against which the steady-state mode is neutrally stable at $I_0 = 105.3\,\mathrm{A}$ possesses no such symmetry. In other words, while the steady-state temperature distribution $T_0\,(x, y, z)$ is even with respect to x, the perturbation $T_1\,(x, y, z)$ is odd with respect to x; the latter can be clearly seen from figure 2.11. It follows that the bifurcation of 3D steady-state modes that occurs at $I_0 = 105.3\,\mathrm{A}$ represents breaking of planar symmetry. Alternatively, one can term this bifurcation the period doubling: while the steady-state temperature distribution corresponding to the mode with two spots at the edge and a spot at the center is periodic over ϕ with the period of π, the steady-state mode that branches from it at $I_0 = 105.3\,\mathrm{A}$ has the period of 2π.

The above results may be summarized as follows. Let us consider a cathode of a current-controlled arc and a 3D steady-state mode with ν spots at the edge of the front surface of the cathode, and maybe also with a spot at the center. The mode branches off from an axially symmetric mode at the bifurcation point $I_0 = I_\nu$ or, in other terms, begins at the initial state $I_0 = I_\nu$. The steady-state mode is neutrally stable against one mode of even perturbations (and proportional to $\cos \nu\phi$) at the initial state. In the vicinity of the initial state, this mode of perturbations is decaying or, respectively, growing depending on

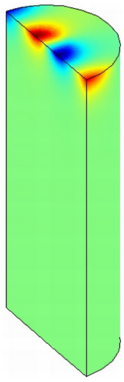

Figure 2.11: Neutrally stable perturbations with $m = 1$ of the steady-state mode with two spots at the edge of the front surface and a spot at the center. $R = 2\,\mathrm{mm}$, $h = 10\,\mathrm{mm}$, $I_0 = 105.3\,\mathrm{A}$.

whether the bifurcation at $I_0 = I_\nu$ is supercritical (the cases plotted in figures 2.9c, 2.9d and 2.10) or subcritical (figures 2.9a and 2.9b). (A bifurcation may be termed supercritical or subcritical if the bifurcating solution branches off into the range of control parameters in which the original solution is unstable or, respectively, stable against the perturbation which possesses the zero increment at the bifurcation point; see appendix B. Taking into account the above results on stability of the fundamental mode and of the first axially symmetric spot mode, one should conclude that in the case of a current-controlled arc, a bifurcation occurring at $I_0 = I_\nu$ is supercritical or subcritical if a 3D spot mode branches off from the axially symmetric mode into the range $I_0 < I_\nu$ or, respectively, $I_0 > I_\nu$.)

If the steady-state spot mode in question possesses no turning points, which is possible only if the bifurcation is supercritical, then this perturbation mode remains decaying in the whole range of existence of the steady-state spot mode in question; figures 2.9c and 2.9d. If the steady-state spot mode in question does possess turning point(s), then this perturbation mode switches between growing and decaying at each turning point; figures 2.9a, 2.9b and 2.10.

Even perturbation modes that are growing at the initial state remain growing in the whole range of existence of the steady-state spot mode in question. Perturbation modes that are decaying at the initial state in most cases remain decaying in the whole range of existence; figures 2.9a to 2.9d and one of the lines with $m = 0$ in figure 2.10. An exception is a perturbation mode with $m = 1$ under conditions of figure 2.10, that is decaying at the initial state but then turns growing.

In many aspects, the above results conform to conclusions of the analytical treatment [118]. In particular, stability in the vicinity of a bifurcation point $I_0 = I_\nu$ against the perturbation which possesses the zero increment at the bifurcation point is related to the bifurcation being sub- or supercritical; an even perturbation mode exists that switches between growing and decaying at each turning point of the steady-state spot mode. On the other hand, a number of the above results are outside the scope of the treatment [118], such as the conclusion that if a 3D steady-state spot mode possesses turning point(s), then the even perturbation mode that switches between growing and decaying at each of these points is the same for all points and the same that possesses the zero increment at the bifurcation point; or conclusion on instability of the mode with a spot at the center of the front surface of the cathode and two spots at the edge; or demonstration of the possibility of breaking of planar symmetry, the consequences being the possibility of branching of 3D steady-state spot modes and the possibility of changes of stability of 3D modes outside turning points.

The above results allow one to suggest plausible assumptions on stability of 3D modes with a spot at the center of the front surface of the cathode and one, three, four, five *etc* spots at the edge, which branch off from the first axially symmetric spot mode at the bifurcation points with $\nu = 1, 3, 4, 5, \ldots$, respectively. There are three growing modes of even perturbations at the bifurcation point with $\nu = 1$ (which coincides with the bifurcation point with $\nu = 3$), that are proportional to $\cos m\phi$ with $m = 0, 1, 2$. One can expect therefore that there are at least three growing even perturbation modes at every steady state belonging to modes with a spot at the center and one or three spots at the edge. Similarly, there are five even perturbation modes, two of them with $m = 1$ and the others with $m = 0$, $m = 2$, and $m = 3$, that are growing at the bifurcation point with $\nu = 4$ and one can expect that there are at least five growing even perturbation modes at every steady state with a spot at the center and four spots at the edge. Continuing this reasoning, one comes to the conclusion that all modes with a spot at the center of the front surface of the cathode and one or more spots at the edge are unstable in the whole range of their existence.

The above results indicate that the only 3D states that may be stable are those with one spot at the edge.

2.5 Concluding discussion

The eigenvalue problem describing stability against small perturbations of steady-state current transfer from high-pressure arc plasmas to thermionic cathodes has been solved numerically. Spectra of perturbations of different modes of steady-state current transfer to cylindrical cathodes have been computed: of the fundamental mode, of the first axially symmetric spot mode, and of several 3D spot modes branching off from the fundamental mode and from the first axially symmetric spot mode. Calculations have been performed both for the case of a current-controlled arc and for the case of a near-cathode region with fixed voltage. As far as 3D steady-state spot modes are concerned, the calculations are done for perturbations that are both even and odd with respect to the plane of symmetry of the 3D spot mode in question.

In all the simulations performed, all the spectra turned out to be real, i.e., included only real values of the increment of perturbations. Note that an analytical proof of this feature [118] employs a specific assumption concerning transfer functions; this assumption leads to the eigenvalue problem being Hermitian (self-adjoint), and consequently its spectrum being real. It is therefore important that this conclusion has been verified in the present work by means of a direct numerical solution to the exact (non-Hermitian) eigenvalue problem. This result conforms to the well-known experimental fact that transitions between the fundamental and spots modes are monotonic, i.e., occur without oscillations of cathode temperature and luminosity.

The present results conform to conclusions of the analytical treatment [118] and supplement them with quantitative data on spectra of different steady-state modes of current transfer. On the other hand, a number of the results are outside the scope of [118], such as the conclusion on instability of the mode with a spot at the center of the front surface of the cathode; the conclusion on instability of modes with a spot at the center and one or more spots at the edge; the possibility of branching of 3D steady-state spot modes and of changes of stability of 3D modes outside turning points, both being caused by breaking of planar symmetry.

The numerical results allow one to establish a complete pattern of stability of all steady-state modes. In the case of a current-controlled arc on a cylindrical cathode, this pattern is as follows.

The fundamental mode is stable beyond the first bifurcation point, i.e., at $I_0 > I_1$, and unstable at lower currents, $I_0 < I_1$. This conclusion conforms to the well-known experimental fact that the fundamental mode is favoured by increasing the arc current and not by decreasing it.

All steady-state modes with spots positioned at the edge of the front surface of the cathode are unstable (in the whole range of existence of each mode) if the number of spots is two or more. All steady-state modes with a spot at the center of the front surface of the cathode and one or more spots at the edge are unstable. It is legitimate to assume that any steady-state mode with multiple spots (i.e., with more than one spot) is unstable. This conclusion conforms to the fact that multiple steady-state spots are not normally observed on thermionic cathodes of high-pressure arc discharges.

The axially symmetric mode with a spot at the center of the front surface of a cylindrical cathode is unstable as well. This conclusion conforms to the experimental fact that a stationary arc spot attached to the center of the (flat) front surface of a cylindrical cathode is not observed in the experiment (e.g., [88]) unless stabilized by an axial gas flow.

The only steady-state spot mode that may be stable at least in a part of its existence region is the 3D mode with a spot at the edge. In the following, this mode will be referred to as the first spot mode. Under typical conditions, this mode branches off from the fundamental mode through a subcritical bifurcation and is unstable between the bifurcation point and the turning point and stable beyond the turning point. The transition between

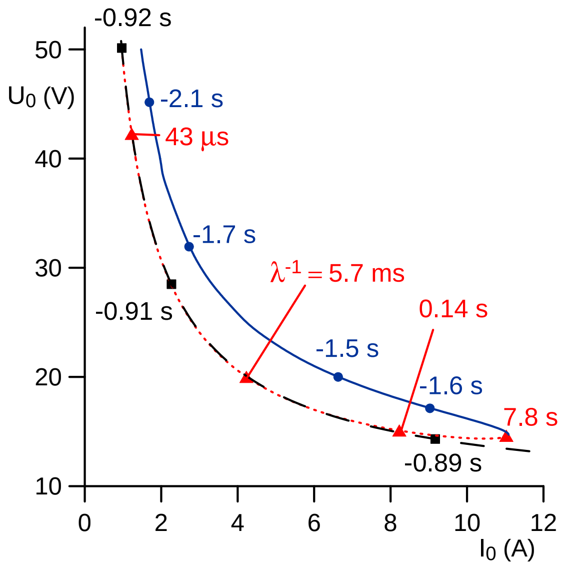

Figure 2.12: CVC's of different modes. Solid, dotted: high-voltage and, respectively, low-voltage branches of the first 3D spot mode. Dashed: fundamental mode. $R = 0.75\,\mathrm{mm}$, $h = 20\,\mathrm{mm}$, the argon pressure 2.6 bar. Numbers: time of development or decay of perturbations.

this mode and the fundamental mode cannot be realized in a quasi-stationary way and is accompanied by hysteresis; also a conclusion that conforms to the experiment.

In figure 2.12, stability of modes of DC current transfer to an arc cathode under conditions of the experiment [88] is illustrated. CVC's of the fundamental mode and of the first spot mode plotted in this figure have been taken from [89]. Bifurcation points positioned on the fundamental mode are located at U_0 well in excess of 100 V and are not seen on the graph. For several steady states which are depicted by points, values of inverse of the biggest increment of perturbations of this state are indicated. Each of these values may be interpreted as time of disruption of the corresponding steady state, if it is positive, or time of decay of perturbations of this state, if it is negative.

One can see that $\lambda < 0$ on the fundamental mode and on the high-voltage branch of the first spot mode and $\lambda > 0$ on the low-voltage branch. This conforms to the above-described general pattern: all the steady states of the fundamental mode shown on the graph are positioned beyond the first bifurcation point, i.e. at $I_0 > I_1$, and should therefore be stable; the low-voltage branch, being a part of the section of the first spot mode which is comprised between the bifurcation point and the turning point, should be unstable; the high-voltage branch, representing the section beyond the turning point, must be stable.

Since the turning point of the first spot mode is neutrally stable, $\lambda = 0$, values of the inverse increment in the vicinity of this point are quite high. Apart from this vicinity, $|\lambda|^{-1}$ on the low-voltage branch is much smaller than on the fundamental mode and the high-voltage branch: while perturbations of the fundamental mode and of the high-voltage branch of the first spot mode decay during intervals of the order of seconds, the instability of the low-voltage branch develops on significantly smaller time scales.

Data on stability shown in figure 2.12 confirm the hypothesis on irreproducibility of transitions between the fundamental and spot modes under typical conditions of experiments with HID lamps, suggested in [89]. Indeed, experiments are usually performed in a limited current and voltage range, say $I_0 \leq 10\,\mathrm{A}$ and $U_0 \leq 100\,\mathrm{V}$, so two stable modes exist in the whole range of conditions of such experiments, the fundamental mode and the high-voltage branch of the first spot mode. Hence, no reproducible transition between fundamental and spot modes can occur in a typical quasi-stationary experiment: if the experiment is well-controlled and quasi-stationary, a mode which has occurred immediately after the ignition of the discharge will be maintained during the whole experimental run; if a mode change is systematically observed in such experiment under quasi-stationary conditions, it means that the experiment is not well-controlled. This conclusion conforms to the general trend that the transition between the fundamental and spot modes is difficult to reproduce in the experiment.

A mode change can be provoked by finite perturbations, e.g., by fast enough variations of experimental parameters. However, if the arc is operated at currents higher than I_t the arc current corresponding to the turning point of the first spot mode, then only the fundamental mode is possible. In other words, operating a discharge at $I_0 > I_t$ will ensure the fundamental mode. Under conditions of figure 2.12, $I_t = 11.1\,\mathrm{A}$ and the above inequality is not easy to satisfy, however the situation is different for thin cathodes since I_t rapidly decreases with a decrease of the cathode radius.

In [88], the low- and high-voltage branches were calculated in the framework of the model of nonlinear surface heating and the assumption was forwarded that it is the low-voltage branch that occurs in the experiment. Under this assumption, the conclusion was drawn that a quantitative agreement between simulations and experimental results can be shown for the spot mode. However, both the numerical results of the present chapter and the analytical theory [118] indicate that the low-voltage branch is unstable, and this conclusion has been obtained in the framework of the model of nonlinear surface heating, which has been used also in the modelling [88]. Hence, the comparison between simulations and experimental results on the spot mode performed in [88] must be revisited.

Chapter 3

Stability of current transfer to cathodes of glow discharges

Stability of different axially symmetric steady-state modes of current transfer of DC glow discharges against small perturbations is investigated in the framework of the linear stability theory with the use of software COMSOL Multiphysics. Conditions of current-controlled microdischarges in xenon are treated as an example. Variations of the increments of perturbations with discharge current are investigated for the 1D glow discharge and different modes of axially symmetric glow discharge. Both real and complex increments have been detected, meaning that perturbations can vary with time both monotonically and with oscillations. In general, results given by the linear stability theory confirm intuitive concepts developed in the literature and conform to the experiment. On the other hand, the theory provides suggestions for further experimental and theoretical work.

3.1 Introduction

In the previous chapter, stability has been studied of multiple steady-state solutions which have been obtained during the last decade in the theory of current transfer to cathodes of high-pressure arc discharges and describe different modes of current transfer to arc cathodes. In this chapter, stability is studied of multiple steady-state solutions which were computed recently for DC glow discharges [128–130] and describe both the normal mode and modes with multiple spots similar to those observed in DC glow microdischarges [20–24].

The patterns of multiple steady-state solutions found for DC glow discharges and for cathodes of high-pressure arc discharges are similar in many aspects. In particular, in both cases the current is distributed over the cathode surface more or less uniformly at higher currents; at lower currents, there are also modes where the current is localized in one or more regions (spots) occupying only a fraction of the cathode surface. This is indeed what is observed in the experiment; note that the fundamental (diffuse) and spot modes on arc cathodes represent analogues of the abnormal and normal modes on glow cathodes.

However, the patterns of modes observed in the experiment on glow and arc cathodes have also important differences: modes with more than one spot observed on glow cathodes have not been observed on arc cathodes; axially symmetric current distributions on planar circular cathodes have not been observed on arc cathodes but seem to have been observed in glow discharges (the upper-left image in figure 3 of [20] and the middle image in figure 4 of [24]). Given that the patterns of multiple steady-state solutions are similar, one should presume that these differences are caused by substantially different properties of stability of these solutions. There is another experimental fact supporting this hypothesis: while transition from the abnormal or fundamental mode at higher currents to a mode with spot(s) occurs on both glow and arc cathodes without temporal oscillations of the luminosity of the cathode surface or of the discharge voltage, the glow discharge operated in the subnormal regime can develop voltage oscillations which have not been observed as far as the near-cathode region of high-pressure arcs is concerned.

Main features of stability of current transfer to arc cathodes have been investigated in the framework of the linear stability theory in chapter 2. On the other hand, no investigations of stability of DC glows have apparently been reported. It should be stressed that, as discussed at the end of section 1.2.2, even if a steady-state solution has been found by means of simulating temporal evolution of the discharge with the use of a non-stationary code, there is no guarantee that this solutions is stable against perturbations of other symmetries.

This chapter is concerned with a numerical investigation of stability of axially symmetric steady-state modes of DC glow discharges, the principal objective being to find out main features of stability of DC glows as predicted by an accurate stability theory and compare them with intuitive concepts developed in the literature and with the experiment. Calculation results are given for conditions of current-controlled microdischarges in xenon.

As in the investigation of stability of current transfer to arc cathodes, described in the previous chapter, the linear stability theory is used. In addition to indicating whether a given stationary state is stable or unstable, this theory allows one to find states where one of perturbation modes is stationary. Such states represent points of bifurcation of steady-state modes and play an important role in computing and understanding different modes of operation of DC glow discharges; [128] and chapter 4, respectively. An eigenvalue boundary-value problem for a system of linear partial differential equations, which appears in the framework of the linear stability theory of DC glows, does not admit an analytic solution except in very special cases. On the other hand, this problem may be treated numerically. A convenient tool is software COMSOL Multiphysics, that was successfully employed in chapter 2.

The outline of the chapter is as follows. A mathematical model is introduced in section

3.2. Relevant aspects of numerical solution with the use of COMSOL Multiphysics are discussed in section 3.3. Numerical results on stability of 1D and different 2D steady-state modes are given and analyzed in sections 3.4 and 3.5. Concluding remarks are given in section 3.6.

3.2 Model

Self-organization in cold glow and glow-like gas discharges is usually simulated by means of a basic glow discharge model assuming a single ion species, direct electron impact ionization, secondary electron emission by ion impact, and electron kinetic and transport coefficients being functions of the local electric field. It was shown that this model can reproduce many features observed experimentally and allows one to understand pattern formation in DBD's [51, 59, 60, 81], pattern formation on DC glow cathodes [128, 130], formation and propagation of filamentary plasma arrays in high-power microwave breakdown at atmospheric pressure [131, 132]. In [129], self-organized patterns on DC glow cathodes have been studied by means of a more realistic model of DC glows, which is in the spirit of models usually employed for detailed simulation of microdischarges in the absence of self-organization [133–138] and which accounts for two ionic species, several ionization channels, non-equilibrium population of excited states and comprises an energy equation for the electrons. It was found that the effect of chemistry and non-locality of electron kinetic and transport coefficients does not cause qualitative changes in self-organization, which explains why the use of the basic model in simulations of self-organization has been successful. The basic model is used also in this work.

3.2.1 System of equations

The system of non-stationary equations comprises equations of conservation of a single ion species (molecular ions) and the electrons, transport equations for the ions and the electrons written in the drift-diffusion local-field approximation, and the Poisson equation:

$$\frac{\partial n_i}{\partial t} + \nabla \cdot \mathbf{J}_i = w, \quad \mathbf{J}_i = -D_i \nabla n_i + n_i \mu_i \mathbf{E}, \tag{3.1}$$

$$\frac{\partial n_e}{\partial t} + \nabla \cdot \mathbf{J}_e = w, \quad \mathbf{J}_e = -D_e \nabla n_e - n_e \mu_e \mathbf{E}, \tag{3.2}$$

$$\nabla \cdot \mathbf{E} = \frac{e(n_i - n_e)}{\varepsilon_0}, \tag{3.3}$$

where

$$w = n_e \alpha \mu_e E - \beta n_e n_i. \tag{3.4}$$

Here n_i, n_e, $\mathbf{J}_i$, $\mathbf{J}_e$, D_i, D_e, μ_i, and μ_e are number densities, densities of transport fluxes, diffusion coefficients, and mobilities of the ions and electrons, respectively; α is Townsend's ionization coefficient; β is the coefficient of dissociative recombination; $\mathbf{E}$ is the electric field; $E = |\mathbf{E}|$ is the electric field strength; ε_0 is the permittivity of free space; e is the elementary charge; and t is time. Since the electric field in the non-stationary case is expressed in terms of both scalar potential φ and vector potential $\mathbf{A}$,

$$\mathbf{E} = -\nabla\varphi - \frac{\partial \mathbf{A}}{\partial t}, \tag{3.5}$$

the above equations must be supplemented by Ampère's law governing the vector potential

$$\nabla \times (\nabla \times \mathbf{A}) = \mu_0 \mathbf{j}_{cond} - \varepsilon_0\mu_0 \frac{\partial}{\partial t}\left(\nabla\varphi + \frac{\partial \mathbf{A}}{\partial t}\right). \tag{3.6}$$

Here $\mathbf{j}_{cond} = e\left(\mathbf{J}_i - \mathbf{J}_e\right)$ is the conduction current density and μ_0 is the magnetic permeability of free space.

The aim is to use the above equations in analysis of stability of the discharge against small perturbations. Let us designate by τ a time scale characterizing a perturbation (e.g., its period or inverse increment). This time should be compared with time scales contained in the equations, which may be defined as

$$\tau_i = \frac{h^2}{\mu_i^{(0)} U^{(0)}}, \quad \tau_e = \frac{h^2}{\mu_e^{(0)} U^{(0)}}, \quad \tau_c = \sqrt{\varepsilon_0\mu_0}\, h, \quad \tau_j = \frac{\varepsilon_0 U^{(0)}}{j_{cond}^{(0)} h}, \tag{3.7}$$

where h is the discharge gap, the upper index (0) denotes a characteristic value, and U is the discharge voltage. τ_i, τ_e, and τ_c have the meaning of characteristic times of, respectively, transport of the ions and the electrons and propagation of electromagnetic waves across the discharge gap. τ_j represents a time scale on which conduction and displacement currents are comparable (Maxwell time). Under typical experimental conditions of interest (microdischarges in xenon, $p = 30\,\text{Torr}$, $h = 0.5\,\text{mm}$, current density $10^{-2}\,\text{A/m}^2$ to $10^3\,\text{A/m}^2$), $\tau_i = O(10^{-6}\,\text{s})$, $\tau_e = O(10^{-9}\,\text{s})$, $\tau_c = O(10^{-12}\,\text{s})$, and $\tau_j = O\left(10^{-3}\,\text{s} - 10^{-8}\,\text{s}\right)$.

Estimating order of magnitude of $\mathbf{A}$ from equation (3.6), one finds

$$\frac{|\partial \mathbf{A}/\partial t|}{|\nabla\varphi|} \sim \frac{\tau_c^2}{\tau^2 + \tau_c^2}\left(1 + \frac{\tau}{\tau_j}\right). \tag{3.8}$$

Taking into account that $\tau_j \gg \tau_c$, one finds that the rhs of this expression is of the order of $\tau_c^2/\tau\tau_j$ for $\tau_j \lesssim \tau$, of the order of $\left(\tau_c/\tau\right)^2$ for $\tau_c \lesssim \tau \lesssim \tau_j$, and of the order of 1 at $\tau \lesssim \tau_c$. It follows that the second term on the rhs of equation (3.5) may be dropped and equations (3.1)-(3.4) become decoupled from equation (3.6) on time scales $\tau \gg \tau_c$.

If one considers perturbations with frequencies of the order of τ_i^{-1}, then the non-stationary term is essential in the equation of conservation of the ions, the first equation in (3.1), but not in the equation of conservation of the electrons, the first equation in (3.2).

The second term on the rhs of equation (3.5) may be dropped as well. There are perturbations of the magnetic field caused by perturbations of the conduction currents and/or potential φ, but these perturbations do not affect the charged particles and the electric field, so equation (3.6) is unnecessary.

If one considers perturbations with frequencies of the order of τ_e^{-1}, then it follows from the first equation in (3.1) that temporal variations of the ion density are small, $\partial n_i/\partial t \approx 0$. In other words, ion transport and ionization and recombination are frozen on time scales that small, so the ion density remains unperturbed. A non-stationary term is essential in the equation of conservation of the electrons. The second term on the rhs of equation (3.5) may be dropped again and equation (3.6) is unnecessary.

If one considers perturbations with frequencies of the order of τ_c^{-1}, then it follows from the equations of conservation of the ions and the electrons that the temporal variations of both the ion and electron densities are small. The non-stationary term is essential in equation (3.5). In physical terms, there are perturbations of the electromagnetic field, which do not perturb the charged particles and are governed by equations (3.3), (3.5), and (3.6). Note that the first term on the rhs of equation (3.6) may be dropped in this case, since $\tau_j \gg \tau_c$.

On frequencies substantially higher than τ_i^{-1}, one of the channels of development of perturbations in the discharge (perturbation of the electric field by perturbations of the ion density) is effectively switched off, since the ion density is not perturbed. Therefore, one can expect that the possibility of enhancement of perturbations on frequencies of the order of τ_e^{-1} and τ_c^{-1} is smaller than that on frequencies of the order of τ_i^{-1}. Thus, one can expect that stability of the discharge is governed by perturbations with frequencies (or increments) of the order of τ_i^{-1}.

In accord to the above, the system of equations (3.1)-(3.5) is employed in this work with the non-stationary term only in the equation of conservation of the ions, first equation in (3.1); the non-stationary terms in the equation of conservation of the electrons and in equation (3.5) are dropped and equation (3.6) is not used. Note that in order to check the above reasoning, calculations have been performed with account of the non-stationary terms both in the ion and electron conservation equations. It has been found that the account of the non-stationary term in the electron conservation equation results in appearance of a high-frequency part of the spectrum; the spectrum of perturbations with frequencies of the order of τ_i^{-1} is not affected appreciably and it is these perturbations than can be growing, in agreement with the above reasoning.

It will be convenient for the purposes of this work to rewrite the first equations in (3.1) and (3.2) in the following form:

$$\frac{\partial n_i}{\partial t} - \nabla \cdot (D_i \nabla n_i) - \nabla (\mu_i n_i) \cdot \nabla \varphi + \frac{e}{\varepsilon_0} \mu_i n_i (n_i - n_e) = w, \tag{3.9}$$

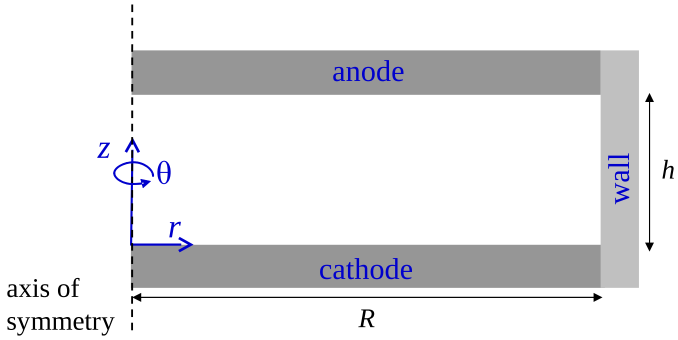

Figure 3.1: Geometry of the problem.

$$-\nabla \cdot (D_e \nabla n_e) + \nabla (\mu_e n_e) \cdot \nabla \varphi - \frac{e}{\varepsilon_0} \mu_e n_e (n_i - n_e) = w. \tag{3.10}$$

Numerical results reported in this work refer to a discharge in xenon under the pressure of 30 Torr. The transport and kinetic coefficients are evaluated in the same way as in [128]. The mobilities of Xe_2^+ ions and electrons in Xe were set equal to $2.2 \times 10^{-3}\,\mathrm{m^2\,V^{-1}\,s^{-1}}$ and, respectively, $0.57\,\mathrm{m^2\,V^{-1}\,s^{-1}}$ in accord to [139, 140]. Townsend's ionization coefficient was evaluated by means of equation (4.6) of [6]. The diffusion coefficients were evaluated by means of Einstein's law with temperatures of the ions and electrons equal to, respectively, 300 K and 1 eV. The coefficient of dissociative recombination of molecular ions Xe_2^+ was set equal to $2 \times 10^{-13}\,\mathrm{m^3\,s^{-1}}$[141, 142].

3.2.2 Boundary conditions

Numerical results reported in this work refer to a microdischarge in a vessel in the form of a right circular cylinder of a radius $R = 1.5$ mm and of a height $h = 0.5$ mm. Let us introduce cylindrical coordinates (r, ϕ, z) with the origin at the center of the cathode and the z-axis coinciding with the axis of the vessel; see figure 3.1. Boundary conditions at the cathode and anode are written in the conventional form:

$$z = 0: \quad \frac{\partial n_i}{\partial z} = 0, \quad J_{ez} = -\gamma J_{iz}, \quad \varphi = 0; \tag{3.11}$$

$$z = h: \quad n_i = 0, \quad \frac{\partial n_e}{\partial z} = 0, \quad \varphi = U, \tag{3.12}$$

where γ is the effective secondary emission coefficient, which was set equal to 0.03 in this modelling. The subscripts z and r here and further denote axial and, respectively, radial projections of corresponding vectors.

The following boundary conditions are applied at the (dielectric) lateral wall of the discharge vessel:

$$r = R: \quad e\,(J_{ir} - J_{er}) - \varepsilon_0 \frac{\partial^2 \varphi}{\partial t\, \partial r} = 0, \quad n_i = n_e = 0. \tag{3.13}$$

These boundary conditions are similar to those used by other authors (e.g., [77, 143]). The first boundary condition means zero of the radial component of the total electric current density, which implies neglect of the radial component of the displacement current inside the dielectric wall. The second boundary condition is written under the assumption that all ions and electrons coming to the wall are absorbed, with eventual neutralization and return of the appearing neutral atoms into the plasma.

The discharge is assumed to be current-controlled. Therefore, the discharge current or, equivalently, the average density of total electric current in the direction from anode to cathode,

$$\langle j \rangle = -\frac{1}{\pi R^2} \int_0^{2\pi} \int_0^R \left[e \left(J_{iz} - J_{ez} \right) - \varepsilon_0 \frac{\partial^2 \varphi}{\partial t \, \partial z} \right] r \, dr \, d\phi, \tag{3.14}$$

is treated as a given parameter. Accordingly, the discharge voltage U is found in the course of simulations.

The above problem, when applied to treatment of stationary states, admits an axially symmetric (2D) solution, $F = F(r, z)$ (here F is any of the quantities n_i, n_e, and φ) which exists at all discharge currents. This solution is designated the fundamental mode. Under certain conditions, the problem admits also other 2D solutions, which exist in a limited current range and represent a closed loop, and 3D solutions, which also exist in a limited current range. In this chapter, stability is studied of 2D steady states belonging to both fundamental and non-fundamental modes.

It is of interest to consider also the case where the second boundary condition in (3.13) is replaced by the condition

$$r = R: \quad \frac{\partial n_i}{\partial r} = \frac{\partial n_e}{\partial r} = 0. \tag{3.15}$$

In this case, the ion and electron fluxes in stationary states vanish at the lateral wall, meaning that all charged particles coming to the wall are reflected rather than absorbed. The fundamental mode of the discharge becomes 1D: all the parameters vary only in the axial direction, i.e., $F = F(z)$. This is the 1D form of glow discharge to which the classical von Engel and Steenbeck theory refers (e.g., [6]). The pattern of stability of this mode is the simplest and the easiest to understand. Besides, investigation of its stability includes a determination of points of bifurcation of steady-state modes, which are important for understanding the pattern of multiple steady-state modes, as will be shown in chapter 4, and calculation of these modes [128]. For this reason, stability of the 1D glow discharge is investigated as well.

3.2.3 Eigenvalue problem for perturbations

Perturbations of 2D stationary states can be 2D or 3D. In the framework of the conventional formalism of the linear stability theory and similarly to how it was done for the case of arc cathode in chapter 2, a solution to the problem (3.9), (3.10), (3.3)-(3.5), (3.11)-(3.14) is sought as sum of a steady-state solution and small perturbations with exponential time dependence. Taking into account that the 3D perturbations are harmonic with respect to the azimuthal angle ϕ, one can write [cf. expansions (2.6), (2.7), (2.12) for the case of arc cathode]

$$n_{i,e}\left(r,\phi,z,t\right)=n_{i0,e0}\left(r,z\right)+e^{\lambda t}n_{i1,e1}\left(r,z\right)\cos m\phi+\ldots, \tag{3.16}$$

$$\varphi\left(r,\phi,z,t\right)=\varphi_0(r,z)+e^{\lambda t}\varphi_1\left(r,z\right)\cos m\phi+\ldots, \tag{3.17}$$

$$U\left(t\right)=U_0+e^{\lambda t}U_1+\ldots. \tag{3.18}$$

Here the first term on the rhs of each expansion represents a solution describing the stationary state stability of which is being studied; the second term represents a perturbation of this state; λ is the increment of growth of the perturbation; and $m=0,1,2,\ldots.$ If $m=0$, the perturbation being considered is 2D. If $m=1,2,\ldots$, the perturbation is 3D with period in ϕ equal to $2\pi/m$.

Substituting expansions (3.16)-(3.18) into the equations (3.9), (3.10), (3.3)-(3.5), boundary conditions (3.11)-(3.13), and equation (3.14), linearizing, and equating linear terms, one obtains

$$\begin{aligned}&\lambda n_{i1}-D_i\nabla^2 n_{i1}+D_i\left(\frac{m}{r}\right)^2 n_{i1}-\mu_i\left(\nabla n_{i1}\cdot\nabla\varphi_0+\nabla n_{i0}\cdot\nabla\varphi_1\right)\\ +\quad&\mu_i\frac{e}{\varepsilon_0}\left[n_{i1}(n_{i0}-n_{e0})+n_{i0}(n_{i1}-n_{e1})\right]=w_1,\end{aligned} \tag{3.19}$$

$$\begin{aligned}&-D_e\nabla^2 n_{e1}+D_e\left(\frac{m}{r}\right)^2 n_{e1}+\mu_e\left(\nabla n_{e1}\cdot\nabla\varphi_0+\nabla n_{e0}\cdot\nabla\varphi_1\right)\\ -\quad&\mu_e\frac{e}{\varepsilon_0}\left[n_{e1}(n_{i0}-n_{e0})+n_{e0}(n_{i1}-n_{e1})\right]=w_1,\end{aligned} \tag{3.20}$$

$$-\nabla^2\varphi_1+\left(\frac{m}{r}\right)^2\varphi_1=\frac{e}{\varepsilon_0}\left(n_{i1}-n_{e1}\right); \tag{3.21}$$

$$\begin{aligned}z=0:\qquad&\frac{\partial\, n_{i1}}{\partial\, z}=0,\quad -D_e\frac{\partial n_{e1}}{\partial z}+\mu_e\left(n_{e1}\frac{\partial\varphi_0}{\partial z}+n_{e0}\frac{\partial\varphi_1}{\partial z}\right)\\ =\quad&\gamma\mu_i\left(n_{i1}\frac{\partial\varphi_0}{\partial z}+n_{i0}\frac{\partial\varphi_1}{\partial z}\right),\quad \varphi_1=0;\end{aligned} \tag{3.22}$$

$$z=h:\quad n_{i1}=0,\quad \frac{\partial n_{e1}}{\partial z}=0,\quad \varphi_1\cos m\phi=U_1; \tag{3.23}$$

$$r=R:\quad e\left(-D_i\frac{\partial n_{i1}}{\partial r}+D_e\frac{\partial n_{e1}}{\partial r}\right)-\varepsilon_0\lambda\frac{\partial\varphi_1}{\partial r}=0,\quad n_{i1}=n_{e1}=0; \tag{3.24}$$

$$\delta_{m0} \int_0^R \left[e \left(-D_i \frac{\partial n_{i1}}{\partial z} - \mu_e n_{e1} \frac{\partial \varphi_0}{\partial z} - \mu_e n_{e0} \frac{\partial \varphi_1}{\partial z} \right) - \varepsilon_0 \lambda \frac{\partial \varphi_1}{\partial z} \right]_{z=h} r \, dr = 0. \tag{3.25}$$

Here

$$w_1 = \mu_e \left[n_{e1} \, \alpha|_{E_0} E_0 + \frac{n_{e0}}{E_0} \left. \frac{d(\alpha E)}{dE} \right|_{E_0} \nabla \varphi_0 \cdot \nabla \varphi_1 \right] - \beta \left(n_{i0} n_{e1} + n_{e0} n_{i1} \right). \tag{3.26}$$

It should be stressed that although equations (3.19)-(3.21) are written in terms of ∇, there are no azimuthal derivatives in these equations since n_{i0}, n_{i1}, n_{e0} *etc* are functions only of r and z. Equation (3.25) reflects the assumption that the discharge current is maintained unperturbed by the external circuit (the limiting case of a very high ballast or, equivalently, a current-controlled discharge) and Kronecker delta δ_{m0} on the lhs originates in integration over ϕ. For definiteness, the discharge current is evaluated at the anode.

In the case $m \neq 0$, equation (3.25) is satisfied trivially: perturbations which are harmonic in ϕ do not perturb discharge current. On the other hand, the last boundary condition in (3.23) cannot be satisfied in the case $m \neq 0$ unless both sides vanish. Therefore, the last boundary condition in (3.23) in the case $m \neq 0$ is equivalent to two relations: $\varphi_1(r,h) = 0$, $U_1 = 0$.

Equations (3.19)-(3.26) represent a linear eigenvalue problem, λ being the eigenvalue. By means of solving this problem for a given m, one will determine a set of eigenvalues λ (spectrum) associated with this m. By means of repeating this procedure for each m and joining the obtained spectra, one will find the whole spectrum of the stationary state being treated. If real parts of all eigenvalues are non-positive, the state is stable; if at least one eigenvalue has a positive real part, the state is unstable.

Perturbations of 1D stationary states, which belong to the (1D) fundamental mode occurring in the case where the second boundary condition in (3.13) is replaced by (3.15), can be 1D, or 2D, or 3D. The above problem for perturbations (3.19)-(3.26) remains valid except that equation (3.24) is replaced with

$$r = R: \quad \frac{\partial \varphi_1}{\partial r} = 0, \quad \frac{\partial n_{i1}}{\partial r} = \frac{\partial n_{e1}}{\partial r} = 0. \tag{3.27}$$

[Note that in this case perturbations of fluxes of charged particles to the wall are zero, in agreement with the interpretation of boundary condition (3.15) as describing a reflecting lateral wall.] The problem admits separation of variables r and z. The radial dependence is described by the Bessel function of the first kind $J_m\left(j'_{m,s} r/R\right)$, where $j'_{m,s}$ is the sth zero of the derivative of the Bessel function of order m, $m = 0, 1, 2, ...$, $s = 1, 2, 3, ...$ (Values of the first five zeros $j'_{m,s}$ are given in table A.1.) Note that $j'_{0,1} = 0$, hence perturbations with $m = 0$, $s = 1$ are 1D. Perturbations with $m = 0$, $s \geq 2$ are 2D, and those with $m \geq 1$ are 3D.

The axial dependence of perturbations of 1D stationary states is described by a 1D eigenvalue problem that is obtained from (3.19)-(3.26) by replacing the operator $\frac{1}{r}\frac{\partial}{\partial r}\left(r\frac{\partial}{\partial r}\right) -$

$\left(\frac{m}{r}\right)^2$ with $-\left(\frac{j'_{m,s}}{R}\right)^2$, introducing the factor $J_m\left(j'_{m,s}r/R\right)$ into the lhs of the last boundary condition (3.23), dropping the boundary conditions (3.24), and replacing integration on the lhs of the equation (3.25) with multiplication by δ_{s1} (note that the integral of the Bessel function vanishes for $m = 0$, $s \geq 2$ and for $m \geq 1$). In the cases of 2D and 3D perturbations the equation that follows from (3.25) is satisfied trivially, while the relation that follows from the last boundary condition (3.23) is equivalent to two relations: the axial dependence of φ_1 vanishes and $U_1 = 0$. By means of solving this problem for each pair (m, s) and joining the spectra obtained, one will determine the whole spectrum for the 1D stationary state being treated.

3.3 Numerical solution of the eigenvalue problem with COMSOL Multiphysics

The approach employed in this chapter for investigation of stability of axially symmetric stationary glow discharges may be viewed as a combination of the two approaches described in section 2.3. Terms involving derivatives with respect to ϕ on the lhs of equations (3.9), (3.10), and (3.3) are replaced with the following terms, respectively: $D_i\,(m/r)^2\,n_i$, $D_e\,(m/r)^2\,n_e$, and $(m/r)^2\,\varphi$. Note that these terms are similar to those present in equations (3.19)-(3.21). The resulting non-stationary equations are introduced in COMSOL as in the first approach described in section 2.3, but in the 2D geometry rather than in 3D. One sets $m = 0$ before invoking the stationary solver and changes m to a desired value before invoking the eigenvalue solver. This approach offers the advantages of the second approach described in section 2.3 while not requiring a manual introduction of the perturbation problem. Besides, it seems to be more robust: when implemented on the same numerical mesh in COMSOL Multiphysics versions 3.5a and 4.0a, the second approach gives spectra which agree between themselves in the case $m = 0$ but not at all discharge currents in the case $m \neq 0$, while spectra given by the present approach under both versions agree between themselves (and also with the spectra given by the second approach under COMSOL 3.5a).

The 1D eigenvalue problem governing stability of 1D stationary states also has been solved with the use of COMSOL. Two approaches which represent analogues of the second and third described approaches in both versions of the software give spectra that agree between themselves.

It has been found that the choice of the mesh affects spectrum of perturbations stronger than it affects results on stationary states. The usual criterion was used: variation of spectrum from one mesh to another should be small, otherwise the results are deemed unreliable. We note right now that it turned out possible to obtain reliable spectra in all the cases except in a narrow current range belonging to the 1D Townsend discharge.

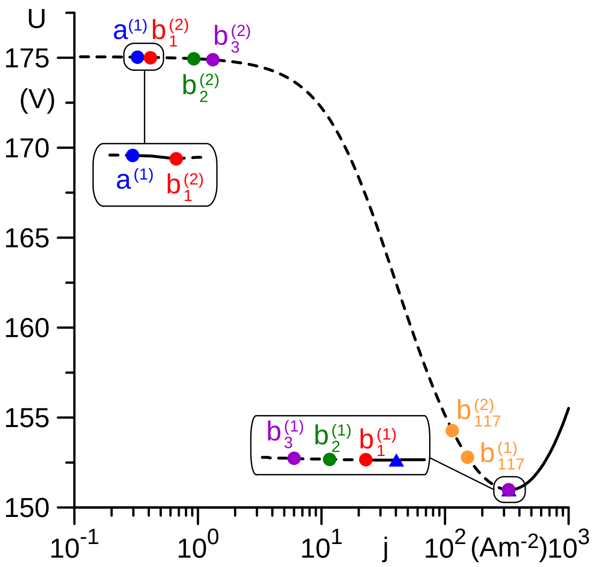

Figure 3.2: CVC of the 1D glow discharge. Solid: stable sections. Dashed: unstable sections. Circles: points of change of stability against a mode of real perturbations or against two complex conjugate modes. Triangle: point of minimum of the CVC.

3.4 Stability of the fundamental mode

In this section, results of numerical calculations of spectra of perturbations are reported and discussed for the fundamental steady-state mode, which is the one existing at all discharge currents.

3.4.1 Numerical results

1D glow discharge

Numerical results reported in this section refer to the case where the lateral wall of the discharge tube reflects charged particles coming from the plasma. In this case, the fundamental mode represents the classic 1D steady-state glow discharge known from the von Engel and Steenbeck theory. Its CVC is shown in figure 3.2. Under the present conditions, the Townsend discharge, where the discharge voltage is approximately constant, occurs at $j \lesssim 3\,\mathrm{A\,m^{-2}}$ and the minimum of the CVC occurs at $j = j_{\min} \approx 328\,\mathrm{A\,m^{-2}}$.

A large number of different perturbation modes have been found, some of them real and others complex. As it should have been expected, increments of real perturbations are real, complex perturbations exist in pairs with perturbations of each pair and their increments being complex conjugate.

It is convenient to introduce "quantum numbers" in order to identify different modes of perturbations. As indicated in section 3.2.3, dependence of perturbations of 1D stationary states on r and ϕ is given by $J_m\left(j'_{m,s} r/R\right)\cos m\phi$, so m and s are natural candidates. One more "quantum number" is needed in order to distinguish between perturbation modes

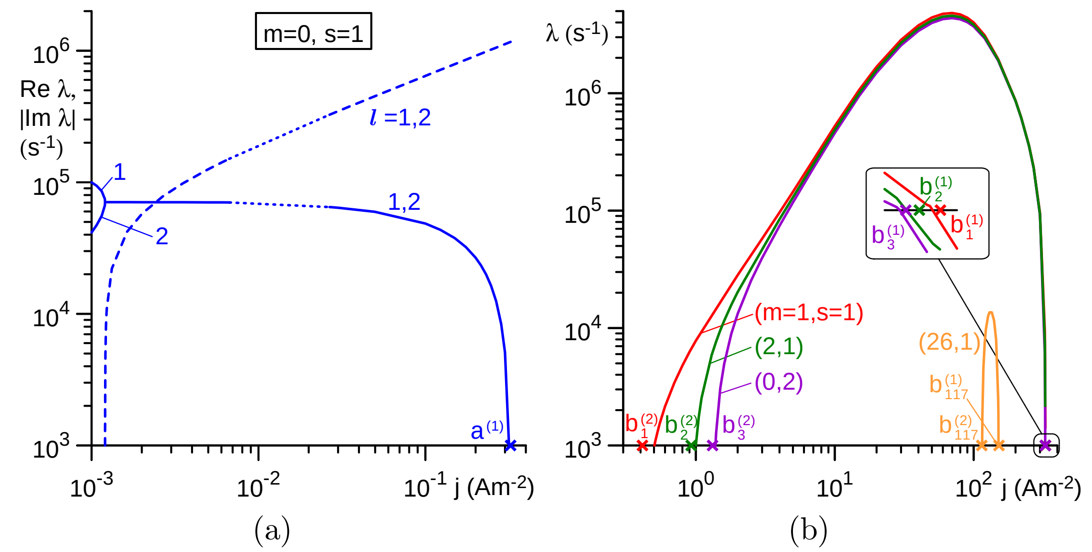

Figure 3.3: Increments of growing perturbations of the 1D glow discharge. Solid: real part of the increment. Dashed: modulus of the imaginary part. Dotted: increments unknown. Crosses: values of j where stability changes against a mode of real perturbations or against two complex conjugate modes. (a) 1D perturbations. (b) Axially symmetric and 3D perturbations.

associated with the same pair (m, s) but with different dependences on z. Let us number such perturbation modes in the order of decrease of $\operatorname{Re}\lambda$; in the case of a pair of complex conjugate perturbations, the one associated with an increment with a positive imaginary part is counted first. Let us designate this number by l and use as the missing "quantum number".

Switching of perturbations of different modes between decay and growth is illustrated by figure 3.3. Note that all 2D and 3D perturbation modes which are growing and are therefore shown in figure 3.3b are associated with different pairs (m, s). In other words, all growing 2D and 3D perturbations are associated with $l = 1$. At $j \geq j_{\min}$, real parts of the increments of all perturbation modes are negative, so all perturbations are decaying and the discharge is stable. As j decreases, real parts of the increments increase and eventually one of them turns positive. This happens at j slightly (some $0.5\,\mathrm{A\,m^{-2}}$) below $j_{\min}$, the corresponding state is designated $b_1^{(1)}$, and the perturbation that becomes growing is one with $m = s = 1$. As j decreases further, real parts of the increments of other perturbations turn positive. This happens in the order of increase of the value of $j'_{m,s}$, hence the second and the third perturbations to become growing are those with $m = 2$, $s = 1$ (at state $b_2^{(1)}$) and $m = 0$, $s = 2$ (at state $b_3^{(1)}$), respectively. As j decreases further, 114 other perturbation modes become growing, the last one being a perturbation mode with $m = 26$, $s = 1$ (at state $b_{117}^{(1)}$). Altogether, 117 perturbation modes become growing between the point of minimum of the CVC and the state $b_{117}^{(1)}$, with 8 of these modes being 2D ($m = 0$; $s = 2, 3, \ldots, 9$) and 109 being 3D [$m = 1, \ldots, 26$; $s = 1, 2, \ldots, s_{\max}$, where $s_{\max} = s_{\max}(m)$

m	1	2-4	5, 6	7-9	10, 11	12-14	15-17	18-21	22-26
$s_{\max}$	9	8	7	6	5	4	3	2	1

Table 3.1: Number of modes of growing 3D perturbations with different azimuthal periods. The 1D glow discharge.

takes values given in table 3.1].

As j decreases further, real parts of the increments of all growing perturbation modes return to negative values. This happens in the order of decrease of $j'_{m,s}$, hence the first perturbation mode to return to being decaying is that with $m = 26$, $s = 1$ (at state $b_{117}^{(2)}$) and the last ones are those with $m = 0$, $s = 2$ (at state $b_3^{(2)}$); $m = 2$, $s = 1$ (at state $b_2^{(2)}$); and $m = s = 1$ (at $j \approx 0.41\,\mathrm{A\,m^{-2}}$; state $b_1^{(2)}$), respectively. The discharge has regained stability at state $b_1^{(2)}$. However, the stability is lost once again at $j \approx 0.32\,\mathrm{A\,m^{-2}}$ (state $a^{(1)}$), where the real part of the increments of two conjugate perturbation modes with $(m = 0, s = 1)$, which are 1D, becomes positive. As current decreases further, no more stability changes occur and the discharge remains unstable.

Increments of all growing 2D and 3D perturbations are real, and this is why there are no dashed lines in 3.3b. Note that increments of the most of decaying 2D or 3D perturbations are complex. The increments of the 1D perturbation modes that switch from decay to growth at the state $a^{(1)}$ are complex at the state $a^{(1)}$ and remain complex down to $j \approx 1.2\,\mathrm{mA\,m^{-2}}$. The imaginary parts of the increments vanish at $j \approx 1.2\,\mathrm{mA\,m^{-2}}$ and there are two real positive increments for lower currents. In other words, there are two 1D growing perturbation modes at currents below $0.32\,\mathrm{A\,m^{-2}}$, their increments being complex conjugate at $1.2\,\mathrm{mA\,m^{-2}} \lesssim j \lesssim 0.32\,\mathrm{A\,m^{-2}}$ and real at $j \lesssim 1.2\,\mathrm{mA\,m^{-2}}$. Note that there is a numerical problem with calculation of spectrum of 1D perturbations in the current range $6.7\,\mathrm{mA\,m^{-2}} \lesssim j \lesssim 26.7\,\mathrm{mA\,m^{-2}}$: values of the increment depend on the mesh being used (although in all the cases the real part of the increment remains positive). The appearance of this problem is surprising, since the calculations are 1D and there are no difficulties in using very fine meshes, and its nature is unclear. However, one can hope that the resulting uncertainty does not affect conclusions.

One can see from figures 3.3a and 3.3b that there are significant variations of increments of growing perturbation modes in the current range $j \lesssim 1\,\mathrm{A\,m^{-2}}$, where U has already attained a constant value corresponding to the Townsend discharge. The strongest variation is shown by the increments of the modes with $m = 0$, $s = 1$, and $l = 1, 2$, i.e., of the first and second modes of 1D perturbations, which switch from complex to real at j as low as $1.2\,\mathrm{mA\,m^{-2}}$. One can conclude that increments of growing perturbations are much more sensitive to variations of current in the range of Townsend discharge, than the discharge voltage is.

$\lambda = 0$ at the states $b_1^{(1)}, \dots, b_{117}^{(1)}, b_{117}^{(2)}, \dots, b_1^{(2)}$. It follows that these states represent points of bifurcation of steady-state modes: a 2D or 3D steady-state mode branches off

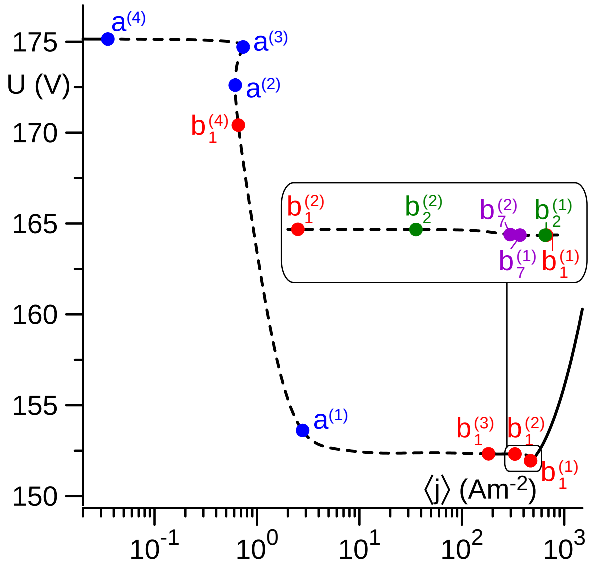

Figure 3.4: CVC of the axially symmetric glow discharge. Solid: stable sections. Dashed: unstable sections. Circles: points of change of stability against a mode of real perturbations or against two complex conjugate modes.

from, or join, the 1D steady-state mode at each of these points. These bifurcations will be analyzed in chapter 4. The bifurcating 2D and 3D steady-state modes have been computed in [128] and [130], respectively. λ is imaginary at the state $a^{(1)}$; a Hopf bifurcation.

Axially symmetric glow discharge

Numerical results reported in this section refer to the case where the lateral wall of the discharge tube absorbs ions and electrons coming from the plasma. The fundamental mode is axially symmetric in this case and its CVC is shown in figure 3.4. Comparing this figure with figure 3.2, one can see that the absorption of the charged particles by the wall results in replacement of the section of the 1D discharge associated with the falling section of the CVC with sections corresponding to the normal and subnormal discharges. An explanation as to why losses of the charged particles due to their diffusion to the wall, which represent a weak effect, cause such a substantial difference will be given in chapter 4. The Townsend discharge and the subnormal discharge join through a Z-shape with turning points designated $a^{(3)}$ and $a^{(2)}$, $\langle j \rangle \approx 0.74\,\mathrm{A\,m^{-2}}$ and $\langle j \rangle \approx 0.62\,\mathrm{A\,m^{-2}}$, respectively. The minimum of the CVC occurs at $\langle j \rangle = \langle j \rangle_{\min} \approx 466\,\mathrm{A\,m^{-2}}$.

As indicated in section 3.2.3, dependence of perturbations of axially symmetric stationary states on ϕ is given by $\cos m\phi$. In order to distinguish between perturbation modes associated with the same m but with different dependences on r and z, we once again number such perturbation modes in the order of decrease of $\mathrm{Re}\,\lambda$ and designate this number by q.

Switching of perturbations of different modes between decay and growth is illustrated

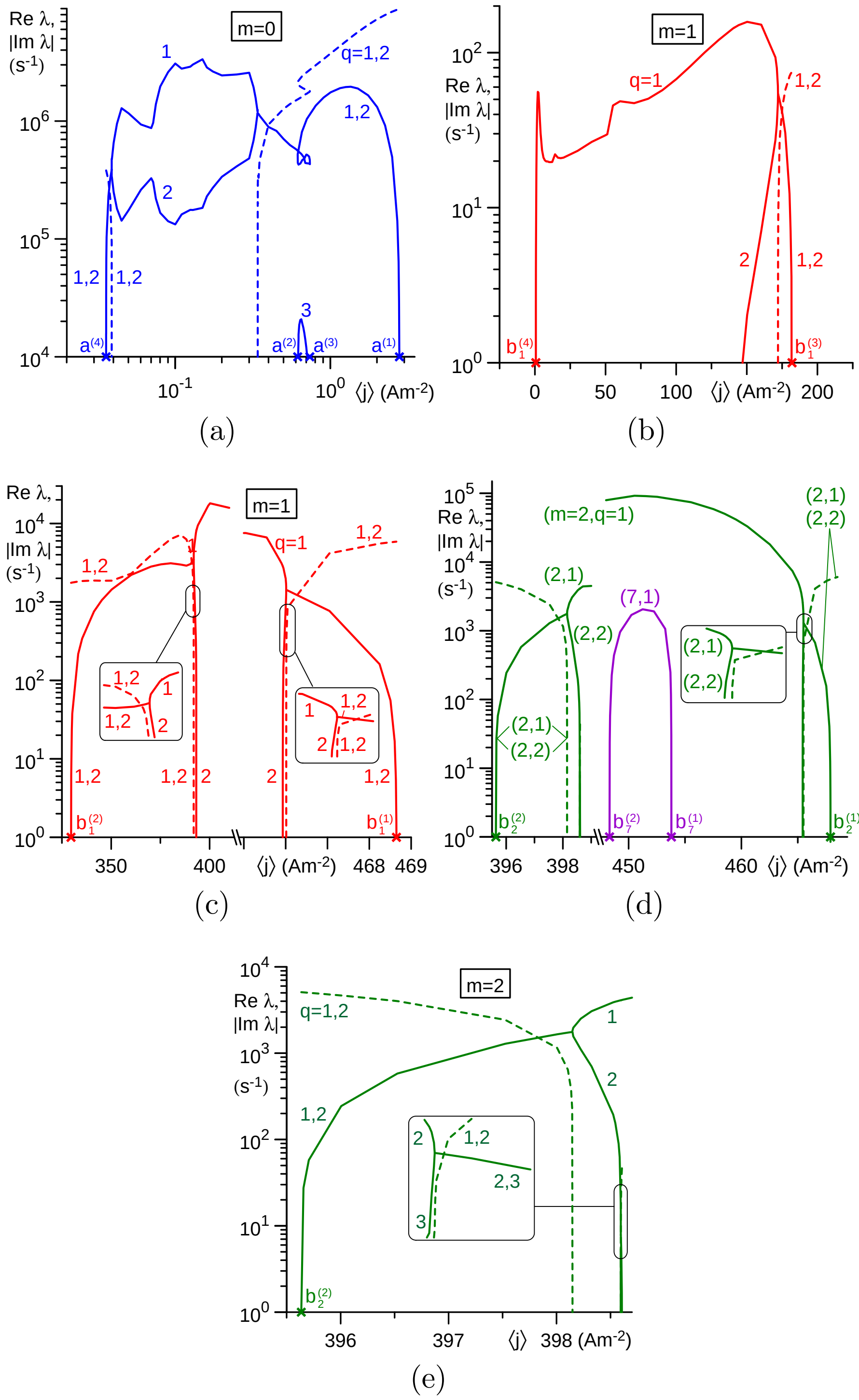

Figure 3.5: Increments of growing perturbations of the axially symmetric glow discharge. Solid: real part of the increment. Dashed: modulus of the imaginary part. Crosses: values of $\langle j \rangle$ where stability changes against a mode of real perturbations or against two complex conjugate modes. (a) Axially symmetric perturbations. (b), (c) 3D perturbations with $m = 1$. (d) 3D perturbations with $m = 2, 7$. (e) Details of 3D perturbations with $m = 2$ in vicinity of state $b_2^{(2)}$.

by figure 3.5. At $\langle j \rangle \gtrsim 469\,\mathrm{A\,m^{-2}}$, real parts of the increments of all perturbation modes are negative and the discharge is stable. As $\langle j \rangle$ decreases, real parts of the increments increase and eventually $\mathrm{Re}\,\lambda$ of two complex conjugate perturbation modes with $m = 1$ becomes positive. This happens at $\langle j \rangle \approx 469\,\mathrm{A\,m^{-2}}$; state $b_1^{(1)}$. Note that the latter state belongs to the rising section of the CVC, however, it is quite close to the point of minimum. As $\langle j \rangle$ decreases further, real parts of the increments of other perturbation modes turn positive. This happens in the order of increase of the value of m, hence the following perturbation modes to become growing are two (complex conjugate) modes with $m = 2$ (at state $b_2^{(1)}$), then two modes with $m = 3$, two modes with $m = 4$, two modes with $m = 5$. After that, a real perturbation mode with $m = 6$ becomes growing. Finally, a real perturbation mode with $m = 7$ becomes growing (at state $b_7^{(1)}$). As $\langle j \rangle$ decreases further, real parts of the increments of all growing perturbation modes return to negative values. This happens in the order of decrease of m, hence the first perturbation mode to return to being decaying is the real mode with $m = 7$ (at state $b_7^{(2)}$) and the last ones are two (complex conjugate) modes with $m = 2$ (at state $b_2^{(2)}$) and two modes with $m = 1$ (at $\langle j \rangle \approx 330\,\mathrm{A\,m^{-2}}$; state $b_1^{(2)}$).

Some growing 3D perturbations are real and other are complex. The latter is in contrast to the case of 2D and 3D perturbations of the 1D glow discharge, which are always real. (The most of decaying perturbations are also complex, as in the case of 1D discharge.) Besides, growing perturbations can switch between real and complex. This switching occurs in the same way as the one which is suffered at $j \approx 1.2\,\mathrm{mA\,m^{-2}}$ by the 1D growing perturbations of the 1D discharge and shown in figure 3.3a. Let us consider, for example, switching of the growing perturbations with $m = 1$ shown in figure 3.5c. One can see that $|\mathrm{Im}\,\lambda| \neq 0$ at the state $b_1^{(1)}$; in other words, what turns growing at this state are two complex conjugate perturbations with $m = 1$. However, $|\mathrm{Im}\,\lambda|$ rapidly decreases with decrease of current and vanishes at $\langle j \rangle \approx 466\,\mathrm{A\,m^{-2}}$: a switching to two real perturbations occurs. The increment of one of these perturbations (the one with $q = 2$) rapidly decreases and at $\langle j \rangle$ still very close to $466\,\mathrm{A\,m^{-2}}$ it vanishes, i.e., the perturbation becomes decaying. There is only one growing real perturbation mode with $m = 1$ at $393\,\mathrm{A\,m^{-2}} \lesssim \langle j \rangle \lesssim 466\,\mathrm{A\,m^{-2}}$. Another real perturbation (the one with $q = 2$) becomes growing at $\langle j \rangle \approx 393\,\mathrm{A\,m^{-2}}$. The increment of the latter perturbation grows very fast and at $\langle j \rangle \approx 392\,\mathrm{A\,m^{-2}}$ becomes equal to the increment of the perturbation with $q = 1$. At smaller currents, the increments become complex conjugate; a switching from two real to two complex perturbations occurs. The latter perturbations become decaying at the state $b_1^{(2)}$.

The above-described switching between real and complex perturbations is manifested also by the growing perturbation modes with $m = 2, 3, 4, 5$, except that the growing perturbations with $m = 4, 5$, after switching to real with decreasing current, remain real until turning decaying. The growing perturbation modes with $m = 6, 7$ are always real, i.e., do not manifest the switching.

After having regained stability at state $b_1^{(2)}$, the discharge remains stable until state $b_1^{(3)}$ ($\langle j \rangle \approx 182\,\mathrm{A\,m^{-2}}$) where two (complex conjugate) modes with $m = 1$ become growing; figure 3.5b. (A theoretically interesting question is whether these are the same perturbation modes that returned to decay at the state $b_1^{(2)}$, however this question is not easy to answer because there are other decaying modes with similar increments and distributions between $b_1^{(2)}$ and $b_1^{(3)}$.) The perturbations turn real at $\langle j \rangle \approx 172\,\mathrm{A\,m^{-2}}$. One of these real perturbations returns to being decaying at $\langle j \rangle \approx 141\,\mathrm{A\,m^{-2}}$ and the other at $\langle j \rangle \approx 0.66\,\mathrm{A\,m^{-2}}$ (state $b_1^{(4)}$).

However, the discharge does not return to stability at state $b_1^{(4)}$ since there are two growing complex perturbation modes with $m = 0$ at this state. These perturbations become growing at state $a^{(1)}$ ($\langle j \rangle \approx 2.8\,\mathrm{A\,m^{-2}}$), switch to being real at $\langle j \rangle \approx 0.34\,\mathrm{A\,m^{-2}}$, switch back to being complex at $\langle j \rangle \approx 40\,\mathrm{mA\,m^{-2}}$, and return to decay at state $a^{(4)}$ ($\langle j \rangle \approx 36\,\mathrm{mA\,m^{-2}}$); see figure 3.5a. Note that the shape with two self-intersection points manifested by the solid line in figure 3.5a at $\langle j \rangle$ slightly below $1\,\mathrm{A\,m^{-2}}$, which resembles the infinity symbol, depicts behavior of $\mathrm{Re}\,\lambda$ between the turning points.

One more perturbation mode (the one with $m = 0$ and $q = 3$) turns growing between turning points $a^{(2)}$ and $a^{(3)}$. Since this mode is real and axially symmetric, i.e., has the same symmetry that the discharge itself, this result is in agreement with the general theory of chapter 4.

For currents below $36\,\mathrm{mA\,m^{-2}}$, the discharge remains stable.

It follows from the above that Hopf bifurcations occur at states $b_m^{(1)}$ with $m = 1, \ldots, 5$, states $b_m^{(2)}$ with $m = 1, 2, 3$, and states $b_1^{(3)}$, $a^{(1)}$, and $a^{(4)}$. Bifurcations of steady-state modes occur at states $b_m^{(1)}$ with $m = 6, 7$, states $b_m^{(2)}$ with $m = 4, 5, 6, 7$, and state $b_1^{(4)}$: a 3D steady-state mode branches off from, or joins, the axially symmetric steady-state mode at each of these states. Besides, stationary bifurcations occur at every state where a real 3D perturbation with $q > 1$ switches between decaying and growing. Strictly speaking, steady-state bifurcations occur also at the turning points $a^{(2)}$ and $a^{(3)}$, however such bifurcations are irrelevant for the purposes of this chapter.

3.4.2 Discussion

Theoretical aspects

In this section, results on 1D and 2D glow discharges are compared between themselves and with results given by the linear stability theory of current transfer to cathodes of high-pressure arc discharges described in chapter 2. The set of growing perturbation modes found in the case of 1D discharge includes two perturbation modes which are of the same symmetry that the discharge (i.e., 1D), 2D perturbation modes, and 3D perturbation modes with $m = 1, \ldots, 26$. In the case of the fundamental mode of axially symmetric discharge, the set of growing perturbation modes includes three perturbation modes which are of the same symmetry that the discharge (i.e., 2D) and 3D perturbation modes with $m = 1, \ldots, 7$.

In addition to the above-described calculations for the limiting cases of reflecting and absorbing lateral walls, calculations have been performed also for intermediate cases. In these calculations, a gradual transition has been performed from the boundary conditions (3.15) to the second condition in (3.13), which amounts to a gradual introduction of absorption at the wall and is similar to the corresponding procedure in the stationary simulations given in chapter 4. In particular, it was found that the state where the discharge regains stability against 3D perturbations is shifted from the state $b_1^{(2)}$ in figure 3.2 to $b_1^{(4)}$ in figure 3.4. However, in general there is no direct correspondence between modes of growing perturbations of the 1D discharge and of the fundamental mode of the axially symmetric glow discharge. One of the reasons is that there is no direct correspondence between the 1D discharge and the fundamental mode of the axially symmetric glow discharge: the latter mode is constituted by states evolving from the section of the 1D discharge before state $b_3^{(2)}$, the section after state $b_3^{(1)}$, and the central-spot branch of the first 2D spot mode; see details in chapter 4. Another reason is that points of change of stability against a given perturbation mode are shifted in the course of the introduction of the absorption and may merge, which results in the disappearance of the instability window for the perturbation mode considered.

The pattern of changes of stability of the 1D glow discharge against 2D and 3D perturbations, seen in figure 3.2 between states $b_1^{(1)}$ and $b_1^{(2)}$, is similar to the pattern of changes of stability of the axially symmetric glow discharge against 3D perturbations between states $b_1^{(1)}$ and $b_1^{(2)}$, seen in the insert in figure 3.4.

The switching of 2D and 3D perturbation modes of the 1D discharge from decay to growth that happens in the vicinity of the point of minimum of the CVC (between the point of minimum and the state $b_{117}^{(1)}$) occurs along exactly the same lines as in the case of 1D current transfer to cathodes of arc discharges described in chapter 2. In the case of arc discharges, perturbation modes do not return to being decaying. However, if one takes into account that the near-cathode voltage in the arc discharge tends at low currents to a finite value (which corresponds to the abnormal glow discharge), rather than to infinitely high values as assumed in chapter 2, then perturbations will return to being decaying and this return will occur along exactly the same lines as the above-described return of perturbations of 1D glow discharge that occurs between the states $b_{117}^{(2)}$ and $b_1^{(2)}$. On the other hand, the above-described loss of stability of the 1D glow discharge against 1D oscillatory perturbations that occurs at the state $a^{(1)}$ has no analogue in the case of 1D current transfer to arc cathodes.

Note that the eigenvalue problem governing perturbations of 1D current transfer to cathodes of arc discharges is Hermitian (self-adjoint) and therefore its spectrum is real [118]; the latter can be seen also from appendix A where this spectrum was calculated for the particular case where thermal diffusivity of the cathode material is constant. Therefore, it is not surprising that the 2D and 3D perturbation modes of 1D glow discharge, which have real increments while being growing, switch between decay and growth similarly to how switching in the case 1D current transfer to arc cathodes occurs, and that there is no such similarity as far as the 1D perturbation mode is concerned, which has a complex increment.

As discussed in section 1.2.2, in order to compute multiple steady-state solutions describing different modes of stationary current transfer, one needs to have in advance an idea of what each solution looks like and in which current range it should be sought. For this reason, numerical calculation [128, 130] of each 2D or 3D steady-state mode branching from the fundamental mode starts in the vicinity of the corresponding bifurcation point. The bifurcation points are determined by means of solving the eigenvalue problem formulated in section 3.2.3. The procedure is as follows. The fundamental steady-state mode is calculated and the eigenvalue problem with a given m solved for different values of $\langle j \rangle$ until close enough values j_1 and j_2 have been localized such that all perturbations with this m decay at $\langle j \rangle = j_1$ and one perturbation mode with this m possesses a real positive increment at $\langle j \rangle = j_2$.

If this perturbation mode is real on the whole interval $[j_1, j_2]$ or at least on the part of the interval where it is growing (e.g., this is the case of 2D and 3D perturbations of the 1D glow discharge), then this perturbation mode switches from decay to growth through a neutrally stable state, i.e., through a steady-state bifurcation. The situation is more involved if the perturbation mode is complex. For example, perturbations proportional to $\cos\phi$ of the 2D fundamental mode (figure 3.5c) are decaying at $\langle j \rangle = 470\,\mathrm{A\,m^{-2}}$ and there is one mode of perturbations proportional to $\cos\phi$ with a positive real increment at $\langle j \rangle = 465\,\mathrm{A\,m^{-2}}$; however, this mode switches from decay to growth (at $\langle j \rangle \approx 469\,\mathrm{A\,m^{-2}}$) through a Hopf bifurcation, rather than a steady-state one, which is followed by switching of the complex conjugate perturbation modes to real ones and a rapid decrease of the (real) increment of one of these modes, the one with $q = 2$, until vanishing. Nevertheless, a steady-state bifurcation associated with $m = 1$ does occur on the interval $\langle j \rangle = 465\,\mathrm{A\,m^{-2}} \leq \langle j \rangle \leq 470\,\mathrm{A\,m^{-2}}$: at a state where the real perturbation mode with $m = 1$ and $q = 2$ switches from growth to decay, $\langle j \rangle \approx 466\,\mathrm{A\,m^{-2}}$.

One concludes that if all perturbation modes with a given m are decaying at $\langle j \rangle = j_1$ and there is one real perturbation mode with a positive increment at a close value $\langle j \rangle = j_2$, then a steady-state bifurcation associated with this m occurs in the interval $[j_1, j_2]$ and one can start looking for a 3D steady-state solution with the azimuthal period of $2\pi/m$ (or for a 2D solution, if $m = 0$) in this interval without finding out whether this perturbation mode switches between decay and growth through a steady-state or Hopf bifurcation.

Stability of different regimes of glow discharge

Let us start with discussing stability of different regimes of 1D glow discharge. As shown in section 3.4.1, the 1D glow discharge is stable on the rising section of the CVC (abnormal discharge), $j \gtrsim 328\,\mathrm{A\,m^{-2}}$. States of the discharge associated with the falling section of the CVC are unstable against perturbations of many different modes, all of them with real increments. If current in the abnormal discharge is reduced to values below $328\,\mathrm{A\,m^{-2}}$, the first perturbation mode to become growing is a 3D mode with the azimuthal period of 2π. A possible result of this instability is a monotonic (in time) transition of the discharge to the first 3D steady-state mode. The latter mode has the period of 2π and was calculated in [130]; a state to which the transition would occur is characterized by a normal spot occupying the whole of the cathode except for a "cold spot" at the edge and is similar to the one corresponding to the current density $428\,\mathrm{A\,m^{-2}}$ in figure 1b of [130]. Since stability of different 3D steady-state modes remains unknown, other possibilities cannot be excluded as well. In particular, if the first 3D steady-state mode is unstable, then higher-order 3D steady-state modes, which are characterized by multiple spots (e.g., figures 1c and 1d of [130]), can occur instead.

The conclusion that the 1D glow discharge is stable in the current range where the CVC is rising and unstable where the CVC is falling, which has been obtained in this chapter by means of the accurate stability theory, conforms to the common knowledge going back to von Engel and Steenbeck. The conclusion that with a reduction of current the abnormal discharge can switch to the normal mode with a normal spot occupying the most part of the cathode or to a mode with multiple spots and this switching occurs monotonically in time, i.e., without oscillations, agrees to what is observed in the experiment. (Note that while the normal spot is observed in the most of the experiments, patterns with multiple spots have been observed in DC glow microdischarges in xenon [20–24].) However, this conclusion should be re-analyzed with account of absorption of the charged particles by the lateral wall before one can say whether the agreement has any significance.

The 1D Townsend discharge is stable in a narrow current range between states $a^{(1)}$ and $b_1^{(2)}$, $0.32\,\mathrm{A\,m^{-2}} \lesssim j \lesssim 0.41\,\mathrm{A\,m^{-2}}$. If the current is increased to values above $0.41\,\mathrm{A\,m^{-2}}$, the first perturbation mode to become growing is again the 3D mode with the azimuthal period of 2π and a real increment, and a possible result of this instability is a monotonic transition to the first 3D steady-state mode. A state to which the transition would occur is characterized by a small normal spot at the edge of the cathode and is similar to the one corresponding to the current density $35\,\mathrm{A\,m^{-2}}$ in figure 1b of [130]. 3D steady-state modes with multiple spots can occur as well. If the current is reduced to values below $0.32\,\mathrm{A\,m^{-2}}$, two 1D perturbation modes with complex (conjugate) increments become growing: oscillations appear.

It is well known that glow discharge can under certain conditions develop oscillations in the range of low currents corresponding to the Townsend or subnormal discharges; e.g., [74, 77, 78, 144–147] and references therein. Therefore, the fact that the linear stability theory predicts an oscillatory instability occurring in the range of Townsend discharge is not surprising. What is surprising is the behavior of the increment of this instability seen in figure 3.3a: while the discharge voltage reaches a constant value corresponding to the limiting case of Townsend discharge already at j of the order of $1\,\mathrm{A\,m^{-2}}$ and increments of other perturbation modes reach constant values at j of the order of $0.1\,\mathrm{A\,m^{-2}}$, the increments of the 1D perturbations shown in figure 3.3a continue to vary down to currents as low as $1\,\mathrm{mA\,m^{-2}}$ and the perturbations remain growing.

Note that the 1D Townsend discharge represents probably the simplest type of a self-sustained discharge and its instability against 1D oscillatory perturbations revealed by the linear stability theory and described above is scientifically very interesting. Understanding of this instability may, in particular, provide important information on the mechanism of onset of oscillations observed in the experiment, supplementing previous investigations on the theory and modelling of oscillations [74, 77, 78, 145–147]. The mechanism of this instability may be elucidated by means of asymptotic solution of the eigenvalue problem formulated in section 3.2.3 in the limiting case of low currents. However, this task proved to be not quite trivial and is left beyond the scope of this work.

Let us proceed to stability of different regimes of axially symmetric glow discharge. As shown in figure 3.4, this discharge is stable beyond the state $b_1^{(1)}$, $\langle j \rangle \gtrsim 469\,\mathrm{A\,m^{-2}}$, in the abnormal regime; in the current range between states $b_1^{(3)}$ and $b_1^{(2)}$, $182\,\mathrm{A\,m^{-2}} \lesssim \langle j \rangle \lesssim 330\,\mathrm{A\,m^{-2}}$, in the normal regime; and before state $a^{(4)}$, $\langle j \rangle \lesssim 36\,\mathrm{mA\,m^{-2}}$, in the Townsend regime.

The state $b_1^{(1)}$ is very close to the point of minimum of the CVC, $\langle j \rangle_{\min} \approx 466\,\mathrm{A\,m^{-2}}$. In other words, the whole abnormal discharge except a very narrow section remains stable while calculated with account of absorption of the charged particles by the lateral wall. Given that the absorption represents a minor effect when a discharge operates in the abnormal regime, this result could have been expected. If current in the abnormal discharge is reduced to a value below $469\,\mathrm{A\,m^{-2}}$, the loss of stability may occur in two ways, depending on whether the value of current after reduction is below, or above, $466\,\mathrm{A\,m^{-2}}$. If the former is the case, a likely scenario is a monotonic transition to the first or a higher-order steady-state 3D mode. If the current is reduced to a value within the range $466\,\mathrm{A\,m^{-2}} \lesssim \langle j \rangle \lesssim 469\,\mathrm{A\,m^{-2}}$, the loss of stability occurs through perturbations oscillating in time. Since the latter current range is very narrow (in fact, its width is close to the limit of accuracy of the computations), the first possibility is more likely, and indeed the transition from abnormal discharge to the steady-state normal mode with a spot at the edge of the cathode or to a steady-state mode with multiple spots observed in the experiments was monotonic. On the other hand, it is of interest to perform experiments on this transition with a fine current step in order to try to detect oscillations.

The conclusion that the axially symmetric normal mode is stable in a rather wide current range, from $182\,\mathrm{A\,m^{-2}}$ to $330\,\mathrm{A\,m^{-2}}$, is theoretically very interesting: while in most cases normal spots are attached to the edge of a (circular) cathode (e.g., the lower-right and adjacent images in figure 3 in [20]), the linear stability theory predicts that a stable normal mode with the spot at the center can exist in microdischarges. It is of interest to check this prediction experimentally.

The theory predicts that the subnormal discharge is unstable under the considered conditions against three modes of 2D perturbations and one mode of 3D perturbations with the period of 2π. The most dangerous, i.e., the ones possessing the biggest real part of the increment are two 2D perturbation modes which become growing at state $a^{(1)}$ ($\langle j \rangle \approx 2.8\,\mathrm{A\,m^{-2}}$) and return to decay at state $a^{(4)}$ ($\langle j \rangle \approx 36\,\mathrm{mA\,m^{-2}}$). We remind that the above-described 1D modes of perturbations of the 1D Townsend discharge become growing at $j \approx 0.32\,\mathrm{A\,m^{-2}}$ (state $a^{(1)}$ in figures 3.2 and 3.3a) and do not return to decay in the current range investigated. One can conclude that loss of the charged particles at the lateral wall suppresses at low currents instability against perturbations of the same symmetry, thus making the Townsend discharge stable at low currents, and shifts the upper boundary of the window of this instability in the direction of higher currents.

If current in the Townsend discharge is increased to a value exceeding $36\,\mathrm{mA\,m^{-2}}$, the loss of stability may occur in two ways, depending on whether the current after the increase is below, or above, $40\,\mathrm{mA\,m^{-2}}$. If the former is the case, the loss of stability is oscillatory. If the latter is the case, the perturbations grow monotonically in time. On the other hand, it is natural to expect that there are no other steady-state solutions in the current range corresponding to the Townsend discharge (note that the first 3D solution branches off at the state $b_1^{(4)}$, i.e., a current value corresponding to the upper boundary of the Townsend discharge). Then the monotonous growth of perturbations which occurs on the linear stage in the case where the increased current exceeds $40\,\mathrm{mA\,m^{-2}}$ is likely to give way to oscillations on the nonlinear stage.

3.5 Stability of axially symmetric non-fundamental modes

In addition to the fundamental mode described above, two other axially symmetric steady-state modes exist in the case of a discharge tube with absorbing wall. Each one of these mode exists in a limited current range ($26\,\mathrm{A\,m^{-2}} \lesssim \langle j \rangle \lesssim 366\,\mathrm{A\,m^{-2}}$ for one mode, which is termed the first mode, and $33\,\mathrm{A\,m^{-2}} \lesssim \langle j \rangle \lesssim 183\,\mathrm{A\,m^{-2}}$ for the second mode), and represents a loop, i.e., is constituted by two branches separated by (two) turning points. CVC's of these modes represent closed curves which are shown in figures 3.6a and 3.6b; $a^{(1)}$ and $a^{(2)}$ designate the turning points limiting the existence region at higher and lower currents, respectively. There are no self-intersections in these figures, so one can designate the two branches of each mode a low-voltage branch and a high-voltage branch, although

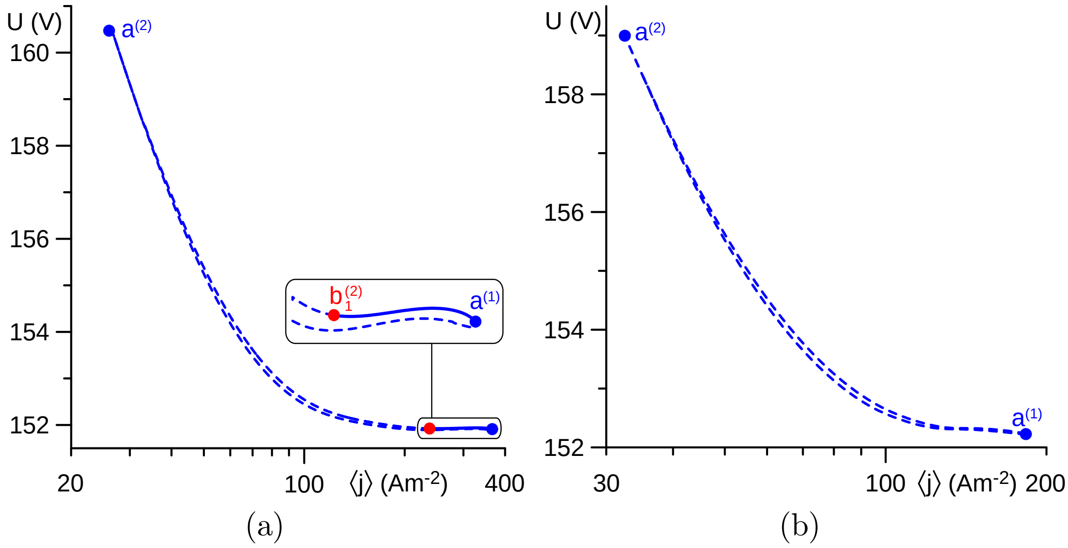

Figure 3.6: CVC's of the first (a) and second (b) non-fundamental axially symmetric steady-state modes of discharge in a tube with absorbing wall. Solid: stable section. Dashed: unstable sections. Circles: points of change of stability against one of perturbation modes.

in reality the discharge voltages corresponding to the two branches are very close. The first mode is associated with a pattern with an interior ring spot, the second mode is associated with a pattern with a spot at the center and an interior ring spot; see [128] for further details. In this section, a summary of results of calculations of stability of these modes is given.

For each mode, a mode exists of real axially symmetric perturbations with the increment vanishing at each of the turning points $a^{(1)}$ and $a^{(2)}$; a result in agreement with section 4.4. For both non-fundamental steady-state modes these perturbations are growing on the low-voltage branch and are decaying on the high-voltage branch.

Switching of 3D perturbations with several values of m between decay and growth is shown in figure 3.7 for the first non-fundamental 2D steady-state mode. Growing perturbation modes, all of them real, have been detected for m up to 33. (More precisely, one growing perturbation mode was detected for each $m = 4, 5, \ldots, 33$. Two growing perturbation modes were detected for each $m = 1, 2, 3$, however the window of growth of one of these modes is positioned inside the window of growth of the other, therefore the former mode is irrelevant and excluded from the following discussion.) Each one of these perturbation modes switches between decay and growth at two states. For most m, one of these states (designated $b_m^{(1)}$) belongs to the low-voltage branch and the other ($b_m^{(2)}$) to the high-voltage branch. It was found that for every m of this group the perturbation mode in question is decaying on the section $b_m^{(1)} a^{(1)} b_m^{(2)}$ and growing on $b_m^{(1)} a^{(2)} b_m^{(2)}$. For others m (e.g., $m = 33$), both points belong to the high-voltage branch. It was found that for every m of this group the perturbation mode in question is growing on the section of the

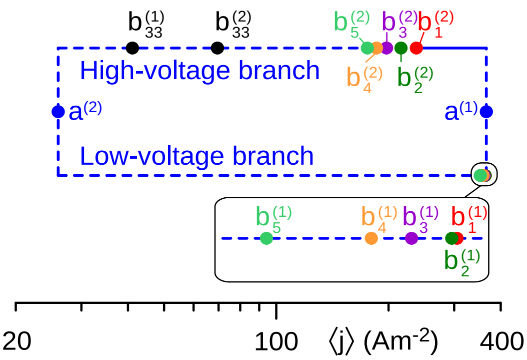

Figure 3.7: Points of change of stability of the first non-fundamental axially symmetric steady-state mode against some of perturbation modes. Solid: stable section. Dashed: unstable sections.

high-voltage branch limited by the states $b_m^{(1)}$ and $b_m^{(2)}$ and is decaying at all the other states of the first non-fundamental 2D steady-state mode.

One can conclude that the first axially symmetric non-fundamental steady-state mode is stable on the high-voltage branch between states $b_1^{(2)}$ and $a^{(1)}$, as shown in figure 3.6a. This is in contrast to what has been found in the case of arc cathode, where the first non-fundamental mode is always unstable; see section 2.4.4. As explained above, state $b_1^{(2)}$, $\langle j \rangle \approx 238\,\mathrm{A\,m^{-2}}$, represents the limit of stability against 3D perturbations with period of 2π and $a^{(1)}$ is the turning point. The stability window is relatively wide, $238\,\mathrm{A\,m^{-2}} \lesssim \langle j \rangle \lesssim 366\,\mathrm{A\,m^{-2}}$, and one can try to observe this mode in the experiment.

In the case of the second axially symmetric non-fundamental steady-state mode, there is, in addition to the above-described 2D perturbations with the increment vanishing at the turning points, another mode of growing 2D perturbations, and these perturbations, which are real as well, grow at all states. Besides, there are several modes of real 3D perturbations that grow at all states. The conclusion is that the second axially symmetric non-fundamental steady-state mode is always unstable.

3.6 Concluding discussion

Main features of stability of different axially symmetric modes of current transfer in DC glow discharges against small perturbations were investigated in the framework of the linear stability theory with the use of software COMSOL Multiphysics, considering as an example conditions of microdischarges in xenon.

Both real and complex increments of perturbations have been detected, meaning that perturbations can vary with time both monotonically and with oscillations. The 1D glow discharge is stable in the current range where the CVC is rising and unstable where the CVC is falling, in agreement with the common knowledge going back to von Engel and Steenbeck.

The 1D Townsend discharge, i.e., a discharge with a spatially uniform electric field is unstable at low current against 1D oscillatory perturbations; a theoretically interesting result which deserves a further elaboration. The fundamental mode of axially symmetric glow discharge, calculated with account of absorption of ions and electrons by the lateral wall, is stable when it operates in the abnormal regime. There is a rather wide window of stability in the axially symmetric normal discharge, which is characterized by a normal spot at the center of the cathode. The subnormal discharge is unstable under the considered conditions. Loss of the charged particles at the lateral wall stabilizes Townsend discharge at low currents.

Loss of stability of the abnormal discharge in the vicinity of the point of minimum of the CVC and loss of stability of the Townsend discharge with increasing current develop in a general case in different ways: monotonically in time and with oscillations, respectively. This conforms to the well-known experimental facts that the transition from the abnormal discharge to the normal discharge or to a discharge with a multiple-spot pattern occurs without oscillations of the luminosity of the cathode or of the discharge voltage, while Townsend discharge is capable of developing voltage oscillations. On the other hand, the linear stability theory predicts that oscillations under conditions of microdischarges can occur also in the transitions from the abnormal discharge to the normal discharge or to a discharge with a multiple-spot pattern, however in a very narrow current range. It is of interest to study these transitions experimentally with a fine current step in order to try to detect the oscillations.

Calculations of stability of the two axially symmetric non-fundamental steady-state modes, which exist under the considered conditions in addition to the fundamental mode, revealed that there is a relatively wide stability window on the first mode, while the second mode is unstable.

Modelling reported in this work has been performed for current-controlled discharges. It is sometimes assumed, by analogy with non-linear electric circuits with inductance, that a gas discharge with a negative differential resistance is stable provided that the ballast is high enough and the total differential resistance of the system is positive. Of course, this conjecture in such a general form is incorrect, an example being the 1D glow discharge (figure 3.2): states between $b_1^{(1)}$ and $b_1^{(2)}$, corresponding to the falling section of the CVC, are unstable against perturbations proportional to $\cos\phi$, which do not perturb the discharge current and therefore are not affected by a ballast. On the other hand, it was proved in the framework of the accurate linear stability theory [118] (see also discussion in section 4.4) that in the case of current transfer to high-pressure arc cathodes this conjecture is valid as far as stability is concerned against perturbations which have the same symmetry that the discharge itself and switch between decay and growth at every turning point.

When applied to the limiting case of a current-controlled discharge, this conjecture means that stability in the vicinity of turning points changes as shown in figure 4.5 of section 4.4: in the vicinity of a turning point which limits the mode in question in the direction of high currents (e.g., state $a^{(3)}$ in figure 3.4) the high-voltage branch is stable and the low-voltage branch unstable; and *vice versa* in the vicinity of a turning point limiting in the direction of low currents (e.g., state $a^{(2)}$ in figure 3.4). One of the consequences of this conjecture is that steady-state modes with loops are forbidden; see discussion in section 3 of [118]. Indeed, steady-state modes with loops on an arc cathode have not been reported in the literature. As far as the fundamental mode of axially symmetric glow discharge is concerned, this conjecture holds: as seen in figure 3.5a, the mode of axially symmetric perturbations with $q = 3$, which is neutrally stable at the turning points, grows between the turning points as it should. For non-fundamental axially symmetric modes (section 3.5), this conjecture holds in the vicinity of the turning point $a^{(1)}$ but is violated in the vicinity of $a^{(2)}$. It follows that this conjecture, while being valid for arc cathodes, in a general case does not apply to glow discharge. The latter explains why steady-state modes with loops, which are forbidden in the case of arc cathode, do occur in the case of glow discharge (e.g., the non-fundamental axially symmetric modes).

The question of existence of stable steady-state axially symmetric self-organized patterns in circular domains is of considerable theoretical interest; see, e.g., discussion in [50]. As far as gas discharges are concerned, axially symmetric self-organized patterns have been observed, in particular, on anodes of glow discharge [25, 28] and in dielectric barrier discharge [50]. It seems that such patterns have been observed also on cathodes of microdischarges in Xe; the upper-left image in figure 3 of [20] and the middle image in figure 4 of [24]. Since, according to the above, axially symmetric self-organized steady-state patterns on cathodes of microdischarges in Xe may be also theoretically stable, it would be very interesting to address this question by means of special experiments.

In general, results given by the accurate stability theory confirm intuitive concepts developed in the literature and conform to the experiment. On the other hand, the theory provides suggestions for further experimental and theoretical work.

Modelling of this work has been performed with account of the simplest mechanisms of glow discharges, which are charge separation, ionization, recombination, drift and diffusion of charged particles, and with electron transport and kinetic coefficients evaluated in the local approximation. This is in part justified by successful application of this approach to modelling of self-organization in DBD's [51, 59, 60, 81] and of formation and propagation of filamentary plasma arrays in high-power microwave breakdown at atmospheric pressure [131, 132], and also by the fact that an account of a more complex chemistry and non-locality of electron coefficients does not affect steady-state solutions qualitatively [129]. Nevertheless, it is desirable to take the latter effects in account also in the investigation of stability. Another possible direction of future work is investigation of stability of 3D steady-state modes with multiple spots, observed in the experiments [20–24].

Chapter 4

Bifurcations of current transfer to cathodes of glow and arc discharges

Bifurcations and/or their consequences are frequently encountered in numerical modelling of current transfer to cathodes of gas discharges, also in apparently simple situations, and a failure to recognize and properly analyze a bifurcation may originate difficulties in the modelling and hinder understanding of numerical results and the underlying physics. This chapter is concerned with analysis of bifurcations that have been encountered in the modelling of steady-state current transfer to cathodes of glow and arc discharges. All basic types of steady-state bifurcations (fold, transcritical, pitchfork) have been identified and analyzed. The analysis provides explanations to many results obtained in numerical modelling. In particular, it is shown that dramatic changes of patterns of current transfer to cathodes of both glow and arc discharges, described by numerical modelling, occur through perturbed transcritical bifurcations of first and second order contact. The analysis elucidates the reason why the mode of glow discharge associated with the falling section of the CVC in the solution of von Engel and Steenbeck seems not to appear in 2D numerical modelling and the subnormal and normal modes appear instead. A similar effect has been identified in numerical modelling of arc cathodes and explained.

4.1 Introduction

Bifurcations of current transfer to cathodes of DC gas discharges or their consequences are sometimes encountered in apparently simple situations. The examples given in section 1.2.2 show that a failure to recognize and properly analyze a bifurcation may originate difficulties in numerical modelling and hinder understanding of numerical results and the underlying physics. In more general terms, the importance of understanding of bifurcations of steady-state current transfer to cathodes of gas discharges may be explained as follows.

Powerful solvers of nonlinear multidimensional differential equations that exist nowadays can be used for finding multiple solutions in the same way as unique ones, provided, however, that one knows that multiple solutions do exist, where they should be sought, and what they are like. Bifurcation analysis is a powerful means of obtaining such qualitative information. Of course, this qualitative information also facilitate analysis and understanding of obtained numerical results and underlying physics. One more reason to study bifurcations of current transfer to cathodes of DC gas discharges is their intimate relation to stability of different steady-state modes.

In order to illustrate the above statements, one can mention a few examples in addition to those given in section 1.2.2. A study of symmetry-breaking bifurcations, such as branching of 2D and 3D solutions from 1D solutions or of 3D solutions from 2D solutions, is probably the simplest way of proving existence of multiple solutions to nonlinear multidimensional differential equations and of establishing the pattern of these solutions including conditions of their existence, thus paving way to finding these solutions numerically. In fact, this is how multiple solutions describing different modes of DC current transfer to both arc and glow cathodes have started to appear. Another example is represented by variations of pattern of steady-state modes of current transfer to arc cathodes under conditions of industrial interest that will be described in chapter 5. As one more example, one can mention the fact that, as will be shown in this chapter, reasoning based on the bifurcation theory provides useful information on behavior of different steady-state modes of current transfer to arc cathodes in the vicinity of turning points.

This chapter is concerned with analysis of bifurcations that have been encountered in numerical modelling of current transfer to cathodes of DC glow and arc discharges. Relevant details of the statement of the problem and of the numerics are discussed in section 4.2. Bifurcations exhibited by multiple solutions describing different modes of current transfer to cathodes of DC glow and arc discharges are identified in section 4.3. Fold, transcritical, and pitchfork bifurcations are analyzed in sections 4.4, 4.5, and 4.6, respectively. The results obtained are discussed in section 4.7 and conclusions summarized in section 4.8. For convenience, a short summary of relevant information from the general bifurcation theory is given in appendix B.

4.2 Models and numerics

As in chapters 3 and 2, the calculation domain is the interelectrode gap in the case of glow discharge and the body of a thermionic cathode in the case of arc discharge, respectively. It is assumed to be a circular cylinder of a radius R and a height h (except in the case of an arc cathode treated in section 4.5.3 where it has a hemispherical tip).

In the case of a glow discharge, the distribution of the ion and electron densities n_i and n_e and the electrostatic potential φ in the interelectrode gap is governed by the model described in sections 3.2.1 and 3.2.2, except the boundary condition for the charged particles densities at the wall that will be described below. Numerical results reported in this chapter refer to a microdischarge in xenon under the pressure of 30 Torr with $R = 1.5$ mm and $h = 0.5$ mm. Kinetic and transport coefficients are the same as in chapter 3.

The simulation of the interaction of high-pressure arc plasmas with thermionic cathodes is performed by means of the model described in section 2.2.2, except that the second boundary condition in equation (2.2) is valid only at the front surface of the cathode; a boundary condition at the lateral surface will be described below. Numerical results reported in this chapter have been obtained for a tungsten cathode, with $R = 2$ mm and $h = 10$ mm, and an argon plasma under pressure of 1 bar. All the results refer to a temperature of the cooling fluid of 293 K unless otherwise specified. Thermal conductivity of the cathode material and functions $q(T, U)$ and $j(T, U)$ are the same as in chapter 2.

As in previous chapters, we introduce cylindrical coordinates (r, ϕ, z) with the axis z coinciding with the axis of the calculation domain and with the origin at the center of the surface of the glow cathode or at the center of the front surface of the arc cathode. In the case of glow discharge, the boundary conditions for the charged particle densities at the wall are written in the form

$$r = R : \quad s \frac{n_{i,e}}{R} + (1 - s) \frac{\partial n_{i,e}}{\partial r} = 0, \tag{4.1}$$

where s is a given parameter that varies between 0 and 1. $s = 0$ corresponds to a (totally) reflecting wall. $s = 1$ corresponds to an absorbing wall. In the case of arc cathode, the boundary condition at the lateral surface of the cathode is written as

$$r = R : \quad \kappa \frac{\partial T}{\partial r} = s\, q(T, U), \tag{4.2}$$

where s again is a given parameter varying between 0 and 1. $s = 0$ corresponds to the lateral surface of the cathode being thermally (and electrically) insulated, $s = 1$ corresponds to the lateral surface being active, i.e., energy- and current-collecting.

In the case of the arc cathode, the discharge current is related to T and U by the formula

$$I = \int j(T, U)\, dS. \tag{4.3}$$

The integral here is evaluated over the front and lateral surfaces of the cathode, the contribution of the lateral surface being multiplied by s. In this chapter, bifurcations and stability will be discussed under the assumption that the discharge is current-controlled.

As discussed in the previous two chapters, the above-stated problems admit axially symmetric (2D) solutions, $f = f(r, z)$, 3D solutions, $f = f(r, \phi, z)$, and, in the particular case $s = 0$, also 1D solutions, $f = f(z)$. Here f designates the set of quantities n_i, n_e, φ in the case of glow discharge and T in the case of arc cathode. In this chapter, 1D and 2D steady-state solutions for the glow discharge and 1D, 2D, and 3D solutions for the arc cathode are considered. Solutions for the glow discharge and 3D solutions for the arc cathode were calculated with the use of the commercial finite element software COMSOL Multiphysics. 1D and 2D solutions for the arc discharge were calculated with the use of the tool [90] except in the case of an arc cathode with a hemispherical tip, treated in section 4.5.3, where COMSOL Multiphysics was employed.

The above-stated problems possess axial symmetry, i.e., are invariant with respect to the transformation of rotation $\phi \to \phi + \alpha$, where α is any constant (a rotation angle). As already discussed in section 2.3, if any of these problems admits a solution $f = f(r, \phi, z)$, then $f = f(r, \phi + \alpha, z)$ is a solution as well. 3D solutions reported in this chapter have been obtained as described in section 2.3: the calculation domain was restricted to half of the cathode, say, $0 \leq \phi \leq \pi$, and the symmetry condition $\partial T/\partial \phi = 0$ was imposed at the plane $\{\phi = 0, \phi = \pi\}$. Of course, this approach allows one to find only solutions that possess planar symmetry. We will come back to this point at the end of section 4.7.

Data on points of transcritical and pitchfork bifurcations of steady-state solutions reported in this chapter were obtained as follows. In the case of glow discharge, one of the bifurcating solutions is 1D and the other is 2D (these bifurcations will be designated $\{1D, 2D\}$ from now on) and the bifurcation points were found by means of solving the eigenvalue problem described in section 3.2.3 with the use of COMSOL Multiphysics. In the case of arc cathode, bifurcations $\{1D, 2D\}$, $\{1D, 3D\}$, $\{2D, 2D\}$, $\{2D, 3D\}$, and $\{3D, 3D\}$ are present. Points of bifurcations $\{1D, 2D\}$, $\{1D, 3D\}$, and $\{2D, 3D\}$ were calculated with the use of the tool [90], points of bifurcations $\{2D, 2D\}$ and $\{3D, 3D\}$ were calculated with the use of COMSOL Multiphysics.

The procedure of calculation of bifurcation points with the use of the tool [90] is as follows. The determinant of a finite-difference problem approximating the 2D differential eigenvalue problem governing axially symmetric and 3D perturbations of the axially symmetric solution is evaluated for different steady states. If the determinant changes its sign between two states, this means that a bifurcation occurs between them.

Bifurcation points calculated with the use of COMSOL Multiphysics have been found as follows. The spectrum is calculated for different steady states. If a real eigenvalue changes its sign between two states, this means that a bifurcation occurs between then. We note right now that calculated positions of bifurcation points in all the cases are in good agreement with results of numerical calculations of steady-state solutions, as evidenced by the graphs that will follow.

Data on stability of current transfer to arc cathodes reported in this chapter were obtained by means of solving the eigenvalue problem described in section 2.2.3 with the use of COMSOL Multiphysics as described in section 2.3.

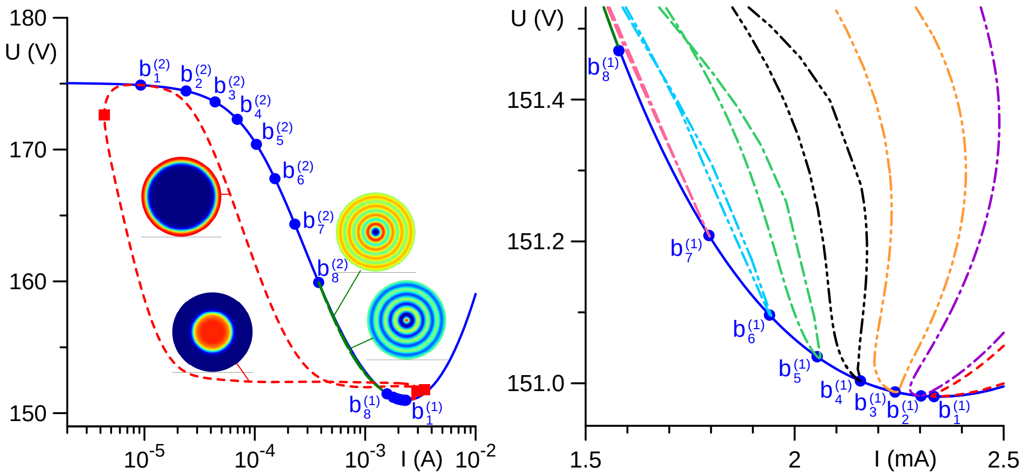

(a) (b)

Figure 4.1: CVC's of different modes of current transfer in glow discharge with reflecting walls and schematics of current density distribution over the cathode surface. (a) The 1D glow discharge and the first and eighth 2D spot modes. The CVC of the eighth 2D spot mode coincides, to the graphical accuracy, with the CVC of the 1D glow discharge, also in figure (b). (b) CVC's in the vicinity of the point of minimum of the CVC of the 1D glow discharge.

4.3 Identifying bifurcations encountered

4.3.1 1D modes and modes bifurcating from it

An appropriate way to analyze multiple steady-state solutions is to start with the limiting case $s = 0$ (the case of reflecting wall of the glow discharge tube or of insulating lateral surface of arc cathode), where the pattern of solutions is the easiest to understand. CVC's for this case are shown in figures 4.1 and 4.2. Squares and circles in these and following figures in the this chapter represent turning points and, respectively, all the other bifurcation points. Also shown in these figures are schematics of distributions of current density over the cathode surface associated with each solution. (In the case of arc cathode, only distributions along the front surface are shown.) The solid line in each figure represents the 1D solution, which describes a mode of current transfer with a uniform distribution of discharge parameters along the cathode surface. (In the case of glow discharge, the 1D solution is the same as the one depicted by the dashed line in figure 1.2 and the one depicted in figure 3.2.) In the theory of the arc cathodes, the mode with an uniform distribution of discharge parameters along the current-collecting surface of the cathode is called diffuse. As before, the mode described by the 1D solution will be called fundamental mode both in the cases of arc cathode and glow discharge, however the terms diffuse mode and 1D glow discharge will also be used.

There is also a number of 2D and 3D solutions describing different spot modes. While

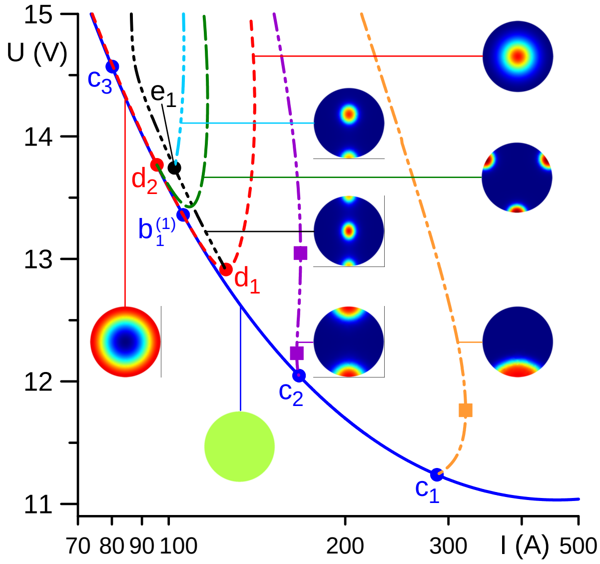

Figure 4.2: CVC's of steady-state modes of current transfer to arc cathode with insulating lateral surface and schematics of current density distribution over the front surface of the cathode.

the fundamental mode exists at all currents, each of the spot (non-fundamental) modes exists in a limited current range.

In the case of glow discharge, eight 2D spot modes were detected. Let us number these modes in the order of shrinking of the range of currents in which they exist. The first and eighth modes, i.e., those with the widest and, respectively, narrowest ranges of existence are shown in the figure 4.1a. Each mode joins the fundamental mode at two bifurcation points, one of these points being designated $b_i^{(1)}$ and positioned in the vicinity of the point of minimum of the CVC of the fundamental mode, at $1.5 \lesssim I \lesssim 2.5\,\mathrm{mA}$ (figures 4.1a and 4.1b) and the other, $b_i^{(2)}$, at low currents, $I \lesssim 0.4\,\mathrm{mA}$ (figure 4.1a); here $i = 1, 2, \ldots, 8$. Let us number bifurcation points $b_i^{(1)}$ from high to low currents, as shown in figure 4.1b, and $b_i^{(2)}$ from low to high currents, as shown in figure 4.1a. (Note that this classification does not have the same meaning that the one used in chapter 3 since in this chapter only 2D spot modes are considered.) A 2D spot mode which branches off from the fundamental mode at a bifurcation point $b_i^{(1)}$ (or $b_i^{(2)}$) re-joins the fundamental mode at the bifurcation point $b_i^{(2)}$ (or, respectively, $b_i^{(1)}$) with the same number i. In the following, values of discharge current that correspond to the bifurcation points $b_i^{(1)}$ and $b_i^{(2)}$ will be designated $I\left(b_i^{(1)}\right)$ and, respectively, $I\left(b_i^{(2)}\right)$.

The bifurcation points divide each 2D spot mode into two branches, one associated with patterns consisting of a spot at the center and possibly concentric ring spots, and the other associated with patterns consisting of concentric ring spots without a spot at the center. The number of inside ring spots (i.e., the number of maxima of the current density inside the interval $0 < r < R$) associated with an i-th mode is $(i-1)/2$ if i is odd. If i is even, the number of inside ring spots is $i/2-1$ on the branch with central spot and $i/2$ on the branch without central spot. There is also a ring spot on the periphery of the cathode (i.e., there is a maximum of the current density at $r=R$) on the branch with or, respectively, without central spot depending on whether i is even or odd.

In the case of arc cathode depicted in figure 4.2, some spot modes join the fundamental mode and some do not. The mode that branches off from the fundamental mode at the bifurcation point $b_1^{(1)}$ is 2D. The CVC of this mode is depicted by the short-dash line and partially coincides with the CVC of the fundamental mode. This mode represents an analog of the first 2D spot mode in the case of glow discharge and comprises two branches separated by the bifurcation point, one associated with a spot at the center of the front surface of the cathode and the other with a ring spot on the periphery. Families of 3D modes with one spot on the periphery, or two spots on the periphery opposite each other, or three symmetrically positioned spots on the periphery branch off from the fundamental mode at the bifurcation points c_1, c_2, and c_3, respectively; the family of modes with three spots that branches off at the point c_3 is not shown in order not to overload the figure.

Comparing figures 4.1 and 4.2, one can say that the current and voltage range shown in figure 4.2 represents the vicinity of the point of minimum of the CVC of the fundamental mode. In other words, the spot modes in the case of arc cathode branch off from the fundamental mode in the vicinity of the point of minimum, similarly to how it happens in the case of glow discharge. A question arises whether they re-join the fundamental mode at low currents. The range of currents down to 0.3 A (voltages of up to 1 kV) was investigated in order to answer this question. No re-joining was found (see in this connection discussion in section 3.4.2); rather branching of two new families of 3D spot modes was detected: modes with four spots at the periphery, then modes with a spot at the periphery and an inside spot positioned opposite each other.

The three dot-dashed line in figure 4.2 represents a family of 3D modes with a spot at the center and two spots on the periphery positioned opposite each other, which branches off from the first 2D spot mode at the bifurcation point d_1. Note that patterns associated with this family possess planar symmetry with respect to two orthogonal axes; e.g., the pattern shown in figure 4.2 is symmetric with respect to the horizontal and vertical axes. One can say that this family branches off from the fundamental mode not directly but rather through the chain of sequential bifurcations which occur at points $b_1^{(1)}$ and d_1.

The long-dash line in figure 4.2 represents a family of 3D modes with three symmetrically positioned spots on the periphery, which branches off from the first 2D spot mode at the bifurcation point d_2 or, as one can say, branches off from the fundamental mode through the chain of sequential bifurcations which occur at points $b_1^{(1)}$ and d_2. The absence of a central spot in patterns associated with this mode is a consequence of the bifurcation point d_2 being positioned on the branch without central spot of the first 2D spot mode.

Another family branches off from the above-described family of 3D modes with a spot at the center and two spots on the periphery at the bifurcation point e_1. This family is depicted by the four dot-dashed line and is associated with patterns that possess planar symmetry with respect to one axis and comprise two spots positioned opposite each other, one of these spots being at the periphery and the other an inside spot. Again, one can say that the family being considered branches off from the fundamental mode not directly but rather through the chain of sequential bifurcations which occur at points $b_1^{(1)}$, d_1, and e_1.

The above results refer to the limiting case of reflecting wall of the glow discharge tube or insulating lateral surface of arc cathode, $s = 0$. Results of numerical calculations of multiple modes for the case of absorbing wall of the glow discharge tube or energy- and current-collecting lateral surface of arc cathode, $s = 1$, can be found in [128] or, respectively, [89] (these results are cited in chapter 3 and 2). 1D modes do not exist in this case. There are several disconnected 2D modes, one existing at all currents and the others in limited current ranges, and 3D modes existing in limited current ranges.

4.3.2 Bifurcations encountered

The numerical solutions shown in figures 4.1 and 4.2 manifest a large number of bifurcations of different types (a brief description of basic types of steady-state bifurcations is given in appendix B). Many of these bifurcations are fold, i.e., turning points; as an example, turning points of the first 2D spot mode are marked in figure 4.1a and turning points of the 3D modes with one and two spots at the periphery are marked in figure 4.2. All the bifurcations that are not fold involve branching of modes of different symmetries: 2D modes branch off from the 1D modes at the bifurcation points $b_1^{(1)}$, $b_2^{(1)}$, ..., $b_8^{(1)}$, $b_1^{(2)}$, $b_2^{(2)}$, ..., $b_8^{(2)}$ in figure 4.1 and $b_1^{(1)}$ in figure 4.2; 3D modes branch off from the 1D mode at the bifurcation points c_1, c_2, and c_3 in figure 4.2; 3D modes branch off from the 2D mode at the bifurcation point d_1 and d_2 in figure 4.2; 3D modes with the period 2π branch off from 3D modes with the period π at the bifurcation point e_1 in figure 4.2.

A bifurcation $\{2D, 3D\}$ represents breaking of axial symmetry: a continuum of non-symmetric solutions, which are related by the transformation of rotation, branches off from an axially symmetric solution. This must be a pitchfork bifurcation similar to those described by equation (B.7) in section B.0.1 and shown in figures B.1c and B.1d, with the difference that the number of bifurcating solutions is infinite in the present case.

A bifurcation $\{1D, 2D\}$ represents breaking of symmetry of another kind: invariance with respect to translations in the radial direction. This invariance is a property of a particular mode rather than of the problem, therefore only one 2D mode bifurcates here. In other words, this bifurcation involves two modes and is transcritical. Since there are no reasons for the modes to be tangent at the bifurcation point, this should be a transcritical bifurcation of first order contact, described by equation (B.6) and shown in figure B.1b.

Breaking of invariance with respect to translations in the radial direction occurs also in a bifurcation $\{1D, 3D\}$. However, this bifurcation represents simultaneously breaking of axial symmetry. Therefore, a continuum of 3D modes which are related by the transformation of rotation bifurcates here and the bifurcation must be pitchfork.

The bifurcation $\{3D, 3D\}$ represents breaking of planar symmetry: two 3D modes possessing planar symmetry with respect to only one (and the same) axis branch off from each 3D mode possessing planar symmetry with respect to two orthogonal axes. This bifurcation again must be pitchfork.

In the vicinity of turning points, the topology of CVC's shown in figures 4.1 and 4.2 is similar to that illustrated by figure B.1a (or by its reflection with respect to the x_0-axis). As far as transcritical bifurcations of first order contact are concerned, one should expect to encounter intersecting lines as shown in figure B.1b. However, no intersections at points $b_i^{(1)}$ and $b_i^{(2)}$ are seen in figures 4.1 and 4.2. Furthermore, in cases where the resolution is sufficient, as is the case of bifurcation points $b_1^{(2)}$ in figure 4.1a and $b_1^{(1)}$ in figure 4.2, one can clearly see that CVC's of the fundamental mode and the 2D spot modes are tangent at the bifurcation point rather than intersect. Similarly, the topology of CVC's in the vicinity of bifurcation points c_1, c_2, d_1, and e_1 in figure 4.2 is clearly different from that of pitchfork bifurcations shown in figures B.1c or B.1d.

The above differences are not surprising, since not every functional relation can play the role of a bifurcation diagram in problems with an infinite number of degrees of freedom. Bifurcations involving axially symmetric modes may be conveniently represented in the coordinates (I, j_c), where j_c is the current density at the center of the cathode. This representation is used in figure 4.3 in the case of glow discharge. (A convenient feature of this representation is a possibility of easy identification of branches with or without central spot: they are positioned above or, respectively, below the fundamental mode.) As far as 3D modes are concerned, each continuum would be represented by a single line in these coordinates, just in the same way as in the CVC plane (I, U). Adequate and convenient for 3D modes are coordinates (I, j_e), where j_e is the current density at a fixed point at the edge of the front surface of the cathode, say, at $(r = R, \phi = 0, z = 0)$. This representation is used in figure 4.4 in the case of arc cathode. Only two limiting lines are shown for each continuum of 3D modes, one corresponding to the case where the temperature distribution over the edge of the front surface of the cathode, $T(R, \phi, 0)$, has at $\phi = 0$ a maximum and the other a minimum. The families of modes with three spots on the periphery that branch off at the points c_3 and d_2 are not shown in order not to overload the figure.

The solid lines in figures 4.3 and 4.4 represent the fundamental mode as before. One can see that the topology of the modes in the vicinity of the bifurcation points $b_i^{(2)}$ in figure 4.3a and $b_1^{(1)}$ in figure 4.4 indeed is similar to that illustrated by figure B.1b (or by its reflection with respect to the μ-axis) and the topologies of the modes in the vicinity of the bifurcation points c_1 and d_1 in figure 4.4 are similar to those shown in figures B.1c or B.1d. Appropriate amplifications show that the topologies of the modes in the vicinity of

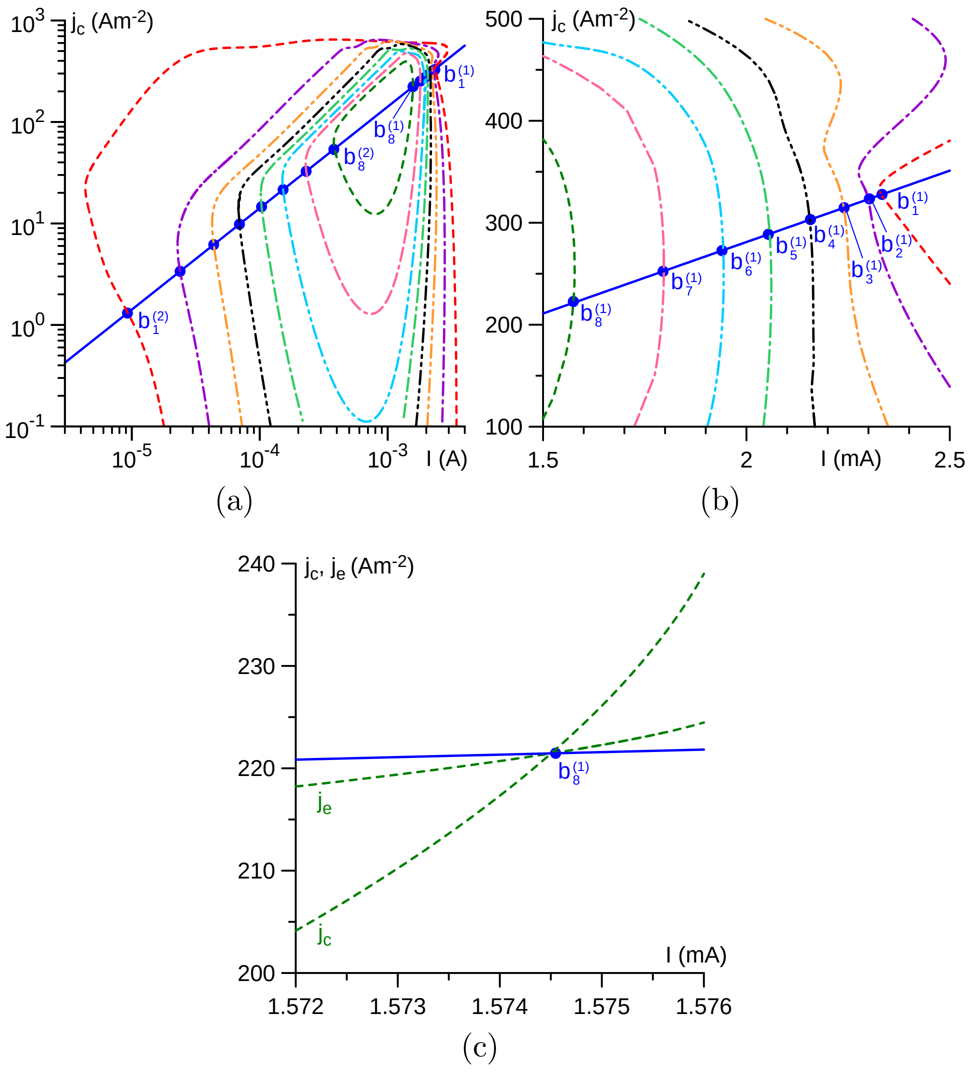

Figure 4.3: Bifurcation diagram. Glow discharge, $s = 0$. (a) General view. (b) Details in the vicinity of the point of minimum of the CVC of the 1D glow discharge. (c) Details in the vicinity of the bifurcation point $b_8^{(1)}$ of figure (b).

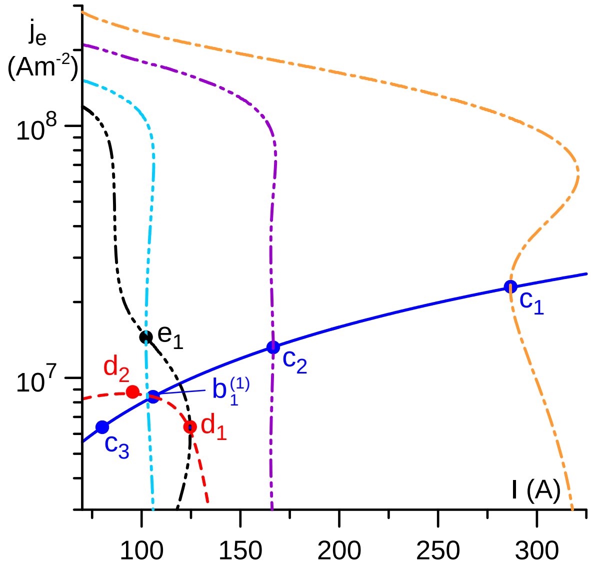

Figure 4.4: Bifurcation diagram. Arc cathode, $s = 0$.

the bifurcation points in figure 4.3b and points c_2 and e_1 in figure 4.4 are similar to those shown in figures B.1b and, respectively, B.1c or B.1d. An example of such amplification is shown in figure 4.3c. Also shown in the latter figure is the current density at the periphery of the cathode. One can see that the current densities at the center and at the periphery become equal at the bifurcation point as they should.

Note that the plateau in the dependence $j_c(I)$ corresponding to the first 2D spot mode in figure 4.3a is a manifestation of the effect of normal current density, as is the plateau in the CVC of the first 2D spot mode in figure 4.1a. This effect is manifested also by higher modes, however it weakens with increase of the order of the mode and finally disappears.

In the following sections, the bifurcations identified above will be discussed in some detail. Also discussed will be transcritical bifurcations of second order contact: $\{1D, 2D\}$, encountered in the modelling of glow discharge [128], and $\{2D, 2D\}$ encountered in the modelling of arc cathodes of complex shapes described in chapter 5.

4.4 Fold bifurcations

A fold, or saddle-node, bifurcation represents not branching of essentially different modes but rather a turning point of the same mode. The importance of understanding these bifurcations originates in their relation with stability of current-controlled discharges. This relation may be explained as follows. Let $f = \tilde{f}(\mathbf{r}; U)$ be a family of solutions describing a particular steady-state mode of current transfer. (Here $\mathbf{r}$ is the space vector and f designates as before the set of quantities n_i, n_e, φ in the case of glow discharge and T in the case of arc cathode.) Suppose that one substitutes $f = \tilde{f}(\mathbf{r}; U)$ into the governing boundary-value problem with the discharge current I being the control parameter, and differentiates the obtained equations and boundary conditions with respect to U. One will arrive at a problem comprising a linear boundary-value problem for the function $\frac{\partial \tilde{f}(\mathbf{r};U)}{\partial U}$ and an expression for parameter $\frac{DI}{DU}$ in terms of the function $\frac{\partial \tilde{f}(\mathbf{r};U)}{\partial U}$, where $\frac{DI}{DU}$ is the derivative evaluated along the steady-state mode being considered. At a turning point, this derivative vanishes and the former problem may be viewed as a homogeneous problem for the function $\frac{\partial \tilde{f}(\mathbf{r};U)}{\partial U}$ supplemented with a normalization condition for this function. This homogeneous problem coincides with the eigenvalue problem governing stability against small perturbations of a current-controlled discharge with the growth increment equal to zero. Thus, at a turning point the function $\frac{\partial \tilde{f}(\mathbf{r};U)}{\partial U}$ represents an eigenfunction of the stability problem associated with the zero eigenvalue (growth increment). In a general case, this means that a steady-state mode of current transfer in a current-controlled discharge at a turning point changes stability against a mode of perturbations that at the turning point is described by the function $\frac{\partial \tilde{f}(\mathbf{r};U)}{\partial U}$. In the following, this perturbation mode will be referred to as fundamental.

As already mentioned in chapter 3, a nonlinear electric circuit with inductance is stable if the total differential resistance of the circuit is positive. By analogy, one can assume that a steady state belonging to the falling section of the CVC of any mode of a gas discharge is stable if the external resistance (ballast) is high enough to compensate the negative differential resistance of the discharge in the state in question. Applying this criterion to the limiting case of a current-controlled discharge, where the external resistance is very high, one arrives at the following rule: if a turning point in the plane (I, U) is traversed in the clockwise direction, states before the turning point are stable against the fundamental perturbation mode (in other words, the increment of this perturbation mode is negative) and states after the turning point are unstable (the increment is positive); if the turning point is traversed in the counterclockwise direction, states before the turning point are unstable and states after it are stable. This rule is illustrated by figure 4.5. Note that scenarios a and b in figure 4.5 conform to the second and, respectively, third scenarios of the fold bifurcation mentioned in section B.0.2.

An alternative formulation of the above rule is as follows: the CVC of a steady-state mode which is stable against perturbations of the fundamental mode can turn only clockwise, after which the steady-state mode becomes unstable; the CVC of an unstable mode can turn only counterclockwise, after which the mode becomes stable.

In the case of arc cathode, an independent proof of the above rule was given in the analytical stability theory [118]. However, this rule is inapplicable in the case of the glow discharge as discussed in section 3.6.

It happens frequently that a steady-state mode manifests more than one turning point. According to the above, there is a change of stability at each point against a mode of perturbations that at the turning point is described by the function $\frac{\partial \tilde{f}(\mathbf{r};U)}{\partial U}$. It seems legitimate to assume that the perturbation mode against which the change of stability

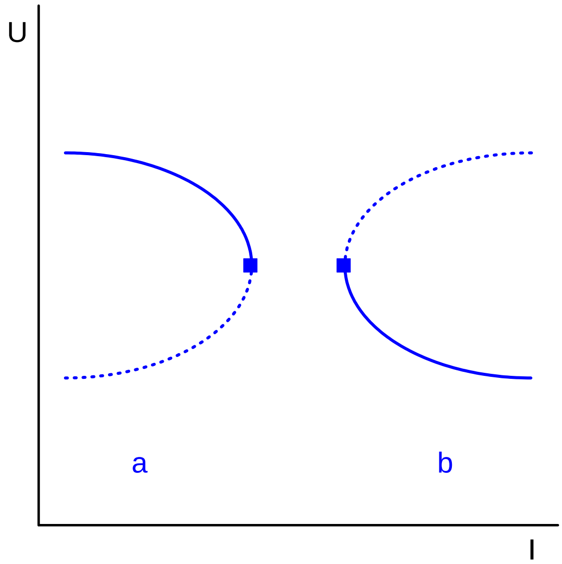

Figure 4.5: Hypothetical pattern of changes of stability of a steady-state mode of current transfer to arc cathode in the vicinity of a turning point against the fundamental perturbation mode. Solid: stable section of the steady-state mode. Dotted: unstable section.

occurs is the same for all turning points of the steady-state mode in question or, in other words, that there is only one fundamental perturbation mode for each steady-state mode. Indeed, this assumption is confirmed by the numerical modelling both in the cases of arc cathode and glow discharge. Then the changes of stability against the fundamental perturbation mode alternate at consecutive turning points: if a steady-state mode has become stable (unstable) on passing through a turning point, it will become unstable (stable) on passing through the next one.

In the case of arc cathode, directions of turns must alternate: a clockwise turn at one turning point is followed by a counterclockwise turn at the next one and *vice versa*; 360°-loops cannot occur. Possible scenarios of passing through two consecutive turning points are shown in figure 4.6 and comprise a Z-shape (scenario a) and an S-shape (scenario b).

The above reasoning refers to the case of a current-controlled discharge. A similar reasoning may be developed for the case of a voltage-controlled discharge, with an application to the behavior of steady-state modes in the vicinity of extrema of the CVC. The conclusion is similar to the above one: a steady-state mode which is stable against perturbations of the fundamental mode can turn only clockwise, and an unstable mode can turn only counterclockwise. However, this line of reasoning seems to give only trivial results.

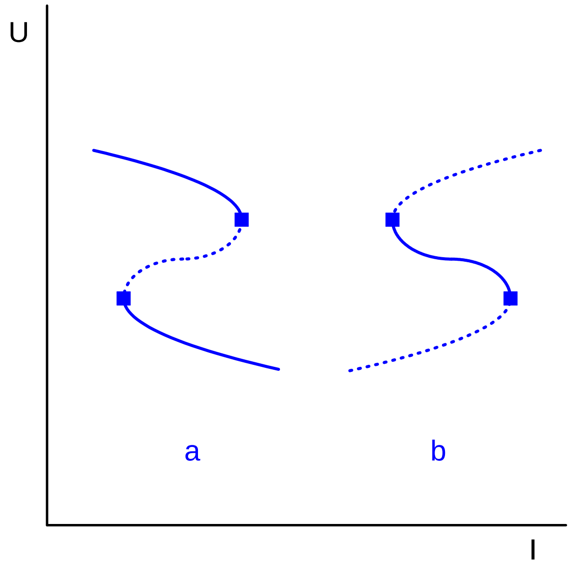

Figure 4.6: Scenarios of passage of a steady-state mode of current transfer to an arc cathode through two consecutive turning points. Solid: sections of the steady-state mode that are stable against the fundamental perturbation mode. Dotted: unstable sections.

4.5 Transcritical bifurcations

4.5.1 Transcritical bifurcations of first order contact

Transcritical bifurcations $\{1D, 2D\}$ were studied in [95] for a glow discharge and in [91] for an arc cathode. In both cases, distribution of discharge parameters associated with the bifurcating 2D mode is given in the vicinity of bifurcation points $b_i^{(1)}$ and $b_i^{(2)}$ $(i = 1, 2, \dots)$ by the formula

$$\tilde{f}^{(2D)}(r, z; U) = \tilde{f}^{(1D)}(z; U) + B_i(z)\ J_0\left(j'_{0,i+1}\frac{r}{R}\right)(U - U_i) + C_i(r, z)(U - U_i)^2 + \dots, \quad (4.4)$$

where $\tilde{f}^{(1D)}(z; U)$ and $\tilde{f}^{(2D)}(r, z; U)$ are solutions describing the fundamental and, respectively, 2D spot modes bifurcating at the point considered, $B_i(z)$ and $C_i(r, z)$ are functions of z and, respectively, r and z (or, in the case of glow discharge, a set of functions of z and, respectively, a set of functions of r and z) which depend on the bifurcation point being considered, U_i is the value of the voltage corresponding to the bifurcation point, $J_\nu(x)$ and $j'_{\nu,m}$ designate Bessel functions and zeros of their derivatives as before. The conclusion that in the vicinity of a bifurcation point radial variations of discharge parameters in the bifurcating 2D mode are proportional to $J_0\left(j'_{0,i+1}r/R\right)$ conforms to results of the numerical modelling. For the case of arc cathode, the function $B_i(z)$ was analytically calculated and thus the second term of expression (4.4). The obtained two-term analytic approximation in the vicinity of the bifurcation point $b_1^{(1)}$ shown in figures 4.2 and 4.4 is depicted by the dashed line in figure 4.7 and conforms to the numerical modelling as it should.

The behavior which is typical for transcritical bifurcations of first order contact and shown in figure B.1b originates in the second term of the expression (4.4). When the

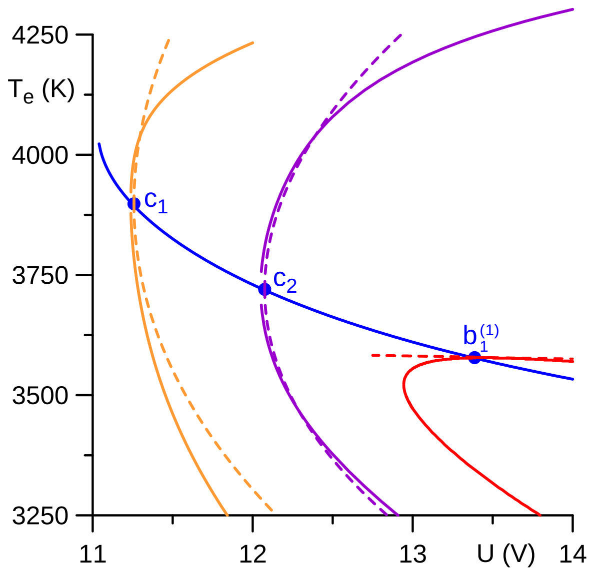

Figure 4.7: Bifurcations $\{1D, 2D\}$ and $\{1D, 3D\}$. Arc cathode, $s = 0$. Solid: numerical modelling. Dashed: analytic approximations.

expression is averaged over the cathode surface, the contribution of this term vanishes, which follows from the fact that this term was obtained [91, 95] by solving the Neumann problem for the Helmholtz equation and the average value of such solutions is zero. (Of course, this can be derived also from properties of integrals of the Bessel functions.) This explains why CVC's do not represent a proper diagram of transcritical bifurcations in the considered problem, and also why CVC's of the fundamental and 2D spot modes are tangent at the bifurcation point as seen in figures 4.1 and 4.2.

Results of a numerical investigation of stability of the fundamental (1D) and 2D spot modes of current transfer to an arc cathode and of an analytical investigation of stability of the fundamental mode, reported in section 2.4.2, have revealed an exchange of stability in the vicinity of points of transcritical bifurcation of first order contact, which is similar to the one occurring in systems with one degree of freedom and illustrated by figure B.1b. This exchange is realized as follows: at a bifurcation point, i.e., at $I = I\left(b_i^{(1)}\right)$, both the fundamental mode and the 2D spot mode that branches off at $b_i^{(1)}$ are neutrally stable against a 2D perturbation mode with a radial dependence described by the function $J_0\left(j'_{0,i+1}r/R\right)$; the fundamental mode is stable and the 2D spot mode is unstable at $I > I\left(b_i^{(1)}\right)$; and *vice versa* at $I < I\left(b_i^{(1)}\right)$.

Results of the numerical modelling described in chapter 2 indicate that the above-mentioned 2D perturbation mode that is neutrally stable at $b_i^{(1)}$ is the same one that changes sign of its increment at all turning points of the steady-state 2D spot mode that branches off at $b_i^{(1)}$. In other words, it represents the fundamental perturbation mode of the steady-state 2D spot mode in question. Note that this perturbation mode, while being proportional to $J_0\left(j'_{0,i+1}r/R\right)$ in all states of the fundamental mode, is no longer propor-

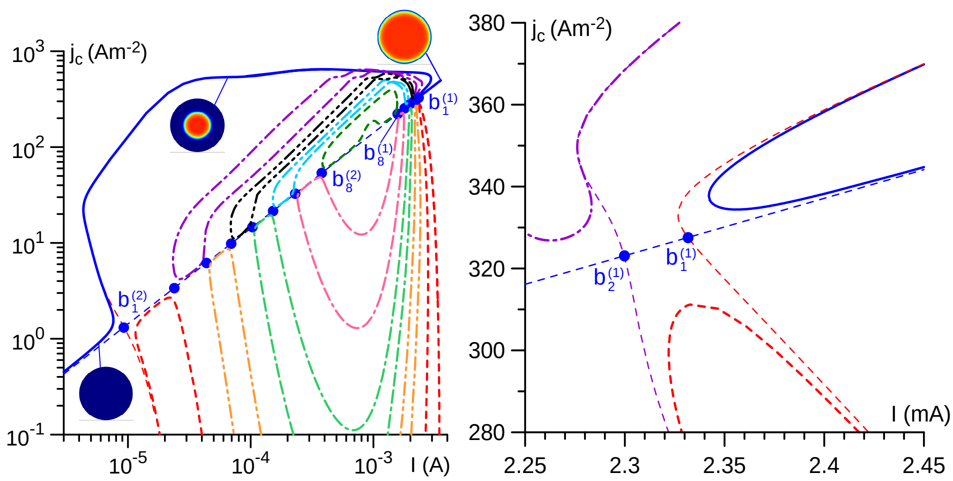

(a) (b)

Figure 4.8: Bifurcation diagram and schematics of current density distribution over the cathode surface in the fundamental mode. Perturbed transcritical bifurcation of first order contact, glow discharge. (a) General view, $s = 0.05$. (b) Details in the vicinity of the point of minimum of the CVC of the fundamental mode, $s = 0.01$.

tional to $J_0\left(j'_{0,i+1} r/R\right)$ in states of the 2D steady-state spot mode outside the bifurcation point $b_i^{(1)}$.

4.5.2 Perturbed transcritical bifurcations of first order contact

Analysis of the preceding section refers to the limiting case $s = 0$ (reflecting wall of a glow discharge tube and insulating lateral surface of an arc cathode). Deviations of s from zero represent imperfections that should break the bifurcations as described in section B.0.3. This is indeed found in the numerical modelling as shown in figures 4.8 and 4.9. Values of s chosen for figures 4.8a, 4.8b, and 4.9 are all different in order that diagrams be transparent. Also shown in these figures are the fundamental mode and the first 2D spot mode for $s = 0$, and in figure 4.8b also the second 2D spot mode for $s = 0$ is shown.

The effect of imperfection at each bifurcation point is the same as discussed in section B.0.3 and shown in figure B.2a: two bifurcating solutions are broken into two isolated solutions with the branches exchanged. In the case of glow discharge, the first scenario discussed in section B.0.3 and illustrated by figure B.2a with $\delta \geq 0$ takes place at bifurcation points $b_2^{(1)}$, $b_4^{(1)}$, $b_6^{(1)}$, $b_7^{(1)}$, $b_1^{(2)}$, $b_3^{(2)}$, $b_5^{(2)}$, $b_7^{(2)}$ and the second scenario (figure B.2a with $\delta \leq 0$) occurs at $b_1^{(1)}$, $b_3^{(1)}$, $b_5^{(1)}$, $b_8^{(1)}$, $b_2^{(2)}$, $b_4^{(2)}$, $b_6^{(2)}$, $b_8^{(2)}$. The sections of the fundamental mode $I < I\left(b_1^{(2)}\right)$ and $I > I\left(b_1^{(1)}\right)$ join the central-spot branch of the first 2D spot mode. The sections of the fundamental mode $I\left(b_1^{(2)}\right) < I < I\left(b_2^{(2)}\right)$ and $I\left(b_2^{(1)}\right) < I < I\left(b_1^{(1)}\right)$ join, on one hand, the branch with a ring spot on the periphery of the first 2D spot mode, and on the other hand, the branch with an inside ring spot of the second 2D spot mode. The

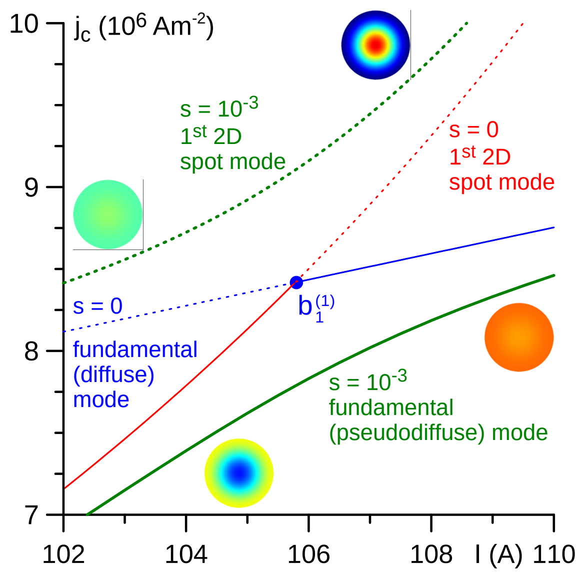

Figure 4.9: Bifurcation diagram and schematics of current density distribution over the cathode surface. Perturbed transcritical bifurcation of first order contact, arc cathode, $s = 10^{-3}$. Solid: sections of the steady-state modes that are stable against axially symmetric perturbations. Dotted: unstable sections.

sections of the fundamental mode $I\left(b_2^{(2)}\right) < I < I\left(b_3^{(2)}\right)$ and $I\left(b_3^{(1)}\right) < I < I\left(b_2^{(1)}\right)$ join, on one hand, the branch with a central spot and a ring spot on the periphery of the second 2D spot mode, and on the other hand, the branch with a central spot and an inside ring spot of the third 2D spot mode. This pattern is repeated and finally the section $I\left(b_8^{(2)}\right) < I < I\left(b_8^{(1)}\right)$ joins the branch with a central spot, three inside ring spots, and a ring spot on the periphery of the eighth 2D spot mode.

In the case of arc cathode, the second scenario occurs at $b_1^{(1)}$. The section of the fundamental mode $I > I\left(b_1^{(1)}\right)$ joins the branch with a ring spot on the periphery of the first 2D spot mode and the section of the fundamental mode $I < I\left(b_1^{(1)}\right)$ joins the branch with a central spot. Also shown in figure 4.9 is a pattern of stability against axially symmetric perturbations (more precisely, against the first mode of axially symmetric perturbations) obtained in the numerical modelling; it conforms to figure B.2a with $\delta \leq 0$ as it should.

One of the consequences of the above-described exchange of branches is that the fundamental mode, i.e., the mode that exists at all I, is no longer diffuse and may be not even close to diffuse: it comprises section(s) of the fundamental mode (or, more precisely, what was the fundamental mode at $s = 0$) and one of the branches of the first 2D spot mode, namely, the branch with a central spot in the case of glow discharge and the branch with a ring spot on the periphery in the case of arc cathode. The fact that the branches are not the same originates in different physics introduced by boundary conditions at $r = R$ in the cases of glow discharge and arc cathode. A non-reflecting wall of a glow discharge tube reduces local intensity of the glow discharge due to losses of the charged particles caused by diffusion to the wall. As a consequence, the diffuse discharge becomes less intense on the periphery than at the center. Thus, the fundamental mode acquires some similarity with the branch with a spot at the center, and it is not surprising that the two join. On the contrary, energy- and current-collecting lateral surface of an arc cathode provides an additional (lateral) heating of the edge of the front surface and thus locally enhances the discharge. As a consequence, the diffuse discharge becomes more intense at the edge than at the center. Thus, the fundamental mode acquires some similarity with the branch with a ring spot on the periphery, and it is not surprising that the two join.

The above-described difference between the fundamental modes for $s \neq 0$ in the cases of glow discharge and arc cathode is seen in the schematics of distributions of the current density shown in figures 4.8a and 4.9. At high currents, $I \gtrsim I\left(b_1^{(1)}\right)$, the distributions are more or less uniform in both cases, however there is a minimum of the current density on the periphery in the case of glow discharge and a maximum in the case of arc cathode. The difference is increased at lower currents, $I \lesssim I\left(b_1^{(1)}\right)$: a well-pronounced spot appears at the center of the glow cathode while the maximum of the current density on the periphery of the arc cathode becomes better pronounced.

A further difference between the fundamental modes at $s \neq 0$ and $I \lesssim I\left(b_1^{(1)}\right)$ in the cases of glow discharge and arc cathode is as follows. The fundamental mode in the case of glow discharge manifests a well-pronounced effect of normal current density, which is attested, in particular, by a plateau in the dependence $j_c(I)$ (solid line in figure 4.8a) at $30\,\mu\mathrm{A} \lesssim I \lesssim 3\,\mathrm{mA}$. Nothing of this kind is manifested by the fundamental mode on the arc cathode. This difference stems from the strongly different aspect ratios. As discussed in section 1.2.2, the effect of normal current density is a particular case of coexistence of phases which is possible in wide systems. In the case of glow discharge, the characteristic dimension in the z-direction is represented by the interelectrode gap or the thickness of the near-cathode space-charge sheath, whichever is smaller. The thickness of the near-cathode space-charge sheath under conditions of the above-mentioned plateau in the dependence $j_c(I)$ corresponding to the fundamental mode is approximately 0.13 mm, which is much smaller than the discharge radius R. Thus, the system represented by the glow discharge indeed may be considered as wide. In the case of arc cathode, the characteristic dimension in the z-direction is the cathode height h, so the aspect ratio h/R is 5. Thus, the arc cathode represents a narrow rather than wide system and it is not surprising that it does not manifest the effect of normal current density.

All the steady-state modes in the case $s \neq 0$ other than the above-described fundamental mode exist in limited current ranges and in the case of glow discharge continue to represent closed loops. The topology of these modes may be understood by means of the same reasoning as above. In particular, the intensity of a ring spot on the periphery is locally reduced in the immediate vicinity of the wall of a glow discharge tube, thus the structure acquires some similarity with an inside ring spot and this is why the corresponding branches

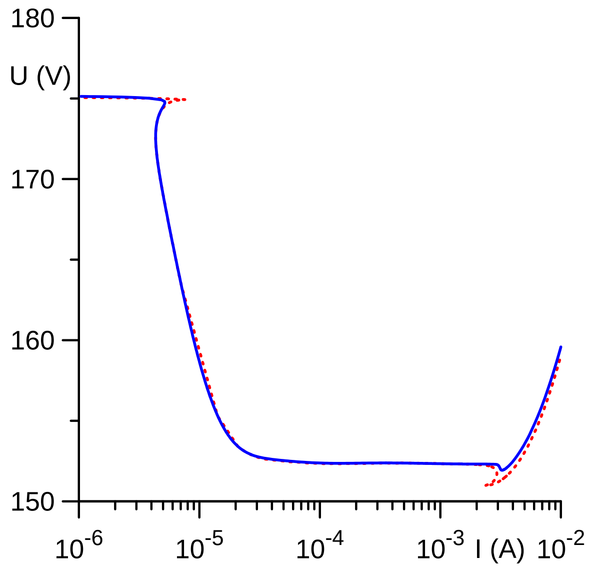

Figure 4.10: CVC's of the 2D glow discharge. Xe plasma, $p = 30$ Torr, the discharge radius 1.5 mm and height 0.5 mm.

join the same section of the fundamental mode.

As s increases from the value of 0.05 shown in figure 4.8a up to unity in the case of glow discharge, the above-described fundamental mode does not suffer dramatic changes. This is illustrated by figure 4.10. A dotted line in this figure depicts the CVC of the fundamental mode for $s = 0.05$, however it is virtually indistinguishable from the solid line, which corresponds to $s = 1$, except in the vicinity of transitions from the Townsend discharge to the subnormal mode and from the normal to the abnormal modes. The range of currents in which each non-fundamental 2D mode shown in figure 4.8 exists shrinks with increasing s and higher-order modes disappear one by one. Only two initial modes remain in existence at $s = 1$, the mode with an inside ring spot and the one with a central spot and an inside ring spot; see section 3.5.

The CVC of the fundamental mode on an arc cathode with $s = 1$ is quite close to the CVC of the fundamental mode on a cathode with $s = 0$, shown in figure 4.2, if the discharge current does not exceed, say, 500 A. Differences between the temperature of the cathode surface in these two modes reach about 400 K. The CVC of the first non-fundamental 2D mode on arc cathode with $s = 1$ also is close to the CVC of the first 2D spot mode on a cathode with $s = 0$, shown in figure 4.2, although differences in the surface temperature reach about 1000 K.

Distributions of the surface temperature of an arc cathode with an energy- and current-collecting lateral surface, $s = 1$, in four states corresponding to the same near-cathode voltage drop $U = 15$ V are shown in figure 4.11. (Note that the range $0 \leq r + z \leq 2$ mm in this figure corresponds to the front surface of the cathode, the range $r + z \geq 2$ mm corresponds to the lateral surface.) The states with the discharge currents of 77.14 A and

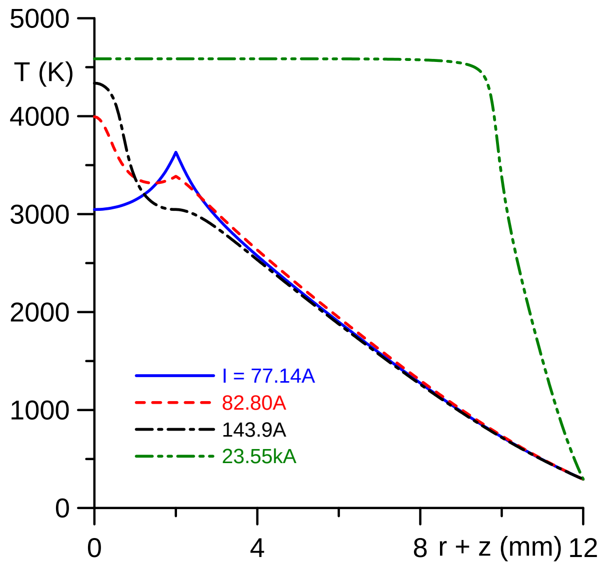

Figure 4.11: Distributions of temperature of the surface of an arc cathode. $s = 1$, $U = 15\,\mathrm{V}$.

23.55 kA belong to the fundamental mode. In the latter state, the temperature is very high and constant ("saturated") along the front surface and the most part of the lateral surface; a feature which is characteristic for the high-current section of the fundamental mode [87]. There is something resembling a ring spot attached to the edge of the front surface of the cathode in the state with $I = 77.14\,\mathrm{A}$. The states with $I = 82.80\,\mathrm{A}$ and 143.9 A belong to the first non-fundamental 2D mode. There is a central spot in the latter state and a central spot and something resembling a ring spot at the edge in the former state. One can say that all four states bear footprints of their origin. In particular, the pattern revealed by the state with $I = 82.80\,\mathrm{A}$ is similar to the pattern associated with one of the branches of the second 2D spot mode, namely, the branch with a central spot and a ring spot at the edge, which, jointly with the fundamental mode and the branch with a central spot of the first 2D spot mode, originates the first non-fundamental 2D spot mode. This similarity is remarkable, given that the bifurcation point $b_2^{(1)}$ at which the second 2D spot mode branches off from the fundamental mode is not present within the range of U considered in this chapter.

Variations of the temperature along the front surface of the cathode operating in the fundamental mode under conditions of figure 4.11 are moderate, and they are still smaller for thinner cathodes, which are used in arc lamps and are best studied experimentally. The thermal regime of the cathode does not appear to be spot-like but rather looks diffuse. As a consequence, the above-described difference between the fundamental modes on cylindrical arc cathodes with insulating and active lateral surfaces has not been appreciated up to now and both are termed "diffuse" in the preceding works. In this chapter, the fundamental mode on a cylindrical arc cathode with $s \neq 0$ is termed "pseudodiffuse" in order to distinguish it from the fundamental mode in the case $s = 0$ (which is associated with a uniform

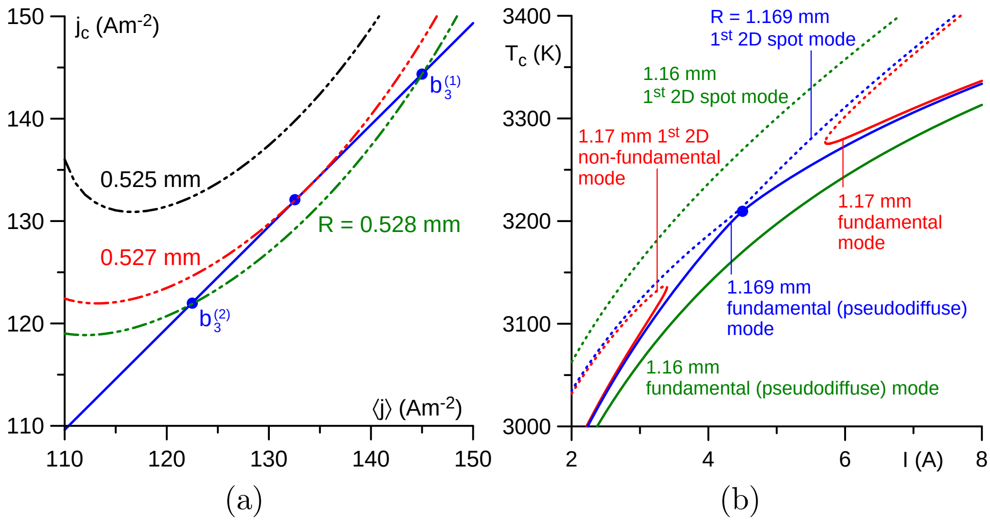

Figure 4.12: Bifurcation diagrams, perturbed transcritical bifurcation of second order contact. (a) Glow discharge, $s = 0$. Solid: fundamental mode. Two dot-dashed: third 2D spot mode. (b) Arc cathode with a hemispherical tip. Solid: (absolutely) stable sections of the steady-state modes. Dotted: unstable sections.

distribution of discharge parameters along the cathode surface, i.e., is truly diffuse). The first non-fundamental 2D mode at $s \neq 0$ is termed the first 2D spot mode.

4.5.3 Transcritical bifurcations of second order contact

Numerical modelling of glow discharge [128] revealed that a decrease of the radius of the discharge tube with reflecting wall causes 2D spot modes to disappear one by one, starting from the higher-order modes. The disappearance of each mode occurs through shrinking of the current range in which the mode exists. At first, shrinking occurs while the spot mode remains connected to the fundamental mode, then the spot mode detaches from the fundamental mode and shrinking continues until the spot mode disappears completely. An example illustrating this detachment is shown in figure 4.12a. [Since dependence $j_c(\langle j \rangle)$ for the fundamental mode is the same for tubes of different radii, there is only one solid line in this figure.] The 2D spot mode and the fundamental mode are connected at two first-order transcritical bifurcation points at $R \gtrsim 0.527$ mm. The two bifurcation points merge to form a transcritical bifurcation of second order contact when R has decreased down to a certain value around 0.527 mm. The 2D spot mode and the fundamental mode become disconnected at $R \lesssim 0.527$ mm.

The topology of modes in figure 4.12a is similar to that shown in figure B.2c. One can conclude that the above-described detachment of a 2D spot mode from the fundamental mode occurs through a perturbed transcritical bifurcation $\{1D, 2D\}$ of second order contact according to scenario shown in figure B.2c.

Numerical modelling of arc cathodes of shapes of industrial interest that is described in chapter 5 revealed a possibility of dramatic changes of the pattern of steady-state modes of current transfer. As an example, figure 4.12b shows the temperature at the center of the front surface of a cathode having the shape of a rod (cylinder) with a hemispherical tip. The temperature of the cooling fluid was 1000 K. The cathode radius is variable, the cathode height is 10 mm, the whole front and lateral surface is energy- and current collecting, all the other parameters are the same as indicated in section 4.2. One can see that the pseudodiffuse and the first 2D spot modes, representing separate modes at $R \lesssim 1.169$ mm, become connected when R has increased up to a certain value around 1.169 mm, then they exchange branches and separate once again. Each of these two new disconnected modes embraces states typical for both fundamental and spot modes as discussed in chapter 5 and cannot be termed (pseudo)diffuse or spot mode. On the other hand, one of these modes exists at all values of the discharge current and may be termed fundamental mode.

The topology of modes in figure 4.12b is similar to that shown in figure B.2b: a transcritical bifurcation of second order contact occurs at $R \approx 1.169$ mm, small deviations of R from this value break the bifurcation. The pattern of stability also is similar. One can conclude that the above-described change of pattern of steady-state modes of current transfer occurs through a perturbed transcritical bifurcation $\{2D, 2D\}$ of second order contact according to scenario shown in figure B.2b.

A very important feature of the latter bifurcation is that it, being of the type $\{2D, 2D\}$, involves modes of the same symmetry. This feature has not been encountered in all the above-described bifurcations (except the fold bifurcations); it is this feature that originates the fact that the bifurcation occurs at only one value of the control parameter R.

4.6 Pitchfork bifurcations

Pitchfork bifurcations $\{1D, 3D\}$ were treated in [95] for a glow discharge and in [91] for an arc cathode. In both cases, distributions of discharge parameters associated with the bifurcating 3D modes are given in the vicinity of a bifurcation point c_i $(i = 1, 2, \dots)$ by the asymptotic expansion

$$\begin{aligned} \tilde{f}^{(3D)}(r, \phi, z; U) \;\; &= \;\; \tilde{f}^{(1D)}(z; U_i) + B_i(z)\; J_\nu\left(j'_{\nu,m}\frac{r}{R}\right)\cos(\nu\phi + \alpha)\sqrt{|U - U_i|} \\ &\quad + C_i(r, \phi, z)(U - U_i) + \dots, \end{aligned} \tag{4.5}$$

where $\tilde{f}^{(3D)}(r, \phi, z; U)$ is a solution describing the 3D spot modes bifurcating at the point considered, ν is an integer equal to i at $i \le 4$ and below i at $i > 4$, $m = 1, 2, \dots$, α is an arbitrary constant, $B_i(z)$, $C_i(r, \phi, z)$, and U_i have the same meaning as above except that $C_i(r, \phi, z)$ depends also on ϕ. The conclusion that in the vicinity of a bifurcation point transversal variations of discharge parameters in the bifurcating 3D modes are proportional to $J_\nu\left(j'_{\nu,m} r/R\right)\cos(\nu\phi + \alpha)$ conforms to results of the numerical modelling of 3D modes. The order of initial nontrivial zeros of the derivatives of the Bessel functions of the first kind (see table A.1) governs the order of branching of different spot modes from the fundamental mode. This is indeed the order detected in the numerical modelling in the case of arc cathode with the insulating lateral surface in the range of currents down to 0.3 A as described in section 4.3.1.

For the case of arc cathode, the function $B_i(z)$ was analytically calculated and thus the second term of asymptotic expansion (4.5). The obtained two-term analytic approximation in the vicinity of the bifurcation points c_1 and c_2 shown in figures 4.2 and 4.4 is depicted by the dashed line in figure 4.7 and conforms to the numerical modelling as it should. Note that there are small gaps in the vicinity of points c_1 and c_2 in the solid lines representing the numerically calculated characteristics of the 3D modes. These gaps stem from divergence of iterations which sometimes occurs in a close vicinity of a bifurcation point.

Pitchfork bifurcations $\{2D, 3D\}$, occurring at the bifurcation points d_1 and d_2 in figures 4.2 and 4.4, represents the most frequent type of bifurcations that can occur in cases where 2D modes exist but 1D modes do not (such as the case $s = 1$ or all cases with non-cylindrical axially symmetric geometries). These bifurcations were treated in [96, 118] for the case of arc cathode. In both cases of glow discharge and arc cathode, distributions of discharge parameters associated with the bifurcating 3D modes are given in the vicinity of a bifurcation point d_i $(i = 1, 2, \dots)$ by the asymptotic expansion

$$\begin{aligned} \tilde{f}^{(3D)}(r,\phi,z;U) &= \tilde{f}^{(2D)}(r,z;U_i) + E_i(r,z)\cos(\nu\phi+\alpha)\sqrt{|U-U_i|} \\ &\quad + C_i(r,\phi,z)(U-U_i) + \dots, \end{aligned} \tag{4.6}$$

where $E_i(r,z)$ is a function of r and z (or, in the case of glow discharge, a set of functions) which depends on the bifurcation point being considered. The harmonic azimuthal variation of discharge parameters in the bifurcating 3D modes in the vicinity of a bifurcation point, predicted by the theory, was found in the numerical modelling.

The behavior which is typical for pitchfork bifurcations and shown in figures B.1c and B.1d originates in the second term of the expansion (4.5) or (4.6). When the expansion is averaged over the cathode surface, the contribution of this term, which is harmonic in ϕ, vanishes. This explains why CVC's do not represent a proper diagram of pitchfork bifurcations in the considered problem, and also why CVC's of the bifurcating 3D spot modes have finite inclinations at the bifurcation points c_1, c_2, d_1, and d_2 in figure 4.2.

Results of analytical and numerical investigation of stability of 2D and 3D spot modes of current transfer to an arc cathode, reported in [118] and in chapter 2, have revealed an exchange of stability in the vicinity of points of pitchfork bifurcation $\{2D, 3D\}$, which is similar to the one occurring in systems with one degree of freedom and illustrated by figures B.1c and B.1d. This exchange is realized as follows. At a bifurcation point, i.e., at $I = I(d_i)$, the 2D steady-state mode and the 3D steady-state modes that branch off at this point are neutrally stable against a 3D perturbation mode with an azimuthal dependence described by the same factor $\cos(\nu\phi + \alpha)$ that describes azimuthal variation of the steady-state 3D modes in the vicinity of the bifurcation point. The 2D mode changes its stability at the bifurcation point, i.e., either it is stable against the above-described 3D perturbation mode at $I > I(d_i)$ and unstable at $I < I(d_i)$, or *vice versa*. [As far as bifurcation points positioned on the pseudodiffuse mode are concerned, the pseudodiffuse mode is stable at $I > I(d_i)$ and unstable at $I < I(d_i)$.] The 3D modes are stable if they are supercritical, i.e., branch off into the current range where the 2D mode is unstable, and unstable if they are subcritical, i.e., branch off into the current range where the 2D mode is stable. The increments of the above-indicated perturbation of the steady-state 2D mode and 3D modes are related by the formula $\lambda^{(3D)} = -2\lambda^{(2D)}$ in the vicinity of the bifurcation point. This formula coincides with the corresponding relation in systems with one degree of freedom, which follows from equation (B.14).

As shown by the numerical modelling of chapter 2, the above-mentioned 3D perturbation mode that is neutrally stable at d_i is the same one that changes sign of its increment at all turning points of the corresponding steady-state 3D mode that branches off at d_i. In other words, it represents the fundamental perturbation mode of the corresponding steady-state 3D mode. Note that this perturbation mode, while being proportional to $\cos(\nu\phi + \alpha)$ in all states of the 2D mode, is no longer proportional to $\cos(\nu\phi + \alpha)$ in states of the 3D steady-state spot mode outside the bifurcation point d_i.

The pitchfork bifurcation $\{3D, 3D\}$, which occurs on an arc cathode at the point e_1 shown in figures 4.2 and 4.4, represents breaking of planar symmetry. For example, symmetry with respect to the horizontal axis is broken in the pattern shown in figure 4.2, although symmetry with respect to the vertical axis is conserved. The pattern of stability against the fundamental perturbation mode in the vicinity of the bifurcation point conforms to scenario B.1d. Note that the possibility of this bifurcation was detected first in the numerical investigation of stability in the case $s = 1$ (see section 2.4.5).

A question arises how a planar symmetry-breaking bifurcation can transform a three-spot pattern into a two-spot one. This may be explained as follows. At states between the bifurcation points d_1 and e_1, the temperature distribution is symmetric, say, with respect to the vertical and horizontal axes and possesses three maxima, associated with the central spot and two spots on the periphery (although the spots on the periphery are still pronounced extremely weakly: the temperature at its centers exceeds the temperature outside the spots by about 1 K). At the bifurcation point e_1, the central spot starts moving up- or downwards. This movement is accompanied by the complete extinction of the upper (or, respectively, lower) peripheral spot and by the enhancement of the opposite peripheral spot. If the central spot moves upwards, the two-spot pattern shown in figure 4.2 appears.

Since in the case of the glow discharge stability of bifurcating multidimensional spot modes has not been studied, we cannot say for sure at the moment if the above conclusions on bifurcations $\{1D, 3D\}$ and $\{2D, 3D\}$, drawn for the case of arc cathode, apply also to the case of glow discharge. A bifurcation $\{3D, 3D\}$ similar to the one discussed above for the case of arc cathode can occur also in the case of glow discharge.

4.7 Discussion

The above analysis provides explanations to many results obtained in numerical modelling. One example is the fundamental mode in the case of arc cathode. This is the only mode that exists at currents high enough, therefore it should be stable at such currents. (This conclusion is confirmed by both the numerical modelling and the experiment.) The steady-state mode with one spot at the periphery of the arc cathode possesses one turning point (square on the dot-dashed line in figure 4.2). Taking into account the behavior of the CVC at this point and applying the analysis of section 4.4, one concludes that the section of this mode comprised between the bifurcation point c_1 and the turning point is unstable against perturbations of one mode (which is the fundamental perturbation mode of the steady-state mode being considered), and the section beyond the turning point is (absolutely) stable. This conclusion conforms to the pattern of stability at points of subcritical pitchfork bifurcation, discussed in section 4.6, and indeed was confirmed by the numerical modelling.

The CVC of the steady-state mode with two spots at the periphery of the arc cathode (two dot-dashed line in figure 4.2) manifests a Z-shape. One concludes that this mode is stable against the fundamental perturbation mode except the section between the turning points. This conforms to the pattern of stability at points of supercritical pitchfork bifurcation, discussed in section 4.6, and indeed was found in the modelling.

While Z-shapes are frequent enough for both arc cathodes and glow discharges (see, in particular, the modelling of arc cathodes of complex shapes reported in chapter 5), 360°-loops have not been found in the case of arc cathodes, however have been found in the case of glow discharge; see section 3.5.

In the case of a cylindrical glow discharge tube with the reflecting wall or of a cylindrical arc cathode with the insulating lateral surface, $s = 0$, the fundamental mode is associated with a uniform distribution of discharge parameters along the cathode surface, i.e., is diffuse. In the case of a cylindrical arc cathode with an active lateral surface, $s = 1$, the fundamental mode is associated with moderate variations of the temperature along the front surface of the cathode provided that the cathode is thin, so this mode appears more or less diffuse (the pseudodiffuse mode, in terms of this chapter). The fundamental mode of glow discharge in a cylindrical tube with the absorbing wall, $s = 1$, embraces states with smooth variations of parameters along the cathode surface (the Townsend discharge and the abnormal discharge), but also states with a current spot (the subnormal and normal discharges). Similarly, the fundamental mode on a non-cylindrical arc cathode may embrace states typical for both fundamental and spot modes. One can conclude, in agreement to what was said in section 2.4.1, that the fundamental mode is diffuse or pseudodiffuse in some situations, but is definitely non-diffuse in others.

A transition between the 1D fundamental mode in the case of a cylindrical glow discharge tube with the reflecting wall or of a cylindrical arc cathode with the insulating lateral surface, $s = 0$, and the 2D fundamental mode in the case of glow discharge in a cylindrical tube with the absorbing wall or of a cylindrical arc cathode with an energy- and current-collecting lateral surface, $s = 1$, is discontinuous. If one starts from a state belonging to the fundamental mode in the case $s = 1$ and then gradually decreases s, one will arrive at $s = 0$ at a state belonging to a "composed" mode comprising section(s) of the 1D mode and one of the branches of the first 2D spot mode, namely, the branch with a spot at the center in the case of glow discharge and the branch with a ring spot on the periphery in the case of arc cathode. Similarly, if one starts from the (1D) fundamental mode in the case $s = 0$ and then gradually increases s, one will not necessarily arrive at $s = 1$ at the fundamental mode: one may also arrive at one of the branches of one of non-fundamental 2D modes, or can obtain no solution at all.

It was shown on section 4.5.2 that the reason of the above-described discontinuity is an exchange of branches that occurs when the transcritical bifurcation $\{1D, 2D\}$ of first order contact is perturbed and the two bifurcating solutions are broken into two isolated solutions with the branches exchanged.

Let us now turn to questions raised in section 1.2.2 in connection with figures 1.1 and 1.2. It was shown in [128] that the subnormal and normal modes of glow discharge are already present in the case $s = 0$, but they represent a part of the first 2D spot mode rather than of the fundamental mode. They become a part of the fundamental mode after the exchange of branches. On the contrary, the mode which is described by the von Engel and Steenbeck solution and is associated with the falling section of the CVC represents a part of the fundamental mode at $s = 0$, but becomes divided between different non-fundamental 2D modes after the exchange of branches. The question that was not answered in [128] was why does the exchange of branches occur. Now the answer to this question has been found: absorption of the charged particles by the wall causes a change of symmetry of the fundamental mode from 1D to 2D; this causes breaking of the transcritical bifurcation of first order contact $\{1D, 2D\}$; and such breaking is always accompanied by the exchange of branches.

The procedure of simulations with the use of the built-in initial approximation implemented in the Internet tool [90] amounts to a transition from the fundamental (diffuse) mode at $s = 0$ to $s = 1$. This transition leads to the fundamental (pseudodiffuse) mode at $s = 1$ provided that U is below the value corresponding to the point at which the bifurcation $\{1D, 2D\}$ occurs (point $b_1^{(1)}$ in figures 4.2 and 4.4), and 13.46 V is precisely this value. In the range of U above the point of minimum of the CVC of the first 2D spot mode in the case $s = 1$, which is 14.04 V, the transition leads to the low-voltage branch of the first 2D spot mode at $s = 1$. The fundamental mode in the case $s = 0$ has no analogue in the case

$s = 1$ in the range of voltages $13.46\,\mathrm{V} \lesssim U \lesssim 14.04\,\mathrm{V}$, whence the lack on convergence in this range of voltages.

The fundamental mode in a glow discharge with $s = 1$ manifests a normal spot and could hardly be confused with the fundamental mode in the case $s = 0$, which is diffuse. Due to a substantially different aspect ratio, the situation in the case of arc cathode is different: the fundamental mode on an arc cathode with $s = 1$ is characterized by modest variations of parameters along the front surface of the cathode and is in this respect similar to the fundamental mode in the case $s = 0$. This similarity masks the above-mentioned discontinuity in the transition between fundamental modes on arc cathodes with $s = 0$ and $s = 1$. It is worth noting that this discontinuity remained unnoticed, although the difficulties arising at low currents in calculations of the (pseudo)diffuse mode on wide cathodes with the use of the fundamental mode at $s = 0$ as an initial approximation have been known for many years, and was realized only recently, after similar difficulties have been encountered in the modelling of glow discharge.

The numerical approach to finding steady-state 3D solutions that has been used in the existing literature allows one to find only solutions possessing planar symmetry. A question arises whether non-symmetric steady-state 3D solutions exist. 3D solutions that branch off from 1D and 2D solutions indeed possess planar symmetry, however one cannot exclude the possibility of breaking of this symmetry through a bifurcation. The latter can happen indeed, as shown by the example of the bifurcation $\{3D, 3D\}$ described in section 4.6.

4.8 Conclusions

Bifurcations of modes of current transfer to cathodes of DC gas discharges do occur in numerical modelling, also in apparently simple situations. A failure to recognize and properly analyze a bifurcation may originate difficulties in the modelling and hinder understanding of numerical results and the underlying physics.

All basic types of steady-state bifurcations (fold, transcritical, pitchfork) are encountered in numerical modelling of current transfer to cathodes of DC glow and arc discharges. Dramatic changes of patterns of DC current transfer occur in both glow and arc discharges through perturbed transcritical bifurcations of first and second order contact.

Analysis of bifurcations allows one to understand main features of patterns of steady-state modes and their stability. For example, the analysis elucidates the reason why the mode associated with the falling section of the CVC in the classic 1D solution of von Engel and Steenbeck seems not to appear in 2D numerical modelling and the subnormal and normal modes appear instead. A similar effect has been identified in numerical modelling of arc cathodes and explained.

Multiple modes of current transfer to DC discharge cathodes represent a self-organization phenomenon. In spite of physical mechanisms of discharges on cold and hot cathodes being very different, the self-organization fits into the same pattern. However, there are some differences, for example different scenarios of exchange of branches in breaking of transcritical bifurcations of first order contact. This difference originates in the fact that an absorbing wall locally quenches the glow discharge due to loss of the charged particles caused by diffusion to the wall, while lateral heating of an arc cathode increases the temperature of the cathode edge and thus locally enhances the discharge. Another difference is that the fundamental mode of a glow discharge in a tube with an absorbing wall manifests a normal spot, while the fundamental mode on an arc cathode with a current- and energy-collecting lateral surface is characterized by modest variations of parameters along the front surface of the cathode and looks rather diffuse. This difference stems from the essentially different aspect ratio. A further difference is that modes with regular patterns of two or more spots are not observed on arc cathodes, but have been observed in glow discharges [20–24]. This difference still remains to be explained.

Chapter 5

Variations of pattern of current transfer to arc cathodes of complex shapes: example of competition between self-organization and geometric factors

Changes of the pattern of steady-state modes of current transfer to thermionic cathodes induced by variations of the cathode geometry and temperature of the cooling fluid are studied numerically. For some combinations of control parameters, only one stable mode in a wide current range exists, which combines features of spot and fundamental modes. This mode, when attached to an elongated protrusion on the cathode surface, may be identified with the so-called super spot mode observed in experiments on low-current arcs. The conclusions on existence under certain conditions of only one stable mode in a wide current range and of a minimum of the dependence of the temperature of the hottest point of the cathode on the arc current, manifested by this mode, may have industrial importance and admit a straightforward experimental verification.

5.1 Introduction

A pattern of different modes of current transfer to arc cathodes studied up to now comprises a fundamental mode that exists at all currents and different spot modes that exist at currents low enough as described in section 2.4.1. Also fit into this pattern results of numerical modelling of cathodes with a rounded edge of the front surface [88, 116, 119] and cathodes with a hemispherical front surface [85, 88], except that the spot modes in [85, 88] were found not in the whole region of their existence. Stability has been studied

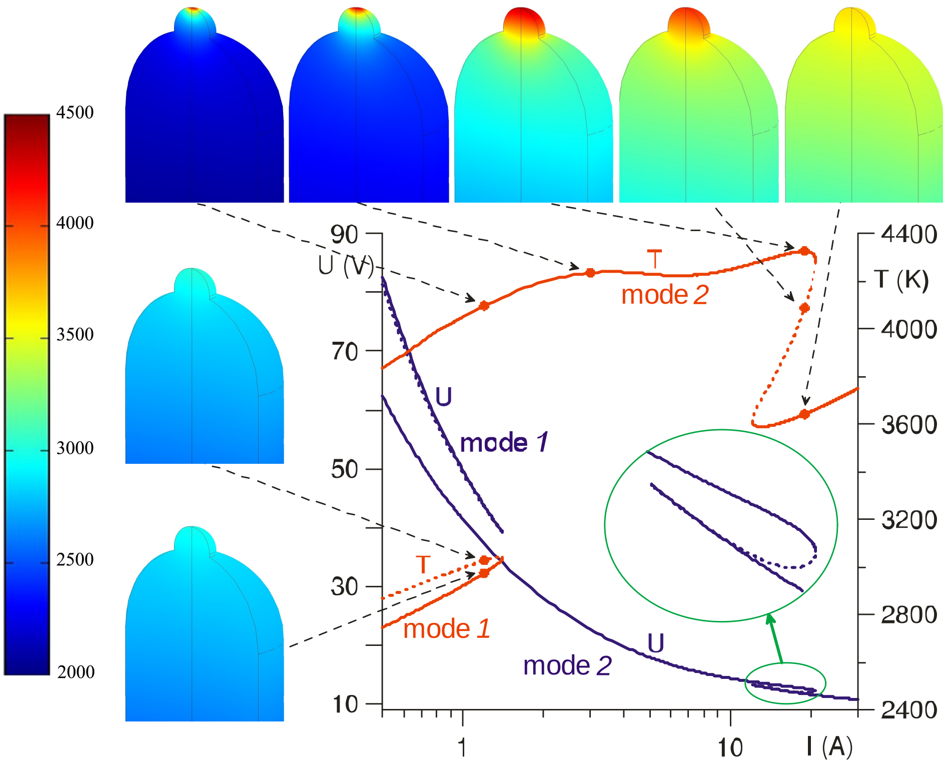

Figure 5.1: CVC's and dependence of the maximum temperature of the cathode surface on the arc current for different modes of current transfer and distributions of the temperature of the cathode for several states (the bar in kelvin).

only for cylindrical cathodes with the flat front surface (see chapter 2) and it was found that the fundamental mode is stable at all currents of interest if the cathode is thin enough and is unstable at low currents otherwise; the high- and low-voltage branches of the mode with a spot at the edge of the front surface are stable and, respectively, unstable; all the other spot modes are unstable, including axially symmetric spot modes.

However, results of simulation of operation of cathodes of complex geometries which are of practical interest, in particular those with protrusions [36, 148] (see also [149]) do not fit into the above-described pattern. In figure 5.1, CVC's are shown of axially symmetric steady-state modes of current transfer to an axially symmetric tungsten cathode in the form of a rod of radius $R = 750\,\mu$m and a height of 12 mm. The cathode has a hemispherical tip. A spherical protrusion of radius of 200 μm is located at the top of the tip. The arc operates in argon under the pressure of 2 bar. Also shown is the dependence of the maximum temperature of the cathode surface on the arc current. Stable and unstable sections of each mode are shown by solid or, respectively, dotted lines.

There are two separate modes in figure 5.1. The mode designated 1 exists only at low currents and comprises branches separated by a turning point. The branch that corresponds to higher values of the near-cathode voltage drop and lower values of the maximum temperature is stable, the branch that corresponds to lower values of the voltage drop and higher temperatures is unstable. The other mode, 2, exists in a broad range of currents and is Z-shaped at currents between 12 A and 21 A.

Apart from this Z-shape, CVC's shown in figure 5.1 are similar to those calculated for cathode in the form of a cylindrical rod with the flat top shown in section 2.4.1. On the basis of this similarity, one would expect that the mode 1 is the axially symmetric spot mode and the mode 2 is the fundamental mode. However, high values of the maximum temperature in mode 2 and low values of the maximum temperature on both branches of the mode 1 do not fit this interpretation.

An inspection of distributions of the temperature of the cathode, shown for several states in figure 5.1, disproves such interpretation: while high-current states belonging to the mode 2 are characterized by smooth temperature distributions typical for the fundamental mode, there is a well-defined spot in low-current states belonging to the mode 2. The stable branch of the mode 1 is diffuse and there seems to be something that can be identified as a poorly pronounced spot on the unstable branch, although this spot can hardly be seen in figure 5.1. In other words, each of the two modes of steady-state current transfer existing in this geometry embraces diffuse states and states with spots.

The above-cited results indicate that more than one pattern of current transfer to thermionic cathodes and of its stability can occur under conditions of industrial interest. It is important to study these patterns in a wide range of conditions and to find out in what conditions each pattern occurs and why a transition between different patterns happens. The present chapter is dedicated to this task. The outline of the chapter is as follows. Numerical results on variations of the pattern of current transfer are given in section 5.2. Section 5.3 is dedicated to discussion of the results; in particular, their relation to the so-called super spot mode observed in experiments with HID lamps is discussed. Possibilities of comparison with data of future experiments are discussed as well. Concluding remarks are given in section 5.4.

5.2 Numerical results

The model for calculation of steady-state current transfer and its stability as well as its numerical realization are the same as the ones described in sections 2.2 and 2.3. Numerical results given in this chapter refer to cathodes made of tungsten. Data on thermal conductivity and work function of tungsten are described in section 2.4. All the results unless otherwise specified refer to an arc operating in argon under the pressure of 1 bar.

Axially symmetric cathodes are considered which consist of a cylindrical section, a tip in the form of the half of spheroid (ellipsoid of revolution) at the top of the cylindrical section, and a hemispherical protrusion at the top of the tip; see figure 5.2. (More precisely, the protrusion represents a part of a sphere which is a little bigger than the hemisphere.) The radius and height of the cylindrical section are designated R and, respectively, $h - d$. The axis of revolution of the spheroidal tip coincides with the axis of the cylindrical section, the

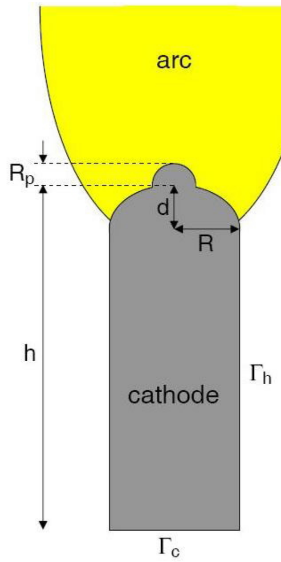

Figure 5.2: Geometry of the problem.

horizontal semi-axis of the spheroid equals the radius R of the cylindrical section and the vertical semi-axis of the spheroid is designated d. The center of the hemispherical protrusion is positioned at the height h with respect to the cathode base on the (common) axis of symmetry of the cylindrical section and the tip. The radius of the protrusion is designated R_p. Note that h has the meaning of the height of the cathode without protrusion.

Given a large number of variable control parameters, the following approach was adopted in order to present the results in a manageable way: one variant is chosen as basic (reference point) and then control parameters are varied one by one, each time starting from the basic variant. In order that such approach allow one to demonstrate all kinds of variations of the pattern of current transfer, care should be employed while choosing the basic variant. In this chapter, the following variant is chosen as basic: $h = 10\,\mathrm{mm}$, $R = d = 1\,\mathrm{mm}$, $R_p = 0$ (that is, a cathode with a hemispherical tip without protrusion), $T_c = 1000\,\mathrm{K}$.

5.2.1 Basic variant

Two axially symmetric steady-state modes have been found in numerical simulations for the above-specified basic variant. CVC's and the dependence of the maximum temperature of the cathode surface on the arc current for these two modes are shown in figure 5.3, U_1 and T_1 referring to one of these modes and U_2 and T_2 to the other. (Note that symbols U_1 and T_1 have other meaning in chapters 2 and 3, where they refer to perturbations, however this is unlikely to cause a confusion.) Stable and unstable sections of each mode in this and following figures are depicted by solid or, respectively, dotted lines. Note that the section of the CVC corresponding to the unstable section of the mode 2 coincides, with the graphic accuracy, with the CVC of the mode 1 and cannot be seen; the same applies to some of

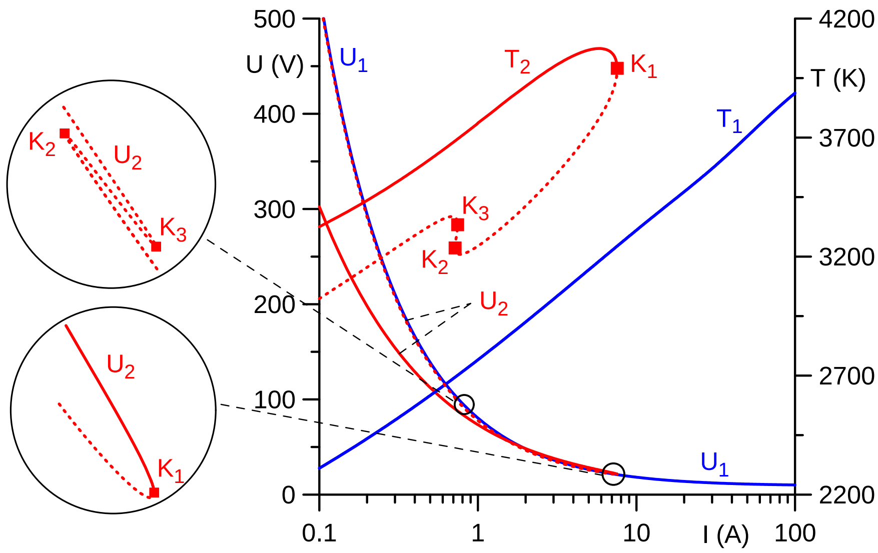

Figure 5.3: CVC's and maximum temperature of the cathode surface. Cathode with a hemispherical tip, $d = R = 1\,\mathrm{mm}$, $h = 10\,\mathrm{mm}$, $T_c = 1000\,\mathrm{K}$. Squares: turning points.

the subsequent figures.

The mode 1 is associated with a smooth distribution of temperature along the front surface of the cathode and is conventionally termed the diffuse mode (although the terms "pseudodiffuse" or "fundamental" mode would be more rigorous). It exists and is stable in the whole current range under consideration. The mode 2 is associated with a distribution of temperature with a maximum at the center of the front surface of the cathode and may be termed the first axially symmetric spot mode. It is composed of two branches separated by a turning point K_1 and exists in a limited current range $I \lesssim 7.6\,\mathrm{A}$. In the following, branches of the spot mode which manifest higher or, respectively, lower values of the maximum temperature of the cathode surface will be referred to as a high- or low-temperature branch.

The high-temperature branch is stable, the low-temperature branch is unstable. The high-temperature branch is associated with a well-pronounced spot, the low-temperature branch is associated with a spot which is somewhat diffuse. The low-temperature branch manifests a shape that resembles Z (the reflected S). The inserts in figure 5.3 show the behavior of the CVC of the spot mode in the vicinity of the turning point K_1 and in the vicinity of the Z-shape. The near-cathode voltage drop on the high-temperature branch of the spot mode is in the vicinity of the turning point slightly higher than the voltage drop on the low-temperature branch (although this difference is small and can be clearly seen only in the insert), and is lower than the voltage drop on the low-temperature branch at $I \lesssim 1.5\,\mathrm{A}$.

Except for the Z-shape, this pattern is similar to the one previously established for a rod cathode with a flat front surface [87, 89]. However, there is a fundamental difference concerning stability of the spot mode: both branches of the first axially symmetric spot mode on a cathode with a flat front surface are unstable; see section 2.4.4.

Under conditions of figure 5.3, the high-temperature branch is stable, i.e., all perturbation modes have negative increments. It follows from the theoretical analysis of stability in the vicinity of a turning point (chapter 4) that there are: one axially symmetric perturbation mode with a positive increment on the section K_1K_2 of the low-temperature branch; two axially symmetric perturbation modes with positive increments on the section K_2K_3; and one axially symmetric perturbation mode with a positive increment beyond the turning point K_3. This is indeed what has been found in the numerical modelling. No 3D perturbation modes with positive increments have been found.

Under conditions of figure 5.3, states in the vicinity of the turning point K_1 that are associated with higher values of the near-cathode voltage and maximum temperature of the cathode surface are stable, and those associated with lower values are unstable. However, the theoretical analysis of chapter 4 indicates that stability of a state in the vicinity of a turning point is unrelated to whether this state is associated with lower or higher values of the near-cathode voltage or maximum temperature of the cathode surface: what matters is whether the turning point in the plane (I, U) is traversed in the clockwise direction or in the counterclockwise direction. In the former case, states before the turning point are stable against one mode of perturbations of the same symmetry that the steady-state mode itself and states after the turning point are unstable. In the latter case, states before the turning point are unstable and ones after it are stable. Therefore, the above-mentioned feature of figure 5.3 is not a general result. Indeed, counter-examples will be encountered in the following.

The above-described modelling predicts stable regimes of current transfer at currents of several hundred milliamperes with near-cathode voltages of several hundred volts, far in excess of near-cathode voltages of up to 50 to 60 V observed in experiments with arc cathodes (e.g., [88, 150]). One should keep in mind, however, that although the current range of several hundred milliamperes has been studied experimentally in connection with high-intensity discharge lamps (e.g., [114]), this was done on substantially smaller cathodes (of a radius of a few hundred micrometers), i.e., at substantially higher average current densities. On the other hand, this current range is well above the range of a few milliamperes, which is characteristic of DC atmospheric-pressure glow discharges (e.g., [20, 151, 152]). Thus, the above regimes are intermediate between those characteristic for arc and glow cathodes and remain unexplored, to the best of our knowledge. It would be very interesting to try to observe such regimes experimentally. (Note that effects neglected by the present model come into play in such regimes, e.g., secondary electron emission and deviations of the electron energy distribution function from the Maxwellian distribution. These effects, however, can hardly render theoretical predictions inaccurate by orders of magnitude.)

This is one of the reasons why CVC's are shown in figure 5.3 and subsequent figures in the range of near-cathode voltages of up to 500 V, a value unusually high from the point of view of arc cathodes. Another reason is that the nature of variations of patterns of current transfer cannot be understood without analysis of data referring to a wide range of conditions, as it will be seen in the following.

In addition to the two above-discussed axially symmetric solutions describing the fundamental mode and the first axially symmetric spot mode, also 3D solutions describing 3D spot modes have been found in the modelling. However, a position of the maximum of the temperature of the cathode surface, described by these solutions, in most cases was found to coincide with the position of maximum in the initial approximation used to compute the corresponding solution. In other words, it was possible to obtain a solution with a spot positioned at virtually any point of the front surface of the cathode. The set of multiple solutions was discrete in all the cases studied before, therefore the existence of a continuum set of 3D spot modes is unexpected and this result requires a special analysis. Such analysis falls beyond the scope of this chapter, therefore the following treatment is focussed on axially symmetric modes.

5.2.2 Effect of the curvature of the cathode tip

The curvature of the cathode tip is defined by the parameter d (see figure 5.2): $d = R$ corresponds to a hemispherical tip, $0 < d < R$ to an oblate spheroidal tip, $d = 0$ to a cathode with a flat front surface and $d > R$ to a prolate spheroidal tip.

Oblate spheroidal tip

CVC's and the dependence of the maximum temperature of the cathode surface on the arc current for several cathodes with $d < R$ are shown in figure 5.4. In all the cases, the indices 1 and 2 continue to designate the fundamental and, respectively, the first axially symmetric spot modes.

A decrease of the curvature of the cathode tip has virtually no effect on the fundamental mode and its stability. There is some effect over the spot mode: the above-described Z-shape which is present on the low-temperature branch of the spot mode in the basic variant (at $d = 1$ mm) becomes less pronounced with a decrease of d and has been extinguished already at $d = 0.98$ mm. The weak non-monotony of the dependence $T(I)$ on the low-temperature branch of the spot mode which is seen in figure 5.4a at I between approximately 1 and 2 A represents a "remnant" of the Z-shape. Otherwise, the effect of a decrease of the curvature of the cathode tip over the spot mode is not strong. Similarly to what is seen in figure 5.3, the near-cathode voltage drop on the high-temperature branch of the spot mode is in all the cases slightly higher than the voltage drop on the low-temperature branch in the vicinity of the turning point (although this difference is small and can hardly be seen in figures 5.4a-5.4c), and is lower than the voltage drop on the low-temperature branch at

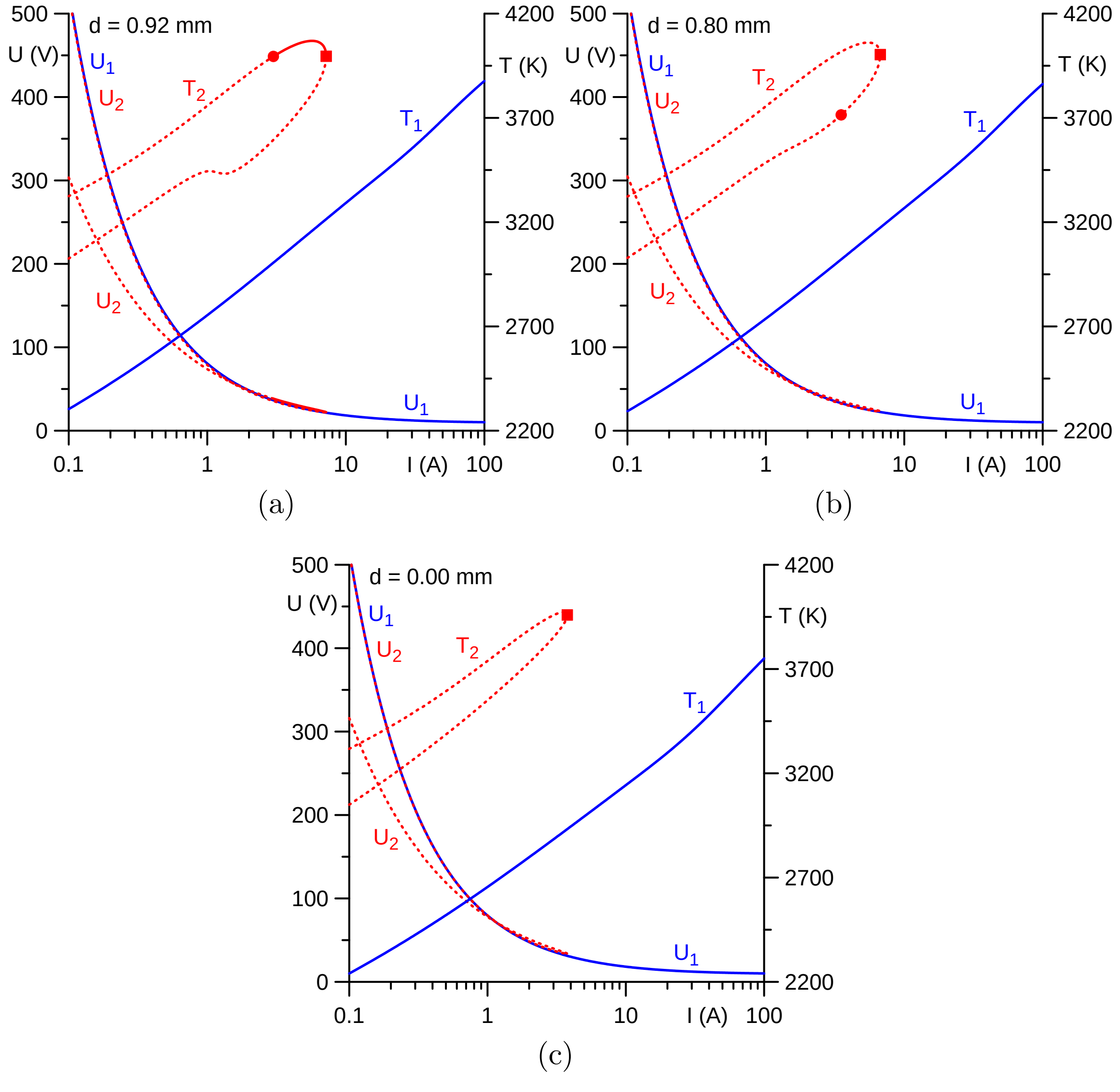

Figure 5.4: Effect of curvature of the cathode tip on the pattern of steady-state modes of current transfer to cathodes with oblate spheroidal tips (a), (b) and a flat tip (c). Circle: state at which the change of stability against the first mode of 3D perturbations occurs. Square: turning point. $R = 1\,\mathrm{mm}$, $h = 10\,\mathrm{mm}$, $T_c = 1000\,\mathrm{K}$.

I below approximately 1.5 A.

There is, however, a dramatic effect over stability of the spot mode. In the basic variant, the high-temperature branch is stable against all perturbations and the low-temperature branch is unstable against axially symmetric perturbations, with the change of stability occurring at the turning point separating these branches. As d decreases, states of the high-temperature branch lose stability against the perturbations proportional to sine or cosine of the azimuthal angle, which represent the first mode of 3D perturbations. The state at which the change of stability against the first mode of 3D perturbations occurs is marked in figure 5.4 by a circle. (Note that a bifurcation of steady-state modes of current transfer occurs at this state: a 3D steady-state mode branches off from the first axially symmetric spot mode.) Initially, this state is positioned in the region of low currents; see figure 5.4a: the high-temperature branch is unstable at lower currents but still stable between the point of change of stability against the first mode of 3D perturbations and the turning point. As d decreases further, the point of change of stability moves in the direction of the turning point; the stable section of the high-temperature branch shrinks. At $d \approx 0.88$ mm the point of change of stability passes over the turning point and moves to the low-temperature branch; the whole of the high-temperature branch becomes unstable.

At still smaller d, the point of change of stability against the first mode of 3D perturbations is shifted in the direction of low currents and eventually displaced from the graph; figure 5.4c. This is a situation familiar from simulations for the cathode with a flat front surface (see section 2.4.4): the high-temperature branch of the first axially symmetric spot mode is unstable against the first mode of 3D perturbations; the low-temperature branch is unstable against the first mode of 3D perturbations and axially symmetric perturbations (and, at low currents, also against higher modes of 3D perturbations).

The above results reveal the first possible scenario of variation of the pattern of current transfer to thermionic cathodes: a change of stability of the first axially symmetric spot mode which occurs through a travel of the point of change of stability against the first mode of 3D perturbations along the whole spot mode.

Prolate spheroidal tip

CVC's and the dependence of the maximum temperature of the cathode surface on the arc current for prolate tips, $d > R$, are shown in figure 5.5. As d increases from 1 mm upwards (figure 5.5a), the above-described Z-shape which is present on the low-temperature branch of the spot mode in the basic variant (figure 5.3) becomes better pronounced and simultaneously is shifted in the direction of low currents. As d increases further, the Z-shape is shifted into the range $I < 0.1$ A and disappears from the graph (figure 5.5b).

Another effect caused by an increase of d and seen on figures 5.5a and 5.5b is approaching of the fundamental and spot modes. At $d \approx 1.383$ mm the two modes become connected: there is a state, corresponding to $I \approx 3.63$ A, which belongs to both modes. In other

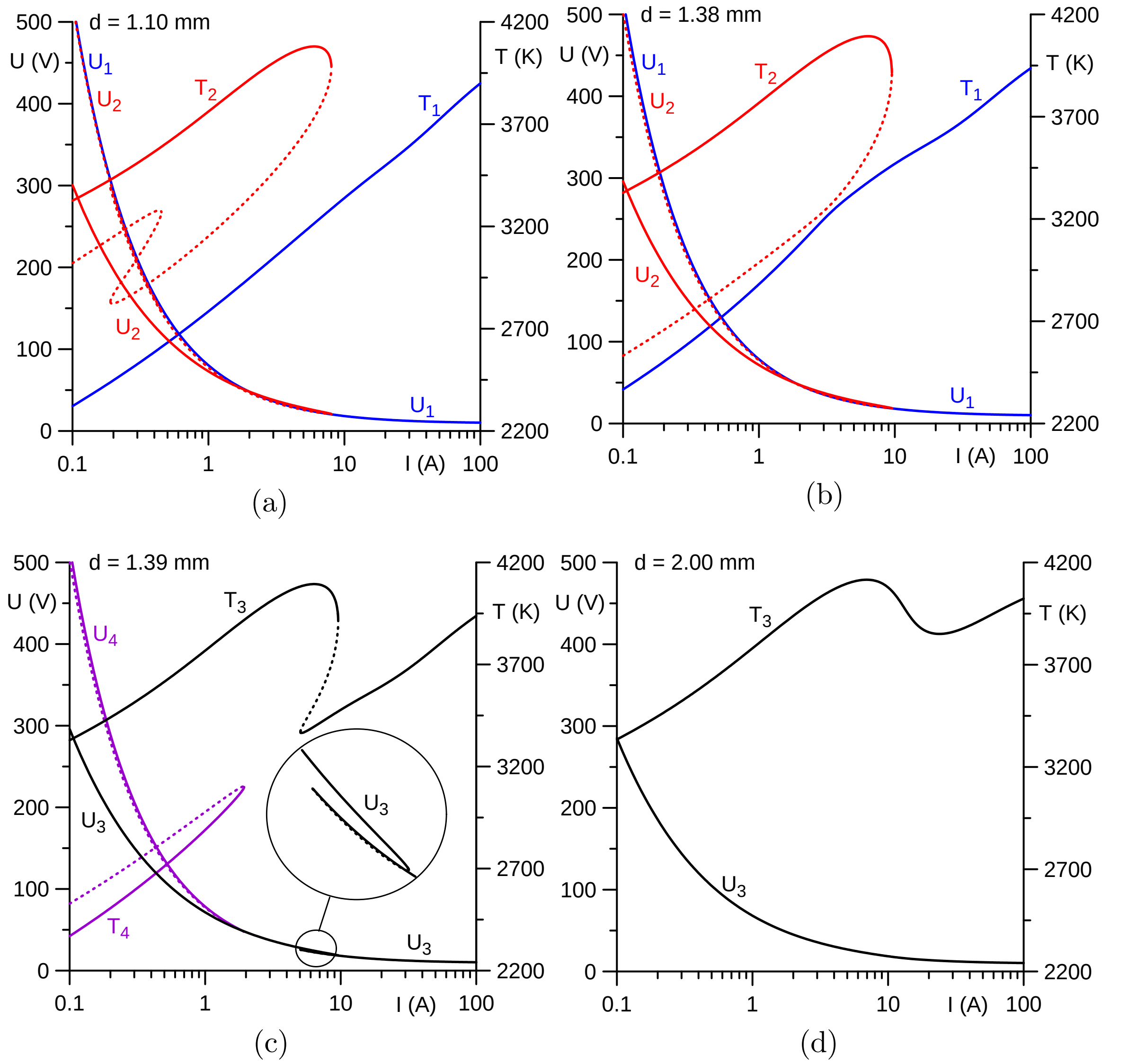

Figure 5.5: Effect of curvature of the cathode tip on the pattern of steady-state modes of current transfer to cathodes with prolate spheroidal tips. $R = 1\,\mathrm{mm}$, $h = 10\,\mathrm{mm}$, $T_c = 1000\,\mathrm{K}$.

words, a bifurcation occurs. There are two disconnected modes once again as d grows further (figure 5.5c), however we will see that these modes cannot be identified with the fundamental and spot modes. The mode to which the index 3 refers exists in the whole current range under consideration and possesses a Z-shape. It is stable with exception of the "retrograde" section of the Z-shape (the section between the turning points). The mode to which the index 4 refers exists only at low currents and comprises two branches separated by a turning point. Again, the branch which manifests higher or, respectively, lower values of the maximum temperature of the cathode surface will be referred to as the high- or low-temperature branch. The low-temperature branch is stable in this case (and is represented by the solid line) while the high-temperature branch is unstable (and is represented by the dotted line), in contrast to what happens in the case of the spot mode depicted in figures 5.3, 5.5a, and 5.5b. The high-temperature branch of the mode 4 in the whole range of existence of this mode is associated with a slightly lower near-cathode voltage drop than the low-temperature branch, although the difference is small and can hardly be seen in figure 5.5c.

As d increases, the Z-shape on the mode 3 becomes less pronounced and eventually is extinguished (figure 5.5d). The mode 4 is shifted in the direction of low currents; eventually it is displaced from the graph and only one mode exists in the whole current range considered (figure 5.5d). Since this mode possesses no Z-shapes, only one thermal regime of the cathode is possible at any current value within the range considered. It is interesting that this mode manifests a minimum in the dependence of the temperature of the hottest point of the cathode on the arc current, positioned at $I \approx 23.9\,\mathrm{A}$.

Apart from the Z-shapes that may be present on the mode 2 (spot mode) and mode 3, CVC's of the modes 3 and 4 shown in figures 5.5c and 5.5d are not fundamentally different from CVC's of the fundamental and, respectively, spot modes in figures 5.3, 5.5a, and 5.5b. However, the maximum cathode temperature in the mode 3 at all currents exceeds the maximum temperature on both branches of the mode 4, and this does not allow one to identify the mode 3 with the fundamental mode and the mode 4 with the first axially symmetric spot mode. Temperature distributions in the body of the cathode for several states belonging to the mode 3 are shown in figure 5.6. While high-current states are characterized by smooth temperature distributions typical for the fundamental mode, there is a well-defined spot in the low-current states. A comparison of distributions of the temperature of the cathode surface for states with the same current belonging to the stable, or low-temperature, and unstable, or high-temperature, branches of the mode 4 is shown in figure 5.7. (Here L is the distance to the center of the front surface of the cathode measured along the generatrix.) States belonging to the stable branch are characterized by smooth temperature distributions typical for the fundamental mode and there is something resembling a poorly pronounced spot on the unstable branch.

In other words, each of the two modes of steady-state current transfer existing in this

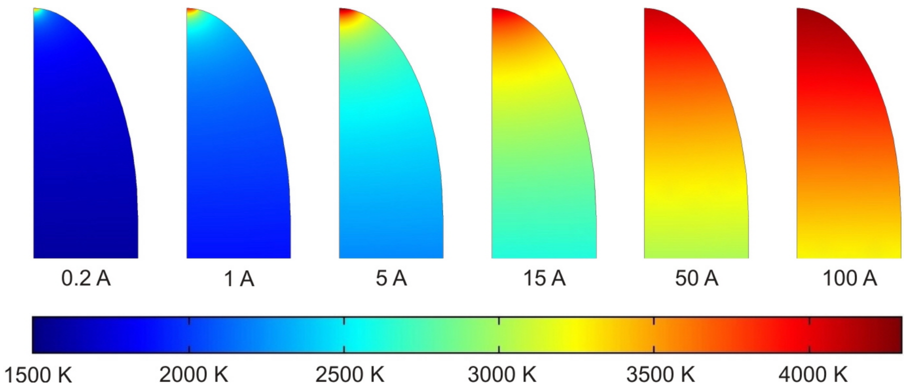

Figure 5.6: Distributions of the temperature inside a cathode with a prolate spheroidal tip in states belonging to mode 3. $d = 2\,\mathrm{mm}$, $R = 1\,\mathrm{mm}$, $h = 10\,\mathrm{mm}$, $T_c = 1000\,\mathrm{K}$.

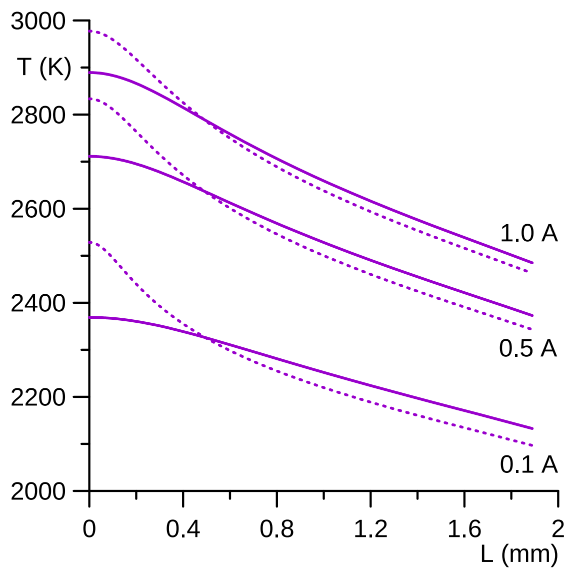

Figure 5.7: Distributions of the temperature along the surface of a cathode with a prolate spheroidal tip in states belonging to mode 4. Solid: stable (low-temperature) branch. Dotted: unstable (high-temperature) branch. $d = 1.39\,\mathrm{mm}$, $R = 1\,\mathrm{mm}$, $h = 10\,\mathrm{mm}$, $T_c = 1000\,\mathrm{K}$.

geometry embraces diffuse states and states with spots; a result similar to the one reported in section 5.1 for a cathode with a protrusion on the top of a hemispherical tip.

One should emphasize that the above-described bifurcation occurring at $I \approx 3.63\,\mathrm{A}$ in the case $d \approx 1.383\,\mathrm{mm}$ involves modes of the same symmetry and occurs at only one value of the parameter d. In this aspect, this bifurcation is similar to the one shown in figure 4.12b of section 4.5.3. One can see from figures 5.5b and 5.5c that the modes exchange branches at this point, and this is why each of the two modes at $d > 1.383\,\mathrm{mm}$ embraces states typical for both fundamental and spot modes.

The above results reveal the second possible scenario of variation of the pattern of current transfer to thermionic cathodes: a perturbed transcritical bifurcation $\{2D, 2D\}$ of second order contact, which is not symmetry-breaking, occurs at a particular value of a control parameter (d, in this case) and is accompanied by an exchange of branches, according to scenario shown in figure B.2b.

5.2.3 Effect of the cathode radius and height

Simulations reported in this section have been performed for a cathode with a hemispherical tip, $d = R$, at $T_c = 1000\,\mathrm{K}$. First, the cathode radius R was varied at fixed height $h = 10\,\mathrm{mm}$. (The results referring to variation of R at fixed h have already been given in section 4.5.3; they are briefly repeated here for completeness.) Second, the height h was varied at fixed radius $R = 1\,\mathrm{mm}$.

The effects of increase of the radius from 1 mm upwards and of decrease of the height from 10 mm downwards are both quite similar to the effect of increase of the curvature of the cathode tip at fixed R and h. The Z-shape which is present on the low-temperature branch of the spot mode in the basic variant (figure 5.3) becomes better pronounced and simultaneously shifted in the direction of low currents. The fundamental and spot modes approach each other and a bifurcation that is not symmetry-breaking appears (at an R value somewhere between 1.16 mm and 1.17 mm or, respectively, at an h value between 8.32 mm and 8.33 mm). This bifurcation is accompanied by an exchange of branches, so each of the two modes emerging at $R \gtrsim 1.17\,\mathrm{mm}$ or, respectively, $h \lesssim 8.32\,\mathrm{mm}$ embraces states typical for both fundamental and spot modes. In other words, the second above-described scenario occurs.

A decrease of the cathode radius from 1 mm downwards and an increase of the height from 10 mm upwards do not cause dramatic changes in the pattern of modes of current transfer. The fundamental and spot modes continue to exist separately. The Z-shape which is present on the low-temperature branch of the spot mode in the basic variant (figure 5.3) becomes less pronounced and eventually is extinguished. The turning point of the spot mode is shifted in the direction of low currents. There is no effect on the stability: the fundamental mode is stable, the high-temperature branch of the spot mode is stable and the low-temperature branch is unstable. Note that some of these features are similar to those characteristic of the decrease of the curvature of the cathode tip at fixed R and h (the separate existence of the fundamental and spot modes and the disappearance of the Z-shape), while the others are different (the shift of the turning point of the spot mode and the lack of effect over stability).

5.2.4 Effect of a protrusion at the top of the cathode tip

In this section, a cathode in the form of a rod with a hemispherical tip and a hemispherical protrusion is considered and modelling results are given for different radii of the protrusion, all the other parameters being fixed. CVC's and the dependence of the maximum temperature of the cathode surface on the arc current are shown in figure 5.8.

Temperature distributions in the body of the cathode for several states belonging to mode 3 under conditions of figure 5.8e are shown in figure 5.9.

Let us first compare figure 5.8a with figure 5.3. The presence of a protrusion produces virtually no effect over the fundamental mode and a strong effect over the spot mode. First, the maximum temperature attained by the cathode surface on the stable branch of the spot mode is much higher than that under conditions of the basic variant: the temperature of the protrusion exceeds 5000 K under conditions of figure 5.8a. Second, the spot mode under conditions of figure 5.8a possesses three turning points, similarly to the spot mode under conditions of figure 5.3, and changes its stability at each of these turning points, in contrast to what happens under conditions of figure 5.3. It is interesting to note that the number of turnings point of the spot mode may vary with an increase of the radius of the protrusion; e.g., five turning points are seen in figure 5.8b.

One can see from figures 5.8a-5.8e that the effect of increase of the radius R_p of the protrusion is similar to the effect of an increase of the curvature of the cathode tip at fixed R and h, or an increase of the ratio R/h of the cathode with a hemispherical tip. The fundamental and spot modes approach each other and a bifurcation that is not symmetry-breaking occurs at an R_p value somewhere between 80 μm and 85 μm. This bifurcation is accompanied by an exchange of branches, so each of the two modes emerging at $R_p \gtrsim 85\,\mu$m embraces states typical for both fundamental and spot modes. In other words, the second above-described scenario occurs.

5.2.5 Effect of the temperature of the cathode base

In this section, a cathode of the same geometry that in the basic variant is considered and modelling results are given for different temperatures T_c of the cathode base. CVC's and the dependence of the maximum temperature of the cathode surface on the arc current are shown in figure 5.10.

Comparing figure 5.10a with figure 5.3, one can see that the decrease of the temperature of the cathode base from 1000 K to 750 K has virtually no effect on the fundamental mode. The Z-shape which is present on the low-temperature branch of the spot mode in the basic variant is not seen in figure 5.10a: it has been shifted to the range of lower currents.

As T_c decreases further, a junction appears between the fundamental and spot modes and these modes form a single mode with a Z-shape; see figure 5.10b. This mode resembles mode 3 in figures 5.5c and 5.8c and is attributed the same designation. As T_c decreases still further, the Z-shape on this mode becomes less pronounced and eventually is extinguished (figure 5.10c). Skipping for brevity temperature distributions in the body of the cathode for different arc currents under conditions of figure 5.10c, we only note that the mode 3 in these conditions embraces states typical for both fundamental and spot modes, similarly to the mode 3 under conditions of figures 5.5c and 5.8c.

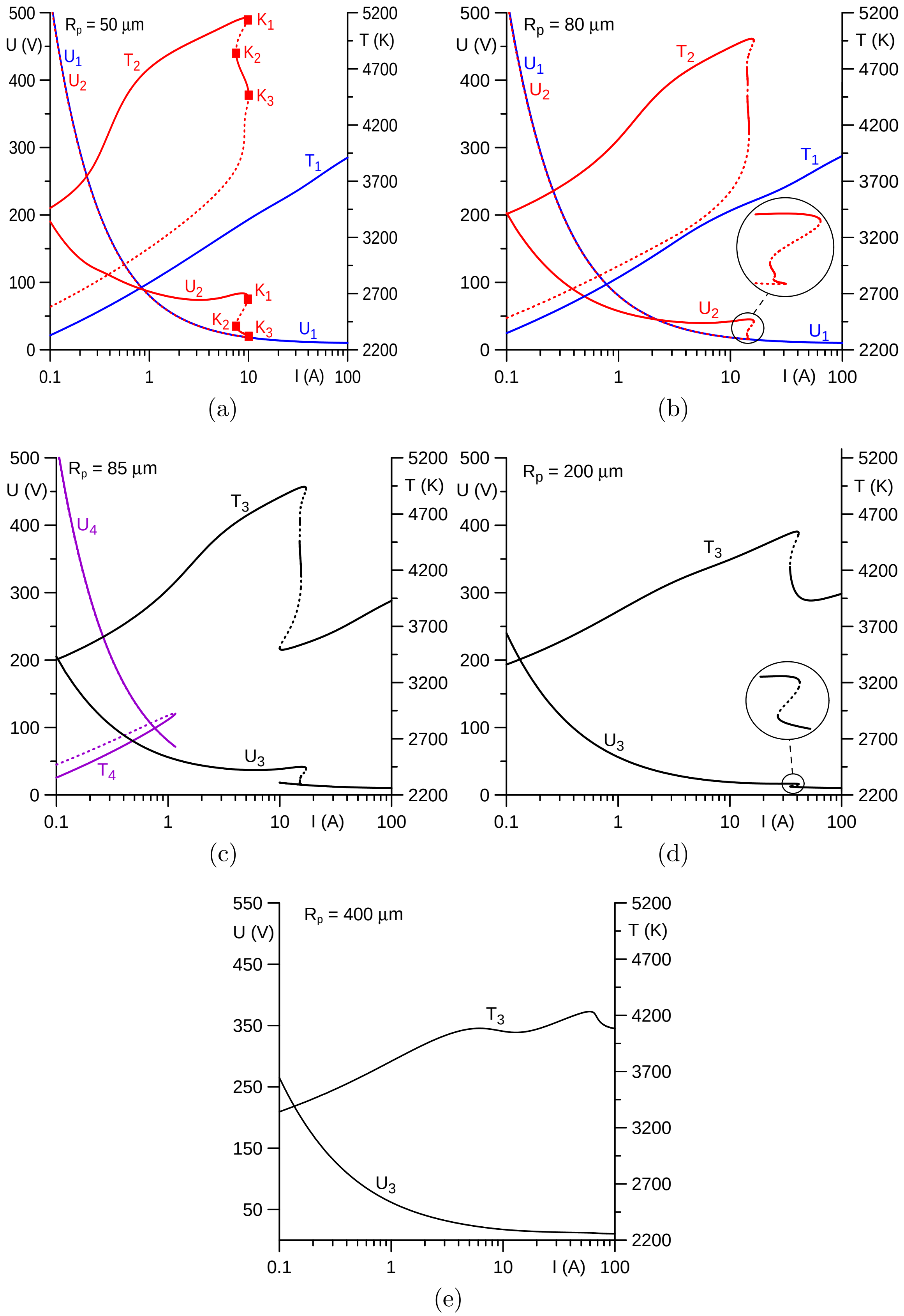

Figure 5.8: Effect of a protrusion on the top of a hemispherical cathode on the pattern of steady-state modes of current transfer. $d = R = 1\,\mathrm{mm}$, $h = 10\,\mathrm{mm}$, $T_c = 1000\,\mathrm{K}$.

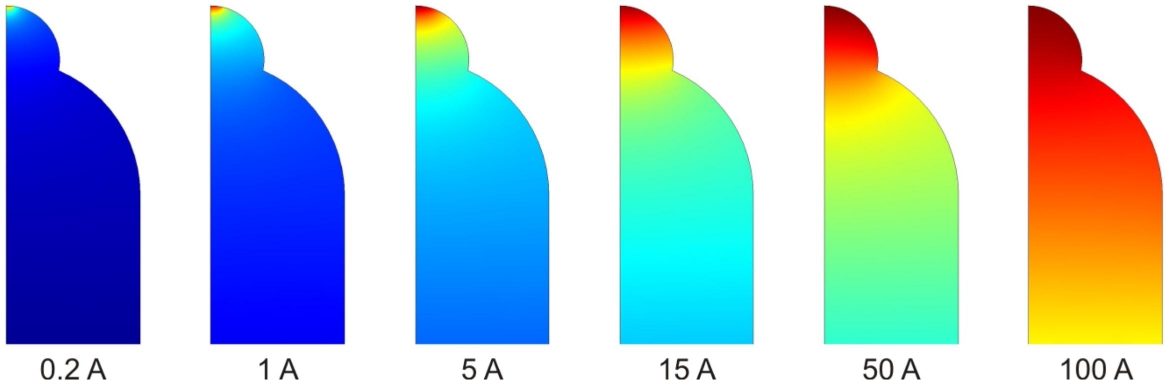

Figure 5.9: Distributions of the temperature inside a cathode with a protrusion in states belonging to mode 3. $R_p = 400\,\mu\mathrm{m}$, $R = 1\,\mathrm{mm}$, $h = 10\,\mathrm{mm}$, $T_c = 1000\,\mathrm{K}$. The temperature bar is shown in figure 5.6.

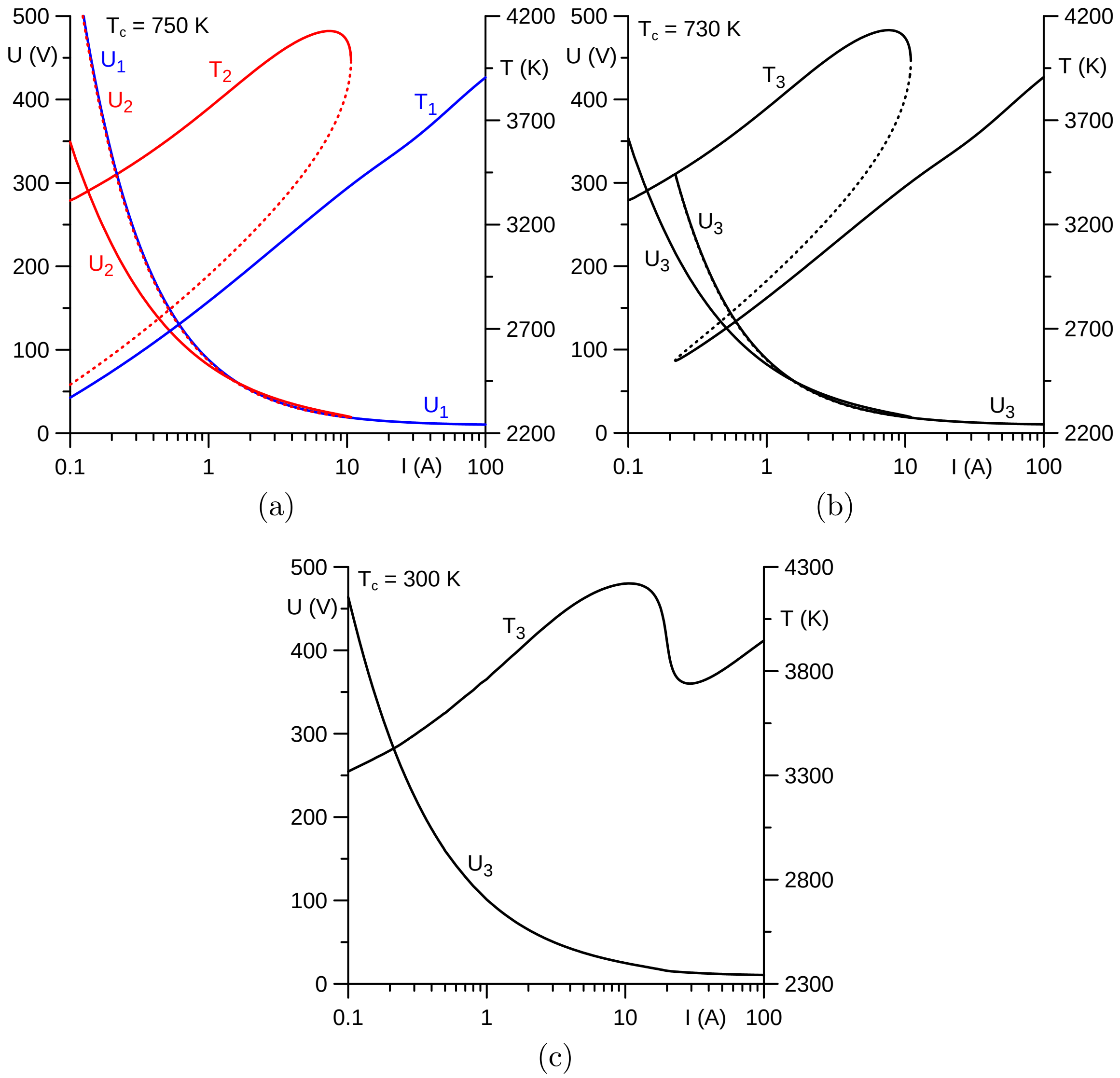

Figure 5.10: Effect of the temperature of the cathode base on the pattern of steady-state modes of current transfer. Cathode with a hemispherical tip, $d = R = 1\,\mathrm{mm}$, $h = 10\,\mathrm{mm}$.

In order to investigate the appearance of the junction, modelling was performed for T_c from 750 K to 730 K in the current range down to 10 mA. The pattern of solutions at $T_c = 749$ K is similar to the one shown in figure 5.10a and comprises two disconnected modes. At $T_c \leq 748$ K, the pattern of solutions is similar to the one shown in figure 5.10b: there is a single mode with a Z-shape. Note that the junction at $T_c = 748$ K occurs at $I \approx 12$ mA. In other words, the junction of the fundamental and spot modes enters the range of I being considered from the region of very low currents.

Thus, one can identify the third scenario of variation of the pattern of current transfer: a junction of the fundamental and spot modes, the result being a single mode existing in a wide current range and comprising states characteristic of the spot mode at low current and of the fundamental mode at high currents. This mode is similar to the mode 3 in the second scenario, however there is a difference in the two scenarios as far as the way of its appearance is concerned: through a junction of the fundamental and spot modes that enters the considered range of I from the region of very low currents in the third scenario, or through a bifurcation that is not symmetry-breaking and occurs at a certain value of I inside the current range being considered in the second scenario. No analogue of the mode 4 exists in the third scenario.

5.3 Discussion

Simulation results reported in this chapter show that variations of control parameters may dramatically change the pattern of steady-state modes of current transfer to a thermionic arc cathode. Three scenarios of these changes have been found. The first one is the movement of the point of change of stability against the first mode of 3D perturbations along the axially symmetric spot mode. This scenario occurs when the curvature of the front surface of the cathode increases starting from zero at fixed radius and height of the cathode. This movement results in the high-temperature branch of the axially symmetric spot mode, while being unstable on the cathode with a flat front surface, becoming stable on a cathode with a hemispherical front surface.

The second scenario is realized through a bifurcation of the fundamental and axially symmetric spot modes that occurs at a certain combination of control parameters and is not symmetry-breaking. The bifurcation is accompanied by an exchange of branches of the modes, which is why each of the two modes appearing as a result of the bifurcation embraces states typical for both fundamental and spot modes. One of these two modes (mode 3) exists at all currents, possesses a Z-shape, and is stable with exception of the retrograde section of the Z-shape. The other mode (mode 4) exists only at low currents and comprises two branches separated by a turning point, one of these branches being stable and the other unstable. Further on from the bifurcation point, the Z-shape on the mode 3 becomes less pronounced and eventually is extinguished, the mode 4 is shifted in the direction of low currents and eventually is displaced into the range $I < 0.1\,\mathrm{A}$. Thus, only one mode remains in the current range of interest and this mode embraces states with a diffuse temperature distribution at high currents and states with a hot spot at low currents. Since this mode possesses no Z-shapes, only one thermal regime of the cathode is possible at any current value within the range considered and this regime is stable. This scenario was encountered when the curvature of the front surface was increased at fixed cathode radius and height, when the radius of a cathode with a hemispherical tip was increased at a fixed height, when the height of a cathode with a hemispherical tip was decreased at a fixed radius, and when the radius of a hemispherical protrusion on top of a cathode in the form of a rod with a hemispherical tip was increased.

The third scenario is realized through a junction of the fundamental and axially symmetric spot modes, which enters the considered range of arc currents from the region of very low currents. This scenario is similar to the second one except that the mode 4 does not appear. This scenario was encountered when the temperature of the cathode base was decreased at fixed geometrical parameters.

The first above-described scenario is intuitively clear: rounding of the cathode tip produces a stabilizing effect over a spot positioned at the center of the tip. The physical meaning of the second scenario may be understood as follows. There are two reasons for appearance of concentrations of current in certain parts of the cathode surface, i.e., of current spots: non-uniformities of geometrical and/or physical properties of the current-collecting surface (such as the presence of protrusions or areas with a reduced work function) and self-organization. A cathode with a flat front surface and thermally and electrically insulated lateral surface [91] represents a limiting case in which the current-collecting surface of the cathode is uniform and the first reason is absent. The fundamental mode of current transfer to such cathode is described by a 1D solution: the temperature in the body of the cathode varies in the axial direction but not in the transversal directions. This solution exists at all arc currents. At arc currents low enough, also axially symmetric and 3D solutions exist describing different spot modes. In other words, a state with uniform distributions of the temperature and current density along the front surface exists at any arc current, and at arc currents low enough also states with non-uniform distributions, i.e., self-organization, exist.

In all the cases other than the above-described limiting case, including in the case of a cathode with a flat tip and an active lateral surface, the current-collecting surface is geometrically non-uniform. Accordingly, the fundamental mode is multidimensional rather than 1D and is associated with the temperature and current density that vary along the cathode surface rather than are constant. One can expect that the non-uniformity, if it is strong enough, is incompatible with the existence of multiple solutions, i.e., with self-organization. Therefore, the second scenario may be understood as a transition from a pattern with two distinct modes, which is a manifestation of self-organization, to a pattern

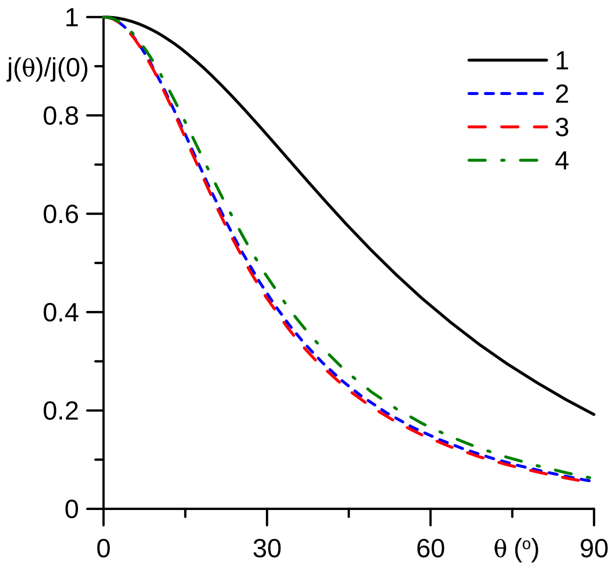

Figure 5.11: Normalized distributions of the current density over the hemispherical cathode tip. $I = 5\,\mathrm{A}$. 1: $d = R = 1\,\mathrm{mm}$, $h = 10\,\mathrm{mm}$, $T_c = 1000\,\mathrm{K}$. 2: $d = R = 1.16\,\mathrm{mm}$ $h = 10\,\mathrm{mm}$, $T_c = 1000\,\mathrm{K}$. 3: $d = R = 1\,\mathrm{mm}$, $h = 8.4\,\mathrm{mm}$, $T_c = 1000\,\mathrm{K}$. 4: $d = R = 1\,\mathrm{mm}$, $h = 10\,\mathrm{mm}$, $T_c = 700\,\mathrm{K}$.

with one mode, which is governed by a non-uniformity of the current-collecting surface. The bifurcation through which this transition is realized may be understood in similar terms: when the non-uniformity of the current-collecting surface reaches a certain level, the cathode temperature distribution associated with the fundamental mode becomes at a certain value of the arc current exactly identical to the temperature distribution associated with the spot mode; the fundamental and spot modes become connected, i.e., a bifurcation occurs. In agreement with the general theory (section 4.5.3), this bifurcation is accompanied by an exchange of branches between the fundamental and spot modes.

The physical meaning of the third scenario is the same: it may be viewed as a transition from a self-organized pattern with two distinct modes, the fundamental mode and the spot mode, to a pattern with a single mode, mode 3, which is governed by a non-uniformity of the current-collecting surface and embraces states with a diffuse temperature distribution at high currents and states with a hot spot at low currents.

An increase in d (at all the other parameters, including the arc current, being fixed) or R_p clearly results in a less uniform current distribution in the fundamental mode. The same effect is produced by an increase of R: the area of the arc attachment is governed primarily by the arc current and does not change much if the current is fixed, while the area of the current-free surface increases. The same effect is produced also by a decrease in h or T_c: a more intense cooling of the arc attachment results in its shrinking. The latter statements are illustrated by figure 5.11, where distributions of the current density over the hemispherical cathode tip are shown for states corresponding to the same arc current $I = 5\,\mathrm{A}$. Here θ is the polar angle, $\theta = 0$ and $\theta = 90\,^\circ$ corresponding to the center of the tip and, respectively, junction of the tip with the cylindrical lateral surface. Lines 1, 2, and 3 correspond to states belonging to the fundamental mode in, respectively, the basic variant, a variant with an increased R, and a variant with a reduced h. Line 4 corresponds to a state belonging to the "base" of the Z-shape in a variant with a reduced T_c; note that the Z-shape in this variant is localized in the current range $2.3\,\mathrm{A} \lesssim I \lesssim 11.4\,\mathrm{A}$. One can see that the distributions described by lines 2-4 manifest considerably more narrow maxima at the center of the tip than the distribution described by line 1, i.e., are less uniform.

Thus, in all the cases the evolution of a self-organized pattern with two distinct modes in the direction of a pattern with one mode is accompanied by an increase of non-uniformity of the fundamental mode, in accord to the above reasoning.

The above reasoning explains the direction of evolution of the patterns caused by a variation of each parameter but does not predict whether this evolution occurs through the second or third scenario. In fact, similar variations of the same parameter may provoke both scenarios, depending on the other parameters. For example, a decrease of h at $d = R = 1\,\mathrm{mm}$ provokes the second scenario when realized at $T_c = 1000\,\mathrm{K}$ (see section 5.2.3) and the third scenario when realized at $T_c = 300\,\mathrm{K}$.

According to the above reasoning, the physics of the spot-like arc attachment at low currents in mode 3 and in the spot mode is not quite the same. The spot in the spot mode is a result of self-organization. The corresponding thermal regime is not the only one possible under the conditions considered: a thermal regime with a diffuse temperature distribution is possible as well, and also a thermal regime associated with the other branch of the spot mode. The spot at low currents in mode 3 represents an attachment of the arc to the center of the cathode tip. No other stationary thermal regime of cathode exists after the Z-shape has disappeared. In fact, the mode 3 may be viewed as a fundamental mode with a strongly variable size of the arc attachment. At high currents, which are sufficient to heat up the whole of the cathode tip, the attachment covers the whole front surface of the cathode. At low currents, that suffice to heat up only a small fraction of the cathode tip, the attachment occupies a small fraction of the front surface. This variation of the size of the arc attachment is clearly seen in figures 5.6 and 5.9.

Results of the present modelling seem to be related to results of experiments [36, 148, 149], which have been performed in low-current arcs typical for high-intensity discharge lamps. The experiments [148, 149] indicate that a protrusion on the front surface of the cathode facilitates a stable operation of the cathode in the spot mode, in particular, helps to eliminate flickering. As discussed in section 1.2.2, three modes of current transfer were observed in experiments of [36], one of them being the super spot mode. Analysis of the experimental data [36], which has been performed with the use of present results in [108], has shown that the super spot mode observed in the work [36] may be explained as mode 3 of the present chapter attached to an elongated protrusion. One can say that the super spot mode appears due to a non-uniformity of the current-collecting surface of the cathode and not due a self-organization.

Let us consider some possibilities to be explored in future experiments. One of the results of the present modelling is the possibility of transition from the pattern with disconnected and stable fundamental and spot modes to a pattern with only one stable mode in a wide current range, which combines features of spot and fundamental modes. In situations where the first pattern occurs, the transition between the fundamental and spot modes is non-stationary and accompanied by hysteresis. Note that from the experimental point of view this situation includes not only cases in which the fundamental and spot modes found in the modelling are exactly disconnected as shown in figure 5.3, but also cases in which mode 3 possesses a Z-shape, as is the case under conditions of figure 5.5c in the current range $I \gtrsim 3\,\mathrm{A}$. In situations where only one stable mode exists in a wide current range (the second pattern), the transition between the diffuse distributions of the cathode surface temperature and distributions with spots may be realized in a quasi-stationary way without hysteresis. Furthermore, a minimum of the dependence of the temperature of the hottest point of the cathode on the arc current occurs during this quasi-stationary transition.

These conclusions may be verified experimentally in a relatively straightforward way. The experiment must be performed in a wide current range, including the range from 5 A to 50 A, which is usually not covered, and be well-controlled, since the sensitivity of the pattern on control parameters is in some cases very high. Cathodes with hemispherical or blunt conical tips may be used, provided that their dimensions and cooling system are suitably chosen. The minimum in the temperature of the hottest point of the cathode can cause similar minima in parameters of the near-cathode plasma and may be traced in this way.

Another conclusion that may be verified experimentally is the one on existence of stable regimes of current transfer which are intermediate between those characteristic for arc and glow cathodes and are associated with currents of several hundred milliamperes and near-cathode voltages of several hundred volts.

5.4 Conclusions

Variations of control parameters may dramatically change the pattern of steady-state modes of current transfer to a thermionic arc cathode. Three scenarios of these changes have been found: movement of the point of change of stability along a mode; bifurcation of modes of the same symmetry occurring at a certain combination of control parameters and accompanied by exchange of branches of the modes; junction of modes of the same symmetry which enters the considered range of arc currents from the region of very low currents.

The first scenario is at the origin of the change of stability of the high-temperature branch of the first axially symmetric spot mode which occurs in a transition from a cathode with the flat front surface to a cathode with the hemispherical front surface. The second or third scenarios are provoked by an increase in the curvature of the front surface of the cathode or in the cathode radius, or by a decrease in the cathode height or the cooling temperature, or by a protrusion on the front surface of the cathode. These scenarios result in a transition from the pattern with disconnected and stable fundamental and axially symmetric spot modes to a pattern with only one stable mode (mode 3) in a wide current range, which combines features of spot and fundamental modes at low and, respectively, high currents.

A pattern with two distinct modes may be viewed as a manifestation of self-organization, while a pattern with one mode is governed by a non-uniformity of the current-collecting surface of the cathode. On the other hand, all the above-mentioned variations of control parameters contribute to the fundamental mode becoming less uniform along the front surface. Therefore, the second and third above-described scenarios may be interpreted as a disappearance of self-organization due to an increasing non-uniformity of the current-collecting surface.

Modelling results provide explanation to some observations made in experiments with low-current arcs typical for high-intensity discharge lamps. In particular, the super spot mode observed in the work [36] may be explained as mode 3 of the present chapter attached to an elongated protrusion. A further work is required, and this work should involve planning of experiments with account of modelling results.

The conclusions on existence under certain conditions of only one stable mode in a wide current range, which combines features of both spot and fundamental modes, and of a minimum of the dependence of the temperature of the hottest point of the cathode on the arc current, manifested by this mode, may have industrial importance and admit a relatively straightforward experimental verification.

Chapter 6

Conclusions of the work

A complete pattern of stability of steady-state modes was established for the case of a current-controlled arc on a cylindrical cathode with a flat tip. The fundamental mode is stable beyond the first bifurcation point and unstable at lower currents. The only steady-state spot mode that may be stable at least in a part of its existence region is the 3D mode with a spot at the edge. Under typical conditions, this mode branches off from the fundamental mode through a subcritical bifurcation and is unstable between the bifurcation point and the turning point and stable beyond the turning point. The transition between this mode and the fundamental mode cannot be realized in a quasi-stationary way and is accompanied by hysteresis. All the spectra found are real. This result conforms to the well-known experimental fact that transitions between the fundamental and spots modes are monotonic. All these conclusions conform to trends observed in experiences.

A pattern of stability of axially symmetric steady-state modes of current transfer in glow discharges was established. Calculation results are given for current-controlled microdischarges in xenon. Both real and complex increments of perturbations have been detected, meaning that perturbations can vary with time both monotonically and with oscillations. The 1D glow discharge is stable in the current range where the CVC is rising and unstable where the CVC is falling. The 1D Townsend discharge is unstable at low current against 1D oscillatory perturbations. The fundamental mode of axially symmetric glow discharge is stable when it operates in the abnormal regime and in a certain current range in the normal regime. The subnormal discharge is unstable. Loss of the charged particles at the lateral wall stabilizes Townsend discharge at low currents. Loss of stability of the abnormal discharge in the vicinity of the point of minimum of the CVC and loss of stability of the Townsend discharge with increasing current develop in different ways: monotonically in time and with oscillations, respectively. There is a current range where the discharge mode associated with a ring spot is stable. In general, results given by the linear stability theory confirm intuitive concepts developed in the literature and conform to the experiment. On the other hand, the theory provides suggestions for further experimental and theoretical work.

Steady-state bifurcations encountered in numerical modelling of current transfer to cathodes of DC glow and arc discharges have been analyzed. The analysis provides explanations to many results obtained in numerical modelling. In particular, it is shown that dramatic changes of patterns of current transfer to cathodes of both glow and arc discharges, described by numerical modelling, occur through perturbed transcritical bifurcations of first and second order contact. The analysis elucidates the mathematical reason why the mode of glow discharge associated with the falling section of the CVC in the solution of von Engel and Steenbeck does not to appear in the 2D solution accounting for absorption of the charged particles by the wall and the subnormal and normal modes appear instead: absorption of the charged particles by the wall causes a change of symmetry of the fundamental mode from 1D to 2D; this causes breaking of the transcritical bifurcation of first order contact {1D,2D}; and such breaking is always accompanied by the exchange of branches. A similar effect has been identified in numerical modelling of arc cathodes and explained.

In spite of physical mechanisms of discharges on cold and hot cathodes being very different, the self-organization fits the same pattern. However, there are also important differences, which have been identified and explained, an example being different scenarios of exchange of branches in breaking of transcritical bifurcations of first order contact. Another example is the difference between 2D fundamental modes on glow and arc cathodes: while the former manifests a normal spot, the latter is characterized by modest variations of parameters along the front surface of the cathode, i.e., is essentially diffuse.

Dramatic changes of the pattern of steady-state modes of current transfer to a thermionic arc cathode, induced by variations of control parameters, have been studied. Three scenarios have been found: movement of the point of change of stability along a mode; bifurcation of modes of the same symmetry occurring at a certain combination of control parameters and accompanied by exchange of branches of the modes; junction of modes of the same symmetry which enters the considered range of arc currents from the region of very low currents. A pattern with two distinct modes may be viewed as a manifestation of self-organization, while a pattern with one mode is governed by a non-uniformity of the current-collecting surface of the cathode. Therefore, the second and third above-described scenarios may be interpreted as a disappearance of self-organization due to an increasing non-uniformity of the current-collecting surface. Results provide an explanation of the mechanism of the so-called super spot mode observed in cathodes of low-current arcs typical for high-intensity discharge lamps.

The lines of future development of this work which are immediately seen include:

- Analytical investigation of stability of the 1D Townsend discharge;
- Investigation of stability of 3D steady-state modes of glow discharge, with the aim to

find out why regular patterns of two or more spots are observed in glow discharges, while not having been observed on arc cathodes;

- Investigation of stability of differents modes of glow discharge with account of multiple ion and excited species, different ionization channels, and non-locality of electron kinetic and transport coefficients;
- Investigation of stability of glow discharge in complex configurations.

Appendix A

Stability of fundamental (diffuse) mode on a cylindrical cathode with an insulating lateral surface: an analytical solution

The model of a cylindrical cathode with an insulating lateral surface has proved previously to give qualitatively - and, in some cases, quantitatively - correct results describing steady-state current transfer to thermionic cathodes of high-pressure arc discharges. The existence of an analytical solution to the eigenvalue problem describing stability of the fundamental mode on such cathodes was pointed out in [84], where also some results have been cited. Results of chapter 2 and of [118] show that this solution provides an useful insight into the physics and reference points necessary for numerical simulations. For completeness, this analytical solution is given in the present appendix.

Let us consider a cathode in the form of a right cylinder, not necessarily circular. The lateral surface of the cylinder is thermally and electrically insulating and collects no energy flux neither electric current. Thermal diffusivity of the cathode material, $\chi = \kappa/\rho c_p$, is constant. The z-axis is directed along the generatrix of the cylinder (cathode) from the front surface inside the bulk. The front (current-collecting) surface Γ_h of the cathode belongs to the plane $z = 0$. The base Γ_c of the cathode belongs to the plane $z = h$, where h is the cathode height.

It is convenient to introduce the heat flux potential $\psi = \int_{T_c}^{T} \kappa(T)\, dT$ as a new dependent variable instead of T. For brevity, ψ will be referred to also as the temperature. The steady-state temperature distribution $\psi_0(\mathbf{r})$, being governed by [118, equations (8) and (9)] supplemented with the boundary condition $\partial\psi_0/\partial n = 0$ at the lateral surface of the cylinder, is 1D and linear in z:

$$\psi_0 = \left(1 - \frac{z}{h}\right)\psi_w. \tag{A.1}$$

Here $\psi_w = \psi_w(U_0)$ is the root of the transcendental equation

$$\frac{\psi_w}{h} = q(\psi_w, U_0) \tag{A.2}$$

and has the meaning of the temperature of the front surface of the cathode. A discussion of this solution can be found elsewhere [91]; here we only note the following. Under typical conditions, equation (A.2) has a trivial root and two positive roots. The CVC, $U_0(I_0)$, is U-shaped and similar to the one depicted by the solid line in figure 2.3. The falling section of the CVC is associated with the smaller positive root of equation (A.2) and the rising section with the bigger root. The inequalities $h\frac{\partial q}{\partial \psi}[\psi_w(U_0), U_0] > 1$ and $h\frac{\partial q}{\partial \psi}[\psi_w(U_0), U_0] < 1$ hold on the falling and growing sections of the CVC, respectively. The temperature of the cathode surface in the fundamental mode monotonically increases with an increase of current, without regard of whether U_0 is growing or decreasing.

The distribution of perturbations $\psi_1(\mathbf{r})$ is governed by an eigenvalue problem comprising [118, equations (11) and (15)] and the boundary condition $\partial\psi_1/\partial n = 0$ at the lateral surface of the cylinder. Note that the derivatives of the functions $q(\psi, U)$ and $j(\psi, U)$ in [118, equation (15)] are evaluated at $\psi = \psi_w(U_0)$ and $U = U_0$, hence these derivatives do not vary along the current-collecting surface. There is therefore no need in averaging $\partial j/\partial\psi$ and $\partial j/\partial U$ over Γ_h, which is present in [118, equation (15)]. (Similarly, there is no need in averaging $\partial j/\partial\psi$ and $\partial q/\partial U$ in [118, equation (18)] and it follows from the latter equation that the spectrum is real in this case.) The eigenvalue problem allows separation of variables: a solution satisfying [118, equation (11)] and the boundary condition $\partial\psi_1/\partial n = 0$ at the lateral surface of the cylinder may be written in the form

$$\psi_1 = \Phi(x, y)\sinh\left[\sqrt{k^2 + \chi^{-1}\lambda}\,(h - z)\right], \tag{A.3}$$

where k^2 is a separation constant and Φ is a solution of the Neumann problem for the two-dimensional Helmholtz equation

$$G: \quad \frac{\partial^2\Phi}{\partial x^2} + \frac{\partial^2\Phi}{\partial y^2} + k^2\Phi = 0, \qquad g: \quad \frac{\partial\Phi}{\partial n_g} = 0. \tag{A.4}$$

Here G is the cross section of the cylinder, g is the boundary of the domain G, and n_g is a direction in the plane (x, y) locally orthogonal to g.

In order that the problem (A.4) have a non-trivial solution, it must be considered as an eigenvalue problem, Φ and k playing the roles of an eigenfunction and an eigenvalue, respectively. It is known that all eigenvalues of this problem are real and of finite degeneracy; the set of eigenvalues is countable and may be numbered in order of their increase. We denote the set of eigenvalues numbered in order of their increase by $k_0, k_1, k_2, \ldots$. Let N_i $(i = 0, 1, 2, \ldots)$ be a degeneracy of the i-th eigenvalue and $\Phi_{i\eta} = \Phi_{i\eta}(x, y)$ $(i = 0, 1, 2, \ldots;$ $\eta = 1, 2, \ldots, N_i)$ a set of eigenfunctions associated with the i-th eigenvalue. Note that $k_0 = 0$, $N_0 = 1$, $\Phi_{01} = 1$; $k_i > 0$, $\langle\Phi_{i\eta}\rangle = 0$ for $i \geq 1$. (Here the angular brackets designate averaging in x and y over the domain G.)

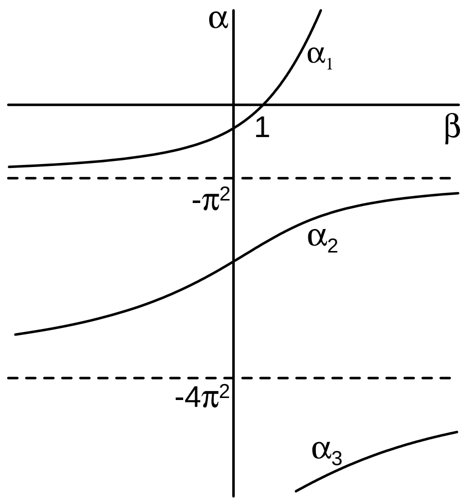

Figure A.1: Solution to equation (A.5) (solid). Dashed: $\alpha = -\pi^2$, $\alpha = -4\pi^2$.

Thus, k and Φ in the expression (A.3) should be replaced with k_i and $\Phi_{i\eta}$, where $i = 0, 1, 2, \dots$ and $\eta = 1, 2, \dots, N_i$. Substituting this expression into the boundary condition [118, equation (15)], one arrives at a transcendental equation governing spectrum of perturbations. In the dimensionless form, this equation may be written as

$$\sqrt{\alpha} \coth \sqrt{\alpha} = \beta, \tag{A.5}$$

where $\alpha = h^2 \left(k_i^2 + \chi^{-1}\lambda\right)$ and

$$\beta = \begin{cases} h\frac{\partial q}{\partial \psi} - h\frac{\partial q}{\partial U}\frac{\omega \frac{\partial j}{\partial \psi}}{1+\omega\frac{\partial j}{\partial U}}, & \text{if} \quad i = 0 \\ h\frac{\partial q}{\partial \psi}, & \text{if} \quad i \geq 1 \end{cases} \tag{A.6}$$

(here $\omega = S_h \Omega$, S_h being area of the front surface of the cathode).

Equation (A.5) has no more than one positive root and a countable set of negative roots; see figure A.1. (It is convenient to rewrite this equation as $\sqrt{-\alpha} \cot \sqrt{-\alpha} = \beta$ while treating negative roots.) Let us designate by $\alpha_1 = \alpha_1(\beta)$ the root of equation (A.5) that takes values exceeding $-\pi^2$, by $\alpha_2 = \alpha_2(\beta)$ the root that takes values between $-4\pi^2$ and $-\pi^2$ *etc.* Note that $\alpha_1(\beta) > 0$ at $\beta > 1$, $\alpha_1(1) = 0$, $\alpha_1(\beta) < 0$ at $\beta < 1$, $\alpha_\epsilon(\beta) < 0$ at all β for $\epsilon \geq 2$. Now the desired spectrum may be written as

$$\lambda = \chi \left[h^{-2}\alpha_\epsilon(\beta) - k_i^2\right], \tag{A.7}$$

where $i = 0, 1, 2, \dots$ and $\epsilon = 1, 2, 3, \dots$. One can see that instability is possible only against perturbations with $\epsilon = 1$. An increase of any of the "quantum numbers" i and ϵ originates a decrease of λ. The physical meaning of this result is quite clear: higher i and/or ϵ correspond to more oscillations of perturbations in the plane (x, y) and/or in the direction z and, consequently, to stronger thermal conduction, which produces a stabilizing effect.

Note that equation (A.3), describing the form of perturbations, can be re-written as

$$\psi_1 = \Phi_{i\eta}(x,y) \sinh\left[\sqrt{\alpha_\epsilon(\beta)}\left(1-\frac{z}{h}\right)\right], \tag{A.8}$$

where $i = 0,1,2,\ldots$, $\eta = 1,2,\ldots,N_i$, and $\epsilon = 1,2,3,\ldots$. One can see that unstable perturbations [i.e., those for which $\alpha_\epsilon(\beta) > 0$] vary with z monotonically, while stable perturbations vary with z non-monotonically.

Equation (A.7) with $i = 0$ assumes the form $\lambda = \chi h^{-2}\alpha_\epsilon(\beta)$, where $\epsilon = 1,2,3,\ldots$, and gives increments of growth of 1D perturbations described by equation (A.8) with $i = 0$. As it should have been expected, the increment of 1D perturbations is affected by the cathode height h but not by the shape and dimensions of the cathode cross section. The instability against (the mode with $\epsilon = 1$ of) 1D perturbations occurs if $\beta > 1$, i.e., if

$$\frac{\partial q}{\partial \psi} - \frac{\partial q}{\partial U}\frac{\omega\frac{\partial j}{\partial \psi}}{1+\omega\frac{\partial j}{\partial U}} > \frac{1}{h}. \tag{A.9}$$

This inequality represents a criterion of instability against 1D perturbations.

The criterion (A.9) may be understood as follows. In the case where the external resistance is absent, $\omega = 0$, this inequality amounts to

$$\frac{\partial q}{\partial \psi} > \frac{1}{h}. \tag{A.10}$$

The physical meaning is quite clear: the instability appears provided that there is a positive feedback (an increase of the cathode temperature causes an increase of the energy flux from the plasma) which is strong enough to overcome the stabilizing effect of heat removal by thermal conduction from the front surface of the cathode to the base.

In the opposite limiting case of a current-stabilized arc, where the external resistance is large, $\omega \gg (\partial j/\partial U)^{-1}$, the inequality (A.9) may be written as

$$\left(\frac{\partial q}{\partial \psi}\right)_j > \frac{1}{h}, \tag{A.11}$$

where the derivative $(\partial q/\partial \psi)_j$ is taken at constant current density and is given by the formula

$$\left(\frac{\partial q}{\partial \psi}\right)_j = \frac{\partial q}{\partial \psi} - \frac{\partial q}{\partial U}\frac{\partial j}{\partial \psi}\left(\frac{\partial j}{\partial U}\right)^{-1}. \tag{A.12}$$

The physical sense of the inequality (A.11) is similar to that of the inequality (A.10), with the difference that what is fixed in the limiting case of large external resistance is current not voltage.

In the general case of arbitrary external resistance, inequality (A.9) may be written in the form

$$\frac{1}{1+\omega\frac{\partial j}{\partial U}}\frac{\partial q}{\partial \psi} + \frac{\omega\frac{\partial j}{\partial U}}{1+\omega\frac{\partial j}{\partial U}}\left(\frac{\partial q}{\partial \psi}\right)_j > \frac{1}{h}, \tag{A.13}$$

with the obvious physical meaning: a weighted average of the inequalities (A.10) and (A.11).

Inequality (A.9) may be explained also in terms of the differential resistance of the cathodic part of the discharge. The slope of the CVC of the fundamental mode is given by [91, equation (9)]

$$\frac{dU_0}{dI_0} = -\frac{1}{S_h \frac{\partial j}{\partial U}} \frac{h \frac{\partial q}{\partial \psi} - 1}{1 - h \left(\frac{\partial q}{\partial \psi} \right)_j}. \tag{A.14}$$

Making use of this formula, one can transform inequality (A.13) to

$$\frac{\frac{\partial j}{\partial U}}{1 + \omega \frac{\partial j}{\partial U}} \left[1 - h \left(\frac{\partial q}{\partial \psi} \right)_j \right] \left(\frac{dU_0}{dI_0} + \Omega \right) < 0. \tag{A.15}$$

If the voltage applied to the near-cathode layer increases while the temperature of the cathode surface remains constant, the density of the electric current coming to the cathode increases. If the temperature of the cathode surface increases at constant current density rather than at constant voltage, an improvement of conditions of current transfer results in a decrease of U and, consequently, of the power deposited in the near-cathode layer. Hence, functions $j(\psi, U)$ and $q(\psi, U)$ of physical interest satisfy the inequalities [91]

$$\frac{\partial j}{\partial U} > 0, \quad \left(\frac{\partial q}{\partial \psi} \right)_j < 0. \tag{A.16}$$

It follows that the first and second multipliers on the lhs of inequality (A.15) are positive and this inequality amounts to

$$\frac{dU_0}{dI_0} + \Omega < 0. \tag{A.17}$$

The physical sense of this result is clear: the 1D instability appears if the external resistance is insufficient to compensate the negative differential resistance of the cathodic part of the discharge. Note that this result is non-trivial, given the thermal nature of the instability being considered.

Equation (A.7) with $i \geq 1$ gives the increment of growth of 3D perturbations, which are described by equation (A.8) with $i \geq 1$. In contrast to the case of 1D perturbations, the increment of 3D perturbations is not affected by the external resistance but is affected by the shape and dimensions of the cathode cross section (through the parameter k_i). The criterion of instability against (the mode with $\epsilon = 1$ of) 3D perturbations is

$$\alpha_1 \left(h \frac{\partial q}{\partial \psi} \right) > (k_i h)^2 \tag{A.18}$$

or, equivalently,

$$\frac{\partial q}{\partial \psi} > k_i \coth k_i h. \tag{A.19}$$

Again, the instability appears provided that the positive feedback is strong enough to overcome the stabilizing effect of thermal conduction.

Let us now relate the above results to the CVC of the fundamental mode. Criterion (A.17) cannot be satisfied on the growing section of the CVC, where $dU_0/dI_0 > 0$, hence all states on the growing section are stable against 1D perturbations. If $\Omega = 0$, criterion (A.17) is satisfied on the falling section of the CVC, where $dU_0/dI_0 < 0$, hence all states on the falling section are unstable against 1D perturbations of the form (A.8) with $i = 0$ and $\epsilon = 1$ if external resistance is absent. A large enough external resistance results in suppression of the 1D instability. In particular, in the case of a current-controlled arc every state belonging to the fundamental mode is stable against 1D perturbations. The latter follows from the inequality (A.11) being not satisfied under conditions of physical interest, which can be seen from incompatibility of this inequality with the second inequality (A.16).

Steady states at which $\partial q/\partial \psi = k_i \coth k_i h$, $i \geq 1$, represent points of neutral stability for 3D perturbations of the form (A.8). Steady-state 3D spot-mode solutions branch off from the 1D fundamental-mode solution at these points [91], therefore the points of neutral stability may be called also bifurcation points. Since $x \coth x > 1$ for real x, all bifurcation points belong to the falling section of the CVC of the fundamental mode, where $h\,\partial q/\partial \psi > 1$.

For states on the growing section of the CVC, $h\,\partial q/\partial \psi < 1$ and the inequality (A.19) is not satisfied for all i. Hence, these states are stable against 3D perturbations. At states between the minimum of the CVC and the first bifurcation point (the one with $i = 1$), the quantity $h\,\partial q/\partial \psi$, while exceeding 1, is still below $k_1 h \coth k_1 h$. Hence, these states as well are stable against 3D perturbations. States between the first and second bifurcation points are unstable against N_1 modes of 3D perturbations, namely against perturbations of the form (A.8) with $i = 1$, $\eta = 1, 2, \ldots, N_1$, $\epsilon = 1$. States between the second and third bifurcation points are unstable against $N_1 + N_2$ modes of 3D perturbations, namely against those with $i = 1$, $\eta = 1, 2, \ldots, N_1$, $\epsilon = 1$ and those with $i = 2$, $\eta = 1, 2, \ldots, N_2$, $\epsilon = 1$ *etc.*

The above conclusions on stability of the 1D fundamental mode conform to conclusions of the approximate treatment [118]. On the other hand, the above conclusions have been derived from an exact expression for spectrum of perturbations, equation (A.7); a more straightforward and transparent, although less general, derivation than the one given in [118].

In order to apply the above results, one needs a solution to the Neumann eigenvalue problem for the two-dimensional Helmholtz equation (A.4). This solution is known for many domains G of a simple shape. In particular, if G is a circle, i.e., if the cathode has the shape of a right circular cylinder with an insulating lateral surface, then spectrum of the problem (A.4) is given by the formula

$$k = j'_{m,s}/R, \tag{A.20}$$

Mode	m	s	ϵ	Type	$j'_{m,s}$	i
a	0	1	1	1D	0	0
b	0	1	2	1D	0	0
c	0	2	1	Axially symmetric	3.832	3
d	1	1	1	3D	1.841	1
e	2	1	1	3D	3.054	2
f	3	1	1	3D	4.201	4

Table A.1: Characteristics of the perturbation modes depicted in figure 2.4.

where $m = 0, 1, 2, \ldots$, $s = 1, 2, 3, \ldots$, R is the radius of the cylinder, and $j'_{m,s}$ is the s-th zero of the derivative of the Bessel function of the first kind of order m (according to the conventional nomenclature [153], $j'_{0,1} = 0$ and $j'_{m,1} > 0$ for $m \geq 1$). Eigenvalues (A.20) with $m = 0$ are simple and are associated with eigenfunctions

$$\Phi_{i1} = J_0 \left(j'_{0,s} \frac{r}{R} \right), \tag{A.21}$$

those with $m \geq 1$ are doubly degenerated and associated with eigenfunctions

$$\left\{ \begin{array}{c} \Phi_{i1} \\ \Phi_{i2} \end{array} \right\} = J_m \left(j'_{m,s} \frac{r}{R} \right) \left\{ \begin{array}{c} \cos m\phi \\ \sin m\phi \end{array} \right\}, \tag{A.22}$$

where r is the distance from the axis of the cylinder, ϕ is the azimuthal angle, and $J_m(x)$ is the Bessel function of the first kind of order m.

Thus, spectrum of perturbations of the fundamental mode on a cathode which has the shape of a right circular cylinder with an insulating lateral surface is governed by three "quantum numbers": $m = 0, 1, 2, \ldots$, $s = 1, 2, 3, \ldots$, and $\epsilon = 1, 2, 3, \ldots$. Perturbations with $m = 0$ and $s = 1$ are 1D, those with $m = 0$ and $s \geq 2$ are axially symmetric, perturbations with $m \geq 1$ are 3D. Note that $i = 0$ for 1D perturbations and $i \geq 1$ for axially symmetric and 3D perturbations, therefore increments of both axially symmetric and 3D perturbations are affected by the cathode radius but not by the external resistance. Again, an increase of any of the quantum numbers m, s, ϵ results in more oscillations of perturbations (in the directions ϕ, r, and z, respectively) and, consequently, in a decrease of λ.

Values of quantum numbers corresponding to perturbation modes depicted in figure 2.4 are given in table A.1. Also shown in the table are type of perturbations, values of $j'_{m,s}$ (i.e., of the normalized eigenvalue) and of the number i of the eigenvalue associated with each mode.

Appendix B

Steady-state bifurcations in systems with one degree of freedom

The bifurcation theory is not a tool of everyday use in the gas discharge physics, therefore a brief summary of relevant information seems to be in place. There is extensive literature on the subject, e.g., [154–157]. On the other hand, the concepts needed for this work are quite natural and may be summarized in a concise and self-sufficient form.

B.0.1 Bifurcations in systems governed by a single parameter

As far as bifurcations are concerned, most problems with a large and even infinite number of degrees of freedom, such as continuum problems, are similar to simple systems with one or two degrees of freedom. (This may be viewed as a consequence of the center manifold theorem; e.g., [154–157].) Of interest for this dissertation are steady-state bifurcations in systems with one degree of freedom. Let us consider a system with one degree of freedom governed by a single parameter μ and described by the equation

$$\frac{dx}{dt} = F, \tag{B.1}$$

where t is time (the independent variable), x is the dependent variable, and F is a known function of μ and x, $F = F(\mu, x)$. The simplest forms of the function F that produce bifurcations are the following:

$$F = \mu - x^2, \tag{B.2}$$

$$F = \mu x - x^2, \tag{B.3}$$

$$F = \mu x \pm x^3. \tag{B.4}$$

The steady-state (equilibrium) solutions of differential equation (B.1) are designated x_0 and governed by algebraic equation $F(\mu, x_0) = 0$. The steady-state solutions for functions

F given by equations (B.2)-(B.4), are, respectively

$$x_0^{(1)} = -\sqrt{\mu}, \quad x_0^{(2)} = \sqrt{\mu}; \tag{B.5}$$

$$x_0^{(1)} = 0, \quad x_0^{(2)} = \mu; \tag{B.6}$$

$$x_0^{(1)} = 0, \quad x_0^{(2)} = -\sqrt{\mp\mu}, \quad x_0^{(3)} = \sqrt{\mp\mu}. \tag{B.7}$$

These solutions are shown in figures B.1a-B.1d.

In all the cases, the origin $\mu = x_0 = 0$ belongs to more than one solution. This phenomenon is called branching, or bifurcation, of solutions; the point $\mu = x_0 = 0$ is called the bifurcation point; and figures B.1a-B.1d are called bifurcation diagrams. The bifurcation described by equation (B.5) and shown in figure B.1a is called fold or saddle-node. Note that functions $x_0^{(1)}(\mu)$ and $x_0^{(2)}(\mu)$ given by equation (B.5) may be viewed not as separate solutions but rather as branches of a single solution, which at $\mu = 0$ reaches a boundary of its existence region, $\mu \geq 0$, and turns back. This is why points of fold bifurcations are also called turning points.

The bifurcation described by equation (B.6) and shown in figure B.1b is called transcritical. It may be viewed as an intersection of two solutions existing on both sides of the bifurcation point (i.e., at both positive and negative μ).

The bifurcations described by equation (B.7) and shown in figures B.1c and B.1d are called pitchfork bifurcations. The function $F(\mu, x)$ given by equation (B.4) is odd with respect to x. In such cases, equation (B.1) is invariant with respect to the transformation of inversion $x \to -x$. Therefore, if such equation admits a solution $x(t)$, then $-x(t)$ is a solution as well. Such equations always admit a trivial solution, which is symmetric with respect to transformation $x \to -x$; non-trivial solutions can appear only in pairs and are related by this transformation. Indeed, the set of solutions given by equation (B.7) includes the trivial solution $x_0^{(1)}$ and two non-symmetric solutions $x_0^{(2)}$ and $x_0^{(3)}$, being $x_0^{(2)} = -x_0^{(3)}$. Thus, the bifurcations described by equation (B.7) and shown in figures B.1c and B.1d represent branching of a pair of non-symmetric solutions that exist at either $\mu \geq 0$ or $\mu \leq 0$ from a symmetric solution that exists on both sides of the bifurcation point, and may be viewed as breaking of symmetry.

The three bifurcations considered above are quite common and treated in all textbooks. It is appropriate for the purposes of this work to consider also a less common bifurcation which represents a special case of transcritical bifurcation and is introduced by a function F slightly different from (B.3): μ is replaced with μ^2 and, for convenience, the sign of the rhs is changed, i.e.,

$$F = x^2 - \mu^2 x. \tag{B.8}$$

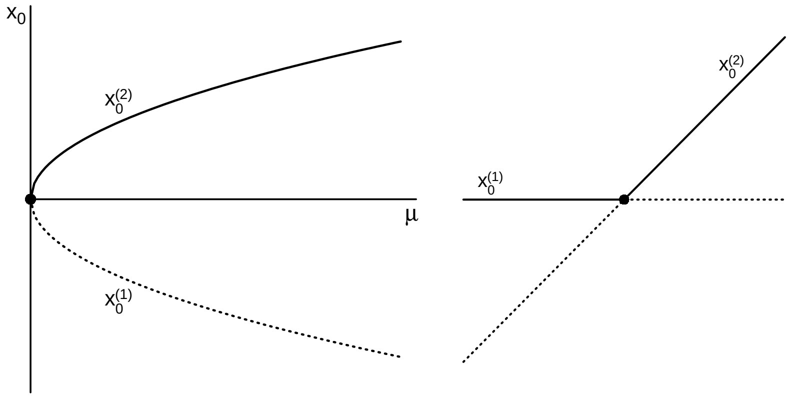

(a) (b)

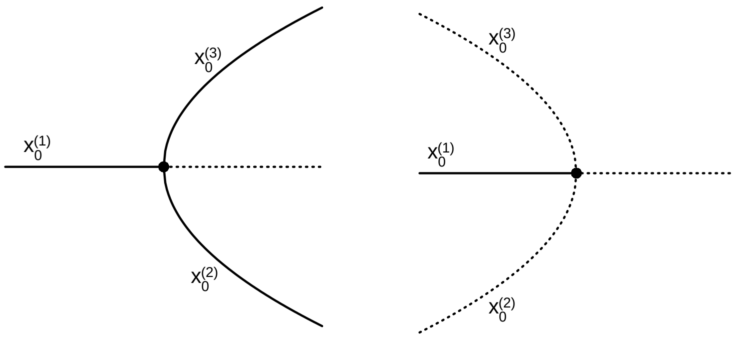

(c) (d)

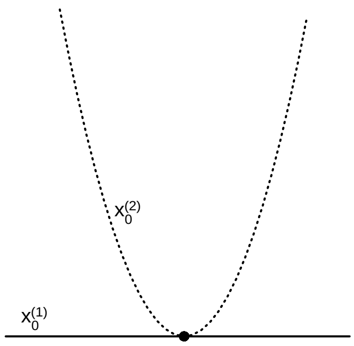

(e)

Figure B.1: Bifurcation diagrams of single-parameter steady-state solutions in one dimension. The origin $\mu = x_0 = 0$ is marked by a circle, axes μ and x_0 in figures (b)-(e) are the same as in figure (a). Solid: stable sections of steady-state solutions. Dotted: unstable sections. (a) Fold bifurcation, equation (B.5). (b) Transcritical bifurcation of first order contact, equation (B.6). (c) Supercritical pitchfork bifurcation, equation (B.7) with the lower sign. (d) Subcritical pitchfork bifurcation, equation (B.7) with the upper sign. (e) Transcritical bifurcation of second order contact, equation (B.9).

There are two steady-state solutions for this function,

$$x_0^{(1)} = 0, \quad x_0^{(2)} = \mu^2, \tag{B.9}$$

which are shown in figure B.1e. The bifurcation is transcritical, similarly to the one described by equation (B.6) and shown in figure B.1b. While the two solutions described by equation (B.6) and shown in figure B.1b cross, i.e., have different first derivatives at the bifurcation point, the two solutions described by equation (B.9) are tangent at the bifurcation point. This bifurcation will be referred to as transcritical bifurcation of second order contact. For consistency, the bifurcation described by equation (B.6) and shown in figure B.1b is referred to in this work as transcritical bifurcation of first order contact.

B.0.2 Stability of bifurcating steady-state solutions

Changes of stability of steady-state solutions frequently occur at bifurcation points. In the framework of the conventional procedure of linear stability analysis, a solution of equation (B.1) is sought as the sum of a steady-state solution and a small perturbation with the exponential time dependence: $x(t) = x_0 + x_1 e^{\lambda t}$, where x_1 is an infinitesimal constant and λ is the growth increment of the perturbation. Substituting this expression into equation (B.1), expanding the rhs in powers of x_1, and retaining only the leading term, one finds

$$\lambda = \frac{\partial F}{\partial x}\left[\mu, x_0(\mu)\right]. \tag{B.10}$$

Using this result, one finds that the increments of growth of perturbations of the steady-state solutions $x_0^{(1)}$ and $x_0^{(2)}$ given by equation (B.5) are, respectively,

$$\lambda^{(1)} = 2\sqrt{\mu}, \quad \lambda^{(2)} = -2\sqrt{\mu}. \tag{B.11}$$

It follows that solutions $x_0^{(1)}$ and $x_0^{(2)}$ are unstable and, respectively, stable in the whole region of their existence (which is $\mu \geq 0$) except the point $\mu = 0$. $\lambda^{(1)} = \lambda^{(2)} = 0$ at $\mu = 0$, i.e., the solutions are neutrally stable at the fold bifurcation point. In fact, the latter is true for any bifurcation: a bifurcation at the point $\mu = 0$ means that the equation $F(\mu, x_0) = 0$ has multiple roots at small μ, which requires that $\frac{\partial F}{\partial x}(0, 0) = 0$. The above conclusions on stability are illustrated by figure B.1a.

Figure B.1a represents an example of a scenario of fold bifurcation, which is conventional in the bifurcation theory. It is convenient for the purposes of this work to mention also the other scenarios, which are obtained by reflection of figure B.1a with respect to the x_0-axis (the second scenario), or with respect to the μ-axis (the third scenario), or with respect to both x_0- and μ-axes (the fourth scenario). Note that these scenarios correspond to replacing equation (B.2) with, respectively, $F = -x^2 - \mu$, or $F = x^2 - \mu$, or $F = x^2 + \mu$.

The increments of growth of perturbations of solutions (B.6) are, respectively,

$$\lambda^{(1)} = \mu, \quad \lambda^{(2)} = -\mu. \tag{B.12}$$

It follows that solutions $x_0^{(1)}$ and $x_0^{(2)}$ are stable and, respectively, unstable at $\mu < 0$ and *vice versa* at $\mu > 0$ as shown in figure B.1b. One can say that the bifurcating solutions exchange stability at the point of transcritical bifurcation of first order contact.

The increments of growth of perturbations of solutions (B.9) are, respectively,

$$\lambda^{(1)} = -\mu^2, \quad \lambda^{(2)} = \mu^2. \tag{B.13}$$

It follows that solutions $x_0^{(1)}$ and $x_0^{(2)}$ are stable and, respectively, unstable at all $\mu \neq 0$. In other words, the bifurcating solutions do not change stability at the point of transcritical bifurcation of second order contact as shown in figure B.1e.

The increments of growth of perturbations of solutions given by equations (B.7) are, respectively,

$$\lambda^{(1)} = \mu, \quad \lambda^{(2)} = \lambda^{(3)} = -2\mu. \tag{B.14}$$

The solution $x_0^{(1)}$ is stable at $\mu < 0$ and unstable $\mu > 0$. In other words, the solution $x_0^{(1)}$ changes its stability at the bifurcation point. In the case depicted in figure B.1c, which corresponds to the lower sign in equations (B.4) and (B.7), both solutions $x_0^{(2)}$ and $x_0^{(3)}$ are stable in the whole region of their existence (except the point $\mu = 0$). In the case depicted in figure B.1d, which corresponds to the upper sign, both solutions are unstable. In other words, if the pair of bifurcating solutions branches off into the region where $x_0^{(1)}$ is unstable, then both bifurcating solutions are stable; figure B.1c. Pitchfork bifurcations of this type are said supercritical. If the pair of bifurcating solutions branches off into the region where the solution $x_0^{(1)}$ is stable, then both bifurcating solutions are unstable (figure B.1d); a subcritical pitchfork bifurcation.

B.0.3 Perturbations of transcritical bifurcations in systems governed by two parameters

It is necessary for the purposes of this work to consider also transcritical bifurcations of first and second order contact in systems governed by two parameters. Let us introduce a new parameter δ and replace expression (B.3) with $F = \mu x - x^2 - \delta$ and (B.8) with $F = x^2 - \mu^2 x + \delta$. Then roots of the equation $F(\mu, x_0) = 0$ are

$$x_0^{(3)} = \frac{1}{2}\left(\mu - \sqrt{\mu^2 - 4\delta}\right), \quad x_0^{(4)} = \frac{1}{2}\left(\mu + \sqrt{\mu^2 - 4\delta}\right) \tag{B.15}$$

and, respectively,

$$x_0^{(3)} = \frac{1}{2}\left(\mu^2 - \sqrt{\mu^4 - 4\delta}\right), \quad x_0^{(4)} = \frac{1}{2}\left(\mu^2 + \sqrt{\mu^4 - 4\delta}\right). \tag{B.16}$$

The case $\delta = 0$ was studied in section B.0.1 and a transcritical bifurcation of first order contact (equation (B.6) and figure B.1b) or second order contact (equation (B.9) and figure B.1e) occurs in this case. Note that the solutions (B.9) may be obtained by setting $\delta = 0$

in equation (B.16), but equation (B.15) with $\delta = 0$ assumes the form $x_0^{(3)} = \mu$, $x_0^{(4)} = 0$ at $\mu \leq 0$ and $x_0^{(3)} = 0$, $x_0^{(4)} = \mu$ at $\mu \geq 0$. In other words, the dependences $x_0^{(3)}(\mu)$ and $x_0^{(4)}(\mu)$ given by equation (B.15) become non-smooth in the case $\delta = 0$ (the first derivative becomes discontinuous), which is why it is natural to use equation (B.6) in this case.

In the case $\delta < 0$, there are two solutions, one described by the dependence $x_0^{(3)}(\mu)$ and the other by $x_0^{(4)}(\mu)$. These solutions do not have any point in common, i.e., are isolated: the bifurcation is broken. Each of these solutions exists on both sides of the bifurcation point, i.e., at both positive and negative μ. In the case $\delta > 0$, there are two isolated solutions as well, one at negative μ and the other at positive μ. Each of the new solutions comprises two branches separated by a turning point, one branch being described by the dependence $x_0^{(3)}(\mu)$ and the other by $x_0^{(4)}(\mu)$. The above-discussed solutions are schematically shown in figures B.2a and B.2b.

Thus, a perturbation represented by a deviation of δ from zero destroys the bifurcation and causes the bifurcating solutions to be broken into two isolated solutions. Such perturbations are called imperfections.

The stability of each one of the steady-state solutions at $\delta \neq 0$ may be worked out as before [in particular, equation (B.10) applies] and is illustrated in figures B.2a and B.2b. Regardless of sign of δ, steady states described by the dependence $x_0^{(3)}$ are unstable and states described by the dependence $x_0^{(4)}$ are stable in the case of the perturbed transcritical bifurcation of first order contact; *vice versa* in the case of the perturbed transcritical bifurcation of second order contact.

The above suggests three possible scenarios of changes of topology of steady-state solutions. The first scenario occurs in the passage from $\delta = 0$ to $\delta > 0$ and represents breaking of the bifurcating solutions $x_0^{(1)}$ and $x_0^{(2)}$ into two isolated solutions formed by joining of branches that exist on the same side of the bifurcation point (i.e., the section of solution $x_0^{(1)}$ in the range $\mu < 0$ joins the section of solution $x_0^{(2)}$ in the same range, the section of $x_0^{(1)}$ in the range $\mu > 0$ joins the section of $x_0^{(2)}$ in the same range). Each one of the new solutions manifests a turning point at which a change of stability occurs according to one of the above-described scenarios of the fold bifurcation.

The second scenario occurs in the passage from $\delta = 0$ to $\delta < 0$ in the case of transcritical bifurcation of first order contact. This scenario again represents breaking of the bifurcating solutions $x_0^{(1)}$ and $x_0^{(2)}$ with exchange of branches, however in this case the isolated solutions are formed by joining of branches that exist on the opposite sides of the bifurcation point. Each one of the new solutions exists on both sides from the bifurcation point, one of these solutions is stable and the other unstable. Note that no change of topology occurs in the passage from $\delta = 0$ to $\delta < 0$ in the case of transcritical bifurcation of second order contact: the bifurcating solutions separate without exchange of branches or changes of stability.

The third scenario occurs in the passage from $\delta < 0$ to $\delta > 0$ or *vice versa*: two isolated solutions approach each other, enter in contact, i.e. a bifurcation occurs, exchange

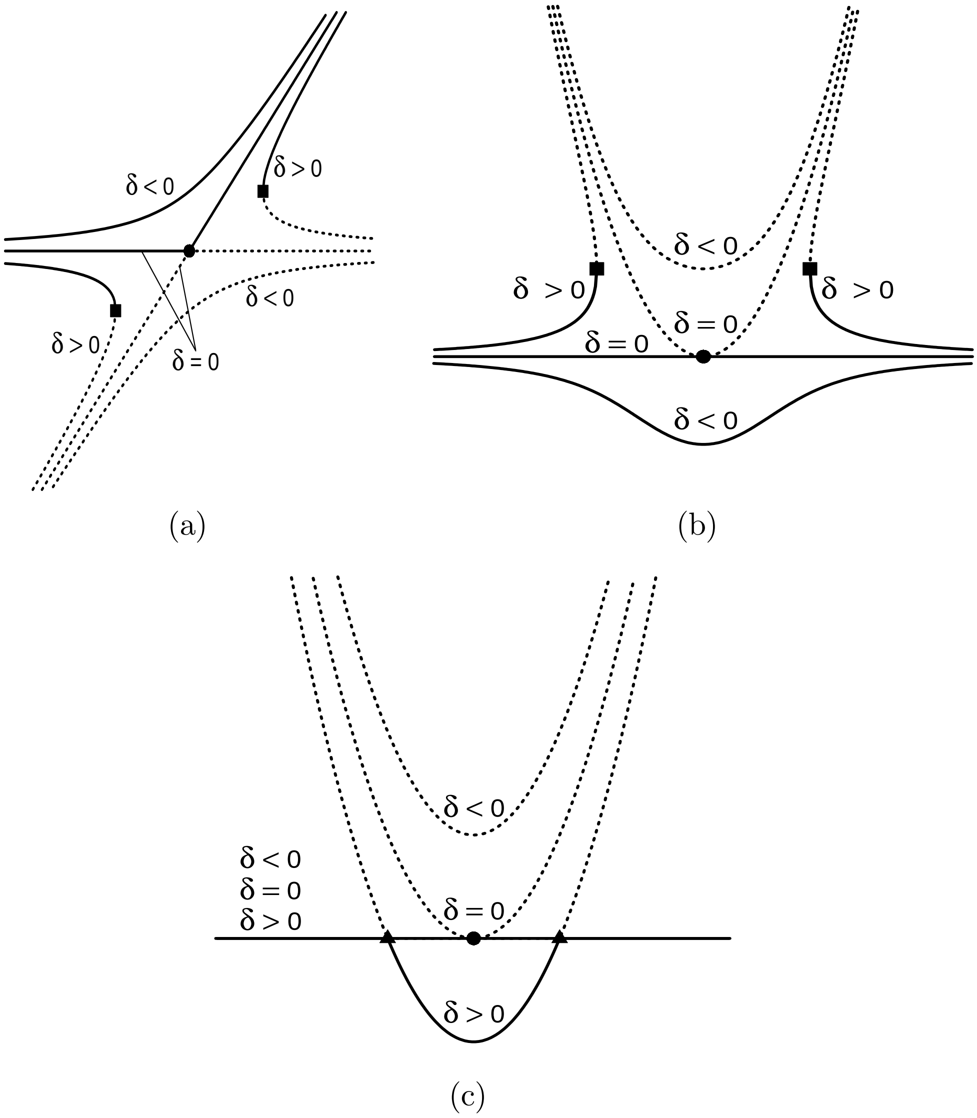

Figure B.2: Diagrams of perturbed transcritical bifurcations in two-parameter systems with one degree of freedom. The origin $\mu = x_0 = 0$ is marked by a circle, axes μ and x_0 are the same as in figure B.1a. Solid: stable sections of steady-state solutions. Dotted: unstable sections. (a) Transcritical bifurcation of first order contact, equation (B.15). (b) Transcritical bifurcation of second order contact, equation (B.16). (c) Transcritical bifurcation of second order contact, equation (B.17).

branches, and then two isolated solutions appear once again. If the change occurs through a perturbed transcritical bifurcation of first order contact, then each of the two solutions develops a vertex (i.e., a discontinuity of the first derivative) immediately before entering in contact, and each of the two appearing solutions also possesses a vertex immediately after the separation. If the change occurs through a perturbed transcritical bifurcations of second order contact, then both solutions remain smooth before entering in contact, and each of the two appearing solutions possesses a cusp immediately after the separation (or *vice versa*: a cusp before entering in contact and smooth solutions after the separation). Therefore, smooth solutions can change their topology through transcritical bifurcations of second (or higher) order contact but not first order contact.

It is convenient for the purposes of this work to consider also another perturbation of transcritical bifurcation of second order contact which is introduced by replacing expression (B.8) with $F = x^2 - \mu^2 x + \delta x$. Steady-state solutions of equation (B.1) read

$$x_0^{(3)} = 0, \quad x_0^{(4)} = \mu^2 - \delta. \tag{B.17}$$

These solutions are schematically shown in figure B.2c. Similarly to figure B.2b, there is a transcritical bifurcation of second order contact in the case $\delta = 0$ and there are two isolated solutions in the case $\delta < 0$. There are two bifurcations of first order contact in the case $\delta > 0$ (rather then two isolated solutions as in figure B.2b); the corresponding points are marked by triangles. Note that in the case $\delta > 0$ the section of solution $x_0^{(3)}$ between the bifurcation points is unstable, which, however, cannot be shown on the graph.

This suggests one more possible scenario of changes of topology of steady-state solutions: two smooth isolated solutions approach each other, enter in second order contact at one point, and remain in first order contact at two points (*or vice versa*).

Bibliography

[1] H. Haken, *Information and Self-Organization: A Macroscopic Approach to Complex Systems*, 3rd ed., Springer Series in Synergetics, Vol. 40 (Springer-Verlag, Berlin, 2006).

[2] G. Nicolis and I. Prigogine, *Self-Organization in Nonequilibrium Systems: From Dissipative Structures to Order through Fluctuations* (John Wiley & Sons, USA, 1977).

[3] H. Haken, *Synergetics: An Introduction*, 3rd ed., Springer Series in Synergetics, Vol. 1 (Springer-Verlag, Berlin, 1983).

[4] H.-G. Purwins, H. U. Bödeker, and Sh. Amiranashvili, Adv. Phys. **59**, 485 (2010).

[5] A. von Engel, *Ionized Gases*, American Vacuum Society Classics (American Institute of Physics, United States of America, 1993).

[6] Yu. P. Raizer, *Gas Discharge Physics* (Springer, Berlin, 1991).

[7] M. Teschke, J. Kedzierski, E. G. Finantu-Dinu, D. Korzec, and J. Engemann, IEEE Trans. Plasma Sci. **33**, 310 (2005).

[8] N. Mericam-Bourdet, M. Laroussi, A. Begum, and E. Karakas, J. Phys. D: Appl. Phys. **42**, 055207 (2009).

[9] Q. Xiong, X. Lu, J. Liu, Y. Xian, Z. Xiong, F. Zou, C. Zou, W. Gong, J. Hu, K. Chen, X. Pei, Z. Jiang, and Y. Pan, J. Appl. Phys. **106**, 083302 (2009).

[10] Y. Xian, X. Lu, Y. Cao, P. Yang, Q. Xiong, Z. Jiang, and Y. Pan, IEEE Trans. Plasma Sci. **37**, 2068 (2009).

[11] A. Shashurin, M. N. Shneider, A. Dogariu, R. B. Miles, and M. Keidar, Appl. Phys. Lett. **94**, 231504 (2009).

[12] X. Lu, Q. Xiong, Z. Xiong, J. Hu, F. Zhou, W. Gong, Y. Xian, C. Zou, Z. Tang, Z. Jiang, and Y. Pan, J. Appl. Phys. **105**, 043304 (2009).

[13] C. Jiang, M. T. Chen, and M. A. Gundersen, J. Phys. D: Appl. Phys. **42**, 232002 (2009).

[14] A. Brockhaus, R. Sauerbier, and J. Engemann, Eur. Phys. J. Appl. Phys. **47**, 22809 (2009).

[15] J. L. Walsh, F. Iza, N. B. Janson, V. J. Law, and M. G. Kong, J. Phys. D: Appl. Phys. **43**, 075201 (14pp) (2010).

[16] M. A. Lieberman and A. J. Lichtenberg, *Principles of Plasma Discharges and Material Processing*, 2nd ed. (Wiley, New York, 2005).

[17] Yu. D. Korolev, V. G. Rabotkin, and A. G. Filonov, High Temp. **17**, 181 (1979).

[18] S. A. Bystrov, A. M. Lushchikova, D. A. Mazalov, A. F. Pal, A. N. Starostin, M. D. Taran, T. V. Taran, and A. V. Filippov, J. Phys. D: Appl. Phys. **27**, 273 (1994).

[19] V. Arkhipenko, A. Kirillov, T. Callegari, Y. Safronau, and L. Simonchik, IEEE Trans. Plasma. Sci. **37**, 740 (2009).

[20] K. H. Schoenbach, M. Moselhy, and W. Shi, Plasma Sources Sci. Technol. **13**, 177 (2004).

[21] M. Moselhy and K. H. Schoenbach, J. Appl. Phys. **95**, 1642 (2004).

[22] N. Takano and K. H. Schoenbach, Plasma Sources Sci. Technol. **15**, S109 (2006).

[23] W. Zhu, N. Takano, K. H. Schoenbach, D. Guru, J. McLaren, J. Heberlein, R. May, and J. R. Cooper, J. Phys. D: Appl. Phys. **40**, 3896 (2007).

[24] B.-J. Lee, D.-L. Biborosch, K. Frank, and L. Mares, J. Optoelectron. Adv. Mater. **10**, 1972 (2008).

[25] C. H. Thomas and O. S. Duffendack, Phys. Rev. **35**, 72 (1930).

[26] V. A. Güntherschulze, W. Bär, and H. Betz, Z. Physik A **109**, 293 (1938).

[27] S. M. Rubens and J. E. Henderson, Phys. Rev. **58**, 446 (1940).

[28] K. G. Müller, Phys. Rev. A **37**, 4836 (1988).

[29] T. Verreycken, P. Bruggeman, and C. Leys, J. Appl. Phys. **105**, 083312 (2009).

[30] T. Braun, J. A. Lisboa, and J. A. C. Gallas, Phys. Rev. Lett. **68**, 2770 (1992).

[31] W. Thouret, W. Weizel, and P. Günther, Z. Physik **130**, 621 (1951).

[32] H. N. Olsen, J. Quant. Spectrosc. Radiat. Transfer **3**, 305 (1963).

[33] J. Haidar, J. Phys. D: Appl. Phys. **28**, 2494 (1995).

[34] J. Reiche, F. Könemann, W. Mende, and M. Kock, J. Phys. D: Appl. Phys. **34**, 3177 (2001).

[35] S. Lichtenberg, D. Nandelstädt, L. Dabringhausen, M. Redwitz, J. Luhmann, and J. Mentel, J. Phys. D: Appl. Phys. **35**, 1648 (2002).

[36] T. Hartmann, K. Günther, S. Lichtenberg, D. Nandelstädt, L. Dabringhausen, M. Redwitz, and J. Mentel, J. Phys. D: Appl. Phys. **35**, 1657 (2002).

[37] N. K. Mitrofanov and S. M. Shkol'nik, Tech. Phys. **52**, 711 (2007).

[38] G. Kühn and M. Kock, Phys. Rev. E **75**, 016406 (2007).

[39] I. G. Kesaev, Sov. Phys. - Tech. Phys. **8**, 447 (1963).

[40] J. C. Sherman, R. Webster, J. E. Jenkins, and R. Holmes, J. Phys. D: Appl. Phys. **8**, 696 (1975).

[41] A. M. Chaly, A. A. Logatchev, K. K. Zabello, and S. M. Shkol'nik, IEEE Trans. Plasma Sci. **31**, 884 (2003).

[42] F. G. Baksht, G. A. Dyuzhev, N. K. Mitrofanov, and S. M. Shkol'nik, Tech. Phys. **42**, 35 (1997).

[43] G. Yang and J. Heberlein, Plasma Sources Sci. Technol. **16**, 529 (2007).

[44] C. Strümpel, H.-G. Purwins, and Yu. A. Astrov, Phys. Rev. E **63**, 026409(7) (2001).

[45] C. Strümpel, Y. A. Astrov, and H.-G. Purwins, Phys. Rev. E **65**, 066210(5) (2002).

[46] E. L. Gurevich, Yu. A. Astrov, and H.-G. Purwins, J. Phys. D: Appl. Phys. **38**, 468 (2005).

[47] Yu. A. Astrov and H.-G. Purwins, Phys. Lett. A **358**, 404 (2006).

[48] W. Breazeal, K. M. Flynn, and E. G. Gwinn, Phys. Rev. E **52**, 1503 (1995).

[49] U. Kogelschatz, IEEE Trans. Plasma Sci. **30**, 1400 (2002).

[50] E. L. Gurevich, A. L. Zanin, A. S. Moskalenko, and H.-G. Purwins, Phys. Rev. Lett. **91**, 154501(4) (2003).

[51] L. Stollenwerk, Sh. Amiranashvili, J.-P. Boeuf, and H.-G. Purwins, Phys. Rev. Lett. **96**, 255001 (2006).

[52] C. Corr, R. Boswell, N. Balcon, C. Samuell, and P. Kenneally, IEEE Trans. Plasma. Sci. **36**, 964 (2008).

[53] K. Takaki, K. Nawa, S. Mukaigawa, T. Fujiwara, and T. Aizawa, IEEE Trans. Plasma. Sci. **36**, 1260 (2008).

[54] F. He, X. Duan, J. Ouyang, J. Wang, and W. Hu, IEEE Trans. Plasma Sci. **36**, 1330 (2008).

[55] X. Duan, F. He, and J. Ouyang, IEEE Trans. Plasma. Sci. **36**, 1332 (2008).

[56] G.-Q. Yang, G.-J. Zhang, Y. Ma, and W.-Y. Zhang, IEEE Trans. Plasma. Sci. **36**, 1346 (2008).

[57] H. Itoh, K. Teranishi, Y. Hashimoto, D. Inada, N. Shimomura, and S. Suzuki, IEEE Trans. Plasma. Sci. **36**, 1348 (2008).

[58] L. Dong, W. Fan, Y. He, and F. Liu, IEEE Trans. Plasma. Sci. **36**, 1356 (2008).

[59] B. Bernecker, T. Callegari, S. Blanco, R. Fournier, and J. P. Boeuf, Eur. Phys. J. Appl. Phys. **47**, 22808 (2009).

[60] B. Bernecker, T. Callegari, and J. P. Boeuf, in *Proc. 12th HAKONE (Bratislava, September 2010)*, edited by J. Országh, P. Papp, and Š Matejčík (Soc. Plasma Res. Appl., Library and Publishing Centre CU, ISBN 978-80-89186-72-3, Bratislava, 2010) pp. 19–30.

[61] P. Mark and K. G. Müller, J. Appl. Phys. **70**, 6694 (1991).

[62] S. Nasuno, Chaos **13**, 1010 (2003).

[63] E. L. Gurevich, Sh. Amiranashvili, and H.-G. Purwins, J. Phys. D: Appl. Phys. **38**, 1029 (2005).

[64] D. D. Šijačić and U. Ebert, Phys. Rev. E **66**, 066410 (2002).

[65] Yu. P. Raizer, U. Ebert, and D. D. Šijačić, Phys. Rev. E **70**, 017401 (2004).

[66] L. B. Loeb, *Electrical Coronas* (University of California Press, Berkely, 1965).

[67] W. Egli, O. Riccius, U. Kogelschatz, R. Gruber, and S. Merazzi, in *Proc. 6th Joint EPS-APS International Conference On Physics Computing*, edited by R. Gruber and M. Tomassini (Lugano, Switzerland, 1994) p. 535.

[68] H. U. Bödeker, M. C. Röttger, A. W. Liehr, T. D. Frank, R. Friedrich, and H.-G. Purwins, Phys. Rev. E **67**, 056220(12) (2003).

[69] Yu. A. Astrov and Yu. A. Logvin, Phys. Rev. Lett. **79**, 2983 (1997).

[70] S. V. Gurevich, H. U. Bödeker, A. S. Moskalenko, A. W. Liehr, and H.-G. Purwins, Physica D **199**, 115 (2004).

[71] M. S. Benilov, Phys. Rev. A **45**, 5901 (1992).

[72] R. S. Islamov, Phys. Rev. E **64**, 046405 (2001).

[73] Sh. Amiranashvili, S. V. Gurevich, and H.-G. Purwins, Phys. Rev. E **71**, 066404(9) (2005).

[74] R. R. Arslanbekov and V. I. Kolobov, J. Phys. D: Appl. Phys. **36**, 2986 (2003).

[75] S. T. Surzhikov, High Temp. **43**, 825 (2005).

[76] R. S. Islamov and E. N. Gulamov, IEEE Trans. Plasma Sci. **26**, 7 (1998).

[77] V. I. Kolobov and A. Fiala, Phys. Rev. E **50**, 3018 (1994).

[78] I. D. Kaganovich, M. A. Fedotov, and L. D. Tsendin, Tech. Phys. **39**, 241 (1994).

[79] D. D. Šijačić, U. Ebert, and I. Rafatov, Phys. Rev. E **71**, 066402(12) (2005).

[80] I. R. Rafatov, D. D. Šijačić, and U. Ebert, Phys. Rev. E **76**, 036206(18) (2007).

[81] I. Brauer, C. Punset, H.-G. Purwins, and J. Boeuf, J. Appl. Phys. **85**, 7569 (1999).

[82] B. Y. Moizhes and V. A. Nemchinskii, Sov. Phys. Tech. Phys. **18**, 1460 (1974).

[83] B. Y. Moizhes and V. A. Nemchinskii, Sov. Phys. Tech. Phys. **20**, 757 (1975).

[84] M. S. Benilov and N. V. Pisannaya, Sov. Phys. - Tech. Phys. **33**, 1260 (1988).

[85] R. Bötticher and W. Bötticher, J. Phys. D: Appl. Phys. **33**, 367 (2000).

[86] M. S. Benilov and M. D. Cunha, J. Phys. D: Appl. Phys. **35**, 1736 (2002).

[87] M. S. Benilov and M. D. Cunha, J. Phys. D: Appl. Phys. **36**, 603 (2003).

[88] L. Dabringhausen, O. Langenscheidt, S. Lichtenberg, M. Redwitz, and J. Mentel, J. Phys. D: Appl. Phys. **38**, 3128 (2005).

[89] M. S. Benilov, M. Carpaij, and M. D. Cunha, J. Phys. D: Appl. Phys. **39**, 2124 (2006).

[90] http://www.arc_cathode.uma.pt.

[91] M. S. Benilov, Phys. Rev. E **58**, 6480 (1998).

[92] M. S. Benilov, Physica Scripta **58**, 383 (1998).

[93] M. S. Benilov, Phys. Letters A **228**, 182 (1997).

[94] M. S. Benilov, Sov. Phys. - Tech. Phys. **33**, 1267 (1988).

[95] M. S. Benilov, Phys. Rev. E **77**, 036408 (2008).

[96] M. S. Benilov and M. D. Cunha, Phys. Rev. E **68**, 056407 (2003).

[97] M. Mitchner and C. H. Kruger, *Partially Ionized Gases* (Wiley, New York, 1973).

[98] I. Rutkevich, Phys. Plasmas **5**, 3054 (1998).

[99] O. A. Sinkevich and V. E. Sosnin, High Temp. **39**, 180 (2001).

[100] O. A. Sinkevich, High Temp. **41**, 609 (2003).

[101] M. Arrayás and U. Ebert, Phys. Rev. E **69**, 036214(10) (2004).

[102] M. S. Benilov and G. V. Naidis, J. Phys. D: Appl. Phys. **43**, 175204 (9pp) (2010).

[103] T. Christen, J. Phys. D: Appl. Phys. **43**, 298001 (2 pp) (2010).

[104] M. S. Benilov and G. V. Naidis, J. Phys. D: Appl. Phys. **43**, 298002 (2pp) (2010).

[105] M. S. Benilov and M. J. Faria, J. Phys. D: Appl. Phys. **40**, 5083 (2007).

[106] P. G. C. Almeida, M. S. Benilov, M. D. Cunha, and M. J. Faria, J. Phys. D: Appl. Phys. **42**, 194010 (21pp) (2009).

[107] M. S. Benilov, M. D. Cunha, and M. J. Faria, IEEE Trans. Plasma Sci. **36**, 1034 (2008).

[108] M. S. Benilov, M. D. Cunha, and M. J. Faria, J. Phys. D: Appl. Phys. **42**, 145205 (17pp) (2009).

[109] S. Coulombe, Bull. Amer. Phys. Soc. **45**, 18 (2000), 53rd Gaseous Electronics Conference, Oct. 2000, Houston, Texas.

[110] W. Graser, in *Proceedings of the 9th International Symposium on the Science and Technology of Light Sources, Cornell University, Ithaca, Aug. 2001*, edited by R. S. Bergman (Cornell University Press, Ithaca, NY, 2001) pp. 211–212.

[111] T. Krücken, in *Proceedings of the 9th International Symposium on the Science and Technology of Light Sources, Cornell University, Ithaca, Aug. 2001*, edited by R. S. Bergman (Cornell University Press, Ithaca, NY, 2001) pp. 267–268.

[112] R. Bötticher and W. Bötticher, J. Phys. D: Appl. Phys. **34**, 1110 (2001).

[113] R. Bötticher, W. Graser, and A. Kloss, J. Phys. D: Appl. Phys. **37**, 55 (2004).

[114] G. M. J. F. Luijks, S. Nijdam, and H. v Esveld, J. Phys. D: Appl. Phys. **38**, 3163 (2005).

[115] R. Bötticher and M. Kettlitz, J. Phys. D: Appl. Phys. **39**, 2715 (2006).

[116] F. H. Scharf, O. Langenscheidt, and J. Mentel, in *Proc. 28th ICPIG (Prague, July 2007)*, edited by J. Schmidt, M. Šimek, S. Pekárek, and V. Prukner (Institute of Plasma Physics AS CR, ISBN 978-80-87026-01-4, Prague, 2007) pp. 1252–1255.

[117] A. L. Lenef, J. Phys. D: Appl. Phys. **41**, 144003 (15pp) (2008).

[118] M. S. Benilov, J. Phys. D: Appl. Phys. **40**, 1376 (2007).

[119] M. S. Benilov, J. Phys. D: Appl. Phys. **41**, 144001 (30pp) (2008).

[120] N. A. Almeida, M. S. Benilov, and G. V. Naidis, J. Phys. D: Appl. Phys. **41**, 245201 (26pp) (2008).

[121] F. Könemann, G. Kühn, J. Reiche, and M. Kock, J. Phys. D: Appl. Phys. **37**, 171 (2004).

[122] M. Redwitz, L. Dabringhausen, S. Lichtenberg, O. Langenscheidt, J. Heberlein, and J. Mentel, J. Phys. D: Appl. Phys. **39**, 2160 (2006).

[123] W. L. Bade and J. M. Yos, *Theoretical and Experimental Investigation of Arc Plasma-Generation Technology. Part II, Vol. 1: A Theoretical and Experimental Study of Thermionic Arc Cathodes. Technical Report No. ASD-TDR-62-729* (Avco Corporation, Wilmington, Mass., USA, 1963).

[124] M. S. Benilov, M. D. Cunha, and G. V. Naidis, Plasma Sources Sci. Technol. **14**, 517 (2005).

[125] M. S. Benilov and M. J. Faria, in *Proc. European COMSOL Conference (Nov. 4-6, 2008, Hannover, Germany)* (COMSOL, ISBN 978-0-9766792-3-3, 2008).

[126] Y. S. Touloukian, R. W. Powell, C. Y. Ho, and P. G. Clemens, *Thermal Conductivity. Metallic Elements and Alloys.*, Thermophysical Properties of Matter, vol. 1 (IFI/Plenum, New York-Washington, 1970).

[127] S. W. H. Yih and C. T. Wang, *Tungsten: Sources, Metallurgy, Properties, and Applications* (Plenum Press, New York, 1979).

[128] P. G. C. Almeida, M. S. Benilov, and M. J. Faria, Plasma Sources Sci. Technol. **19**, 025019 (13pp) (2010).

[129] P. G. C. Almeida, M. S. Benilov, and M. J. Faria, Bull. Amer. Phys. Soc., Proc. 63rd Gaseous Electronics Conf. and 7th Int. Conf. on Reactive Plasmas **55**, 166 (2010).

[130] P. G. C. Almeida, M. S. Benilov, and M. J. Faria, IEEE Trans. Plasma Sci. **39**, (2011, to appear).

[131] J. P. Boeuf, B. Chaudhury, and G. Q. Zhu, Phys. Rev. Lett. **104**, 015002 (2010).

[132] B. Chaudhury, J. P. Boeuf, and G. Q. Zhu, Phys. Plasmas **17**, 123505 (2010).

[133] J. P. Boeuf, L. C. Pitchford, and K. H. Schoenbach, Appl. Phys. Lett. **86**, 071501 (2005).

[134] E. Muñoz-Serrano, G. Hagelaar, Th. Callegari, J. P. Boeuf, and L. C. Pitchford, Plasma Phys. Control. Fusion **48**, B391 (2006).

[135] K. Makasheva, E. Muñoz-Serrano, G. Hagelaar, J. P. Boeuf, and L. C. Pitchford, Plasma Phys. Control. Fusion **49**, B233 (2007).

[136] T. Deconinck and L. L. Raja, Plasma Processes Polym. **6**, 335 (2009).

[137] X. Zhang, X. Wang, F. Liu, and Y. Lu, IEEE Trans. Plasma. Sci. **37**, 2055 (2009).

[138] S. He, J. Ouyang, F. He, and S. Li, Phys. Plasmas **18**, 032102 (2011).

[139] M. A. Biondi and L. M. Chanin, Phys. Rev. **94**, 910 (1954).

[140] L. C. Pitchford, J. P. Boeuf, and W. L. Morgan, "Boltzmann simulation software and database," (1998), http://www.siglo-kinema.com/bolsig.htm.

[141] J. Meunier, P. Belenguer, and J. P. Boeuf, J. Appl. Phys. **78**, 731 (1995).

[142] A. Fridman and L. A. Kennedy, *Plasma Physics and Engineering* (Taylor and Francis, New York, 2004).

[143] C. Punset, J.-P. Boeuf, and L. C. Pitchford, J. Appl. Phys. **83**, 1884 (1998).

[144] V. N. Melekhin, N. Yu. Naumov, and N. P. Tkachenko, Sov. Phys. Tech. Phys. **32**, 274 (1987).

[145] A. V. Phelps, Z. Lj. Petrović, and B. M. Jelenković, Phys. Rev. E **47**, 2825 (1993).

[146] A. A. Kudryavtsev and L. D. Tsendin, Tech. Phys. Lett. **28**, 1036 (2002).

[147] Yu. P. Raizer, E. L. Gurevich, and M. S. Mokrov, Tech. Phys. **51**, 185 (2006).

[148] L. Dabringhausen, U. Hechtfischer, T. Vos, W. van Erk, and M. Haacke, in *Proc. 11th Int. Symp. Sci. Technol. Light Sources (LS:11) (Shanghai, May 2007)*, edited by M. Q. Liu and R. Devonshire (FAST-LS, ISBN 978-0-9555445-0-7, Sheffield, UK, 2007) pp. 529–530.

[149] M. Rahmane, E. Croquesel, and S. Selezneva, "High pressure discharge lamp control system and method," (2007), United States Patent US 7250732 B2.

[150] J. Mentel, J. Luhmann, and D. Nandelstädt, Industry Applications Conference, 2000, Rome. Conference Record of the 2000 IEEE **5**, 3293 (2000).

[151] Y. Yang, J. J. Shi, J. E. Harry, J. Proctor, C. P. Garner, and M. G. Kong, IEEE Trans. Plasma Sci. **33**, 302 (2005).

[152] D. Staack, B. Farouk, A. Gutsol, and A. Fridman, Plasma Sources Sci. Technol. **17**, 025013 (13pp) (2008).

[153] M. Abramowitz and I. A. Stegun, eds., *Handbook of Mathematical Functions* (Dover, New York, 1965).

[154] J. Guckenheimer and P. Holmes, *Nonlinear Oscillations, Dynamical Systems, and Bifurcations of Vector Fields*, Applied Mathematical Sciences, Vol. 42 (Spinger-Verlag, New York, 1983).

[155] G. Iooss and D. D. Joseph, *Elementary Stability and Bifurcation Theory*, 2nd ed. (Springer, New York, 1990).

[156] J. D. Crawford, Rev. Mod. Phys. **63**, 991 (1991).

[157] M. C. Cross and P. C. Hohenberg, Rev. Mod. Phys. **65**, 851 (1993).